Development of fluorescent FRET receptor sensors for investigation of conformational changes in adenosine A_1 and A_{2A} receptors

Entwicklung fluoreszenter FRET Rezeptor-Sensoren zur Untersuchung von Konformationsänderungen in Adenosin A_1 und A_{2A} Rezeptoren

Doctoral Thesis for a doctoral degree
at the graduate school of life sciences,
Julius-Maximilians-Universität Würzburg
Section: Biomedicine
submitted by

Anette D. Stumpf

from Aalen

Würzburg 2015

Contents

List of Figures

VI

List of Tables

1 Introduction

1.1 G protein-coupled receptors

Guanine nucleotide binding protein-coupled receptors (GPCRs) are the largest receptor super-family consisting of transmembrane-spanning receptors [1] that are widely distributed throughout living organisms [2][3][4][5][6]. They consist of seven transmembrane domains, linked with three extracellular and three intracellular loops. Receptor structures start with an extracellular N-terminus and end with an intracellular located C-terminus. GPCRs can be activated by various exogenous ligands, such as photons, biogenic amines, lipids, eicosanoids, nucleosides, hormones and small molecules like neurotransmitters and calcium [7][8]. A wide array of effects occur with the help of dynamical movements of GPCRs, following the binding of a ligand and are regulated with help of heterotrimeric guanine-binding proteins (G proteins) [9][10][11], β-arrestins [12][13] and other mediators [14].

1.1.1 Classification of GPCRs

Until now, genes of almost 1000 human GPCRs have been identified [15][16][17]. Apart from their previously mentioned common structural and activation properties, these receptors are very diverse. There have been many attempts to classify this huge super-family of receptors. One of the first methods to classify GPCRs was the division into a class system A-F [18]. A previously investigated system for the classification of GPCRs is the GRAFS system which distinguishes between Glutamate, Rhodopsin, Adhesion, Frizzled/Taste2 and Secretin class [16]. Rhodopsin receptors represent the largest class in this classification and are grouped in α, β, γ and δ main groups.

Two systems were established for the localization of positions in GPCRs. The first nomenclature was based on the amino acid position in the transmembrane regions [19][20]. The second nomenclature, which was developed by Ballesteros and Weinstein assigned the number 50 to the most conserved amino acid in each trans-

membrane region and all other positions were correlated to that position [21]. The Ballesteros and Weinstein nomenclature was applied throughout this work.

1.1.2 GPCRs as targets for drugs - increasing structural knowledge

It was recently stated that GPCRs represent the target for approximately 50 % of all drugs on the market [22]. However, there are still a lot of GPCRs that are not targeted by drugs because ligands with high efficacy and high selectivity are missing due to lack of structural knowledge.

In the last years crystal structures of numerous GPCRs have been solved revealing information about their receptor function. The first high resolution crystal structure resolved was rhodopsin [23]. More receptor structures belonging to class A GPCRs were resolved in the following years. These structures are important for gaining insight into the binding mode between receptor and a particular ligand, giving a snapshot of all movements that occur when a ligand binds to a receptor. Crystal structures of one particular receptor in the active and inactive state can provide insight into the major regions that are moving when a receptor switches between its active and inactive state. It is challenging to crystallize GPCRs due to their flexibility and their thermal instability [24][25].

1.1.3 Adenosine receptors

The adenosine receptor family consists of four members (Adenosine A_1, A_{2A}, A_{2B} and A_3 receptor, abbreviated as A_1R, $A_{2A}R$, $A_{2B}R$ and A_3R) and belongs to the GPCR class A or α group of rhodopsin-like receptors. This group is the largest and best-characterized GPCR class up to date [26]. The adenosine receptor family includes a highly conserved sequence similarity among receptor subtypes and species [27][28]. Single amino acid positions, such as the histidine residues in position 6.52 and 7.43, are conserved amongst adenosine receptors except for the A_3R where histidine 7.43 is not present [27]. Adenosine receptors are involved in numerous regulatory processes throughout the human body, such as cardiac control, coordination of blood perfusion, perfusion of the kidneys or reperfusion in general after ischemic events, angiogenesis, nociceptive regulation concerning inflammatory occurrences [29], regulation of the sleep-wake cycle and mediation in neurodegenerative disorders and thus represent an attractive target for drugs. Today, the only

2

drug that selectively targets a member of the adenosine receptor family approved by the European Medicines Agency and the U.S. Food and Drug Administration is the $A_{2A}R$ selective agonist regadenoson. However, this drug is only indicated as an analytic reagent for cardiac stress testing in special cases and its area of application has been further restricted due to severe adverse drug events that came up during the past years. Theophylline, an unspecific antagonist on all four receptor subtypes, is clinically approved in the treatment of asthma bronchiale in special cases. Adenosine, the physiological agonist that acts as the full agonist on all adenosine receptors [30] is used for two different applications: paroxysmal supraventricular tachycardia and as an adjunct in a special case of cardiac imaging. However, drugs that have been specifically designed to target these receptors have continuously failed in the early phases of clinical trials [31] due to their lack of selectivity, which results in a lot of adverse drug effects and missing potency.

1.1.3.1 Adenosine A_{2A} receptor

Adenosine A_{2A} receptors ($A_{2A}R$) mediate their effects through the use of a G_s protein [32] and partly through a G_{olf} protein [33][34]. $A_{2A}R$ is involved in the regulation of platelet aggregation, blood pressure and in the development of pain [35]. It has also been shown to play a role in ischemic brain damage in mice [36] and reduces inflammation following an ischemic event [37]. Antagonists of this receptor seemed to have a beneficial effect on Parkinson's disease [38]. However, as mentioned before, the only specifically approved $A_{2A}R$ agonist is regadenoson.

$A_{2A}R$ is also the only member of the adenosine receptor family where detailed structural information is available from its crystal structures. An up-to-date overview of all ligands that have been successfully crystallized with the $A_{2A}R$ is given in table 1.1. High resolution crystal structures of $A_{2A}R$ bound to antagonist ZM241385 exist where the third intracellular loop of receptor was fused to the T4-Lysozyme and the C-terminus was truncated [25] (see figure 1.1). The modified receptor which led to this crystallization was named A_{2A}-T4L-ΔC. Amino acids found to be strongly involved in ligand binding include leucine 85 (3.33), tryptophan 247 (6.48) and histidine 264 (6.66) (figure 1.1). Furthermore, $A_{2A}R$ was stabilized using the so-called StaR-technology (*sta*bilized *r*eceptor) with the help of amino acid mutation and co-crystallized with the antagonists ZM241385, XAC and caffeine [39]. The resulting receptor construct was named A_{2A}-StaR2. The same A_{2A}-StaR2 construct technique was also used for 1,2,4-triazine derivatives, which represent $A_{2A}R$ antagonists

that are potential candidates for the therapy of Parkinson's disease [40]. More-over, the receptor structure was locked into the inactive conformation with help of an antibody Fab fragment. This led to the A_{2A}R-Fab2838 receptor construct that was co-crystallized with ZM241385 [41]. Another crystallization approach that was utilized was the replacement of the third intracellular loop of the receptor by a thermostabilized apocytochrome resulting in the construct A_{2A}AR-BRIL-ΔC. This allowed for further refinement of the resolution of the crystals and made it possible to see water molecules that were clustered within the receptor structure. These water molecules were involved in receptor stabilization and function when A_{2A}R was crystallized with ZM241385 [42]. The crystal structures named until now represent the inactive conformation of A_{2A}R. The active conformation of A_{2A}R was investigated with the A_{2A}-T4L-ΔC receptor that was co-crystallized with the agonist UK-432097 [43]. A_{2A}R that was stabilized with the help of thermo-stabilizing amino acid mutations was additionally resolved using the agonists adenosine [44], NECA [45] and CGS 21680 [46]. This structural data were taken as a starting point for the computational prediction of which effect distinct amino acid mutations have concerning ligand binding behavior [47][48].

Ligand		stabilized A_{2A}R construct
1,2,4,-triazine and derivatives	Antagonists	A_{2A}-StaR2 [40]
adenosine	Agonist	A_{2A}R-GL31 [44][45]
caffeine	Antagonist	A_{2A}-StaR2 [39]
CGS 21680	Agonist	A_{2A}R-GL31 [46]
NECA	Agonist	A_{2A}R-GL31 [45]
UK-432097	Agonist	A_{2A}-T4L$-\Delta$C [43]
XAC	Antagonist	A_{2A}-StaR2 [39]
ZM241385	Antagonist	A_{2A}-T4L-ΔC [25]
		A_{2A}-StaR2 [39]
		A_{2A}R-Fab2838 [41]
		A_{2A}AR-BRIL-ΔC [42]

Table 1.1: Previously published ligands that have been crystallized with the A_{2A}R

In earlier studies, A_{2A}R has been extensively characterized with the help of mutational analysis that found the involvement of threonine 88 (3.36) in ligand binding [49]. The same principle was also found in newer investigations, where the receptor

activity was tested with help of a yeast-assay [50]. The impact of threonine 88 (3.36) was further confirmed with a previously published computational simulation that showed its involvement in agonist binding [51]. Histidine 250 (6.52) and asparagine 253 (6.55) were also found to be important for general ligand binding [52].

The crystal structures of $A_{2A}R$ combined with the results of former mutational analysis performed with the help of radioligand binding studies revealed amino acids which play a major role in ligand binding. Asparagine 253 (6.55) and histidine 250 (6.52) were found to be important in the ligand binding process [53]. Other studies revealed that isoleucine 66 (2.64) and serine 277 (7.42) are also involved in ligand binding [54][55]. Previously published computational simulations of $A_{2A}R$ demonstrated that serine 277 (7.42) is part of the agonist bound receptor conformation and that tryptophan in position 246 (6.48) is involved in the intracellular transfer of the signal evoked by the agonist binding process [51].

Modification of the 2-position of adenosine enhances the ligand selectivity for $A_{2A}R$ [56]. This fact also holds true for CGS 21680 which is an agonist that has an increased specificity for $A_{2A}R$ compared to other adenosine receptor subtypes [57].
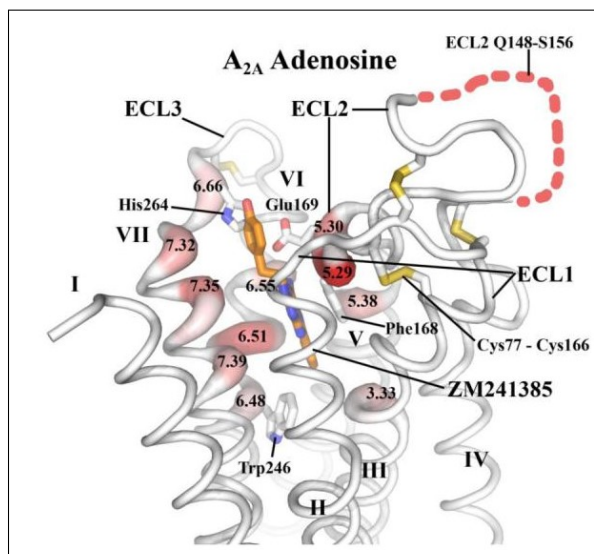
Figure 1.1: A_{2A}-T4-ΔC co-crystallized with ZM241385. Depiction of the ligand binding pocket and the surrounding amino acids which have an impact on ligand binding. Obtained from Jaakola et al. 2008, [25].

1.1.3.2 Adenosine A_1 receptor

The $G_{i/o}$ coupled adenosine A_1 receptor (A_1R) is highly conserved among species and mediates its effects in the body through the inhibition of adenylate cyclase [58].

A_1R is involved in the regulation of many functional processes throughout the body, including negative inotropic and chronotropic effects upon heart function [59], regulation of the sleep-wake cycle [60][61] and nociceptive regulation [62]. For example it was shown that an A_1R selective agonist has beneficial effects on inflammation in rats [63] and acts negatively chronotropic upon rat hearts [64]. Additionally this receptor is involved in the regulation of renal function [65][66]. This versatile involvement throughout the body makes A_1R a desirable target for multiple therapeutic approaches. Therefore detailed knowledge of the structure and dynamical behavior of A_1R is required. However, the crystal structure of A_1R is not yet available and many attempts to design drugs that target this receptor still fail in early phases of clinical trials because of the lack of selectivity and a wide variety of adverse side effects [31]. So far this receptor was mainly characterized with the help of radioligand binding studies [67][27] and the results suggested that modifications of the physiological agonist adenosine at the N^6-position enhance the selectivity of ligands for A_1R [56]. There were also successful attempts of investigating non-adenosine agonists that showed enhanced specificity for the A_1R [68].

To find more potential ligands for the A_1R four homology models of this receptor, based on the $A_{2A}R$ structure revealed from its crystallization data, were established in a previous study. Receptor models were docked to various potential new ligands. However, due to structural resemblance of adenosine receptor subtypes, many substances that were investigated appeared to have a remarkable affinity for all receptor subtypes examined [69].

One of the early performed A_1R homology-modeling studies modeled the receptor with the A_1R selective ligand CPA [70]. Modeling was performed based upon the canine A_1R sequence [71] and the structure of bacteriorhodopsin [72]. In this study it was proposed that threonine 91 (3.36), tryptophan 247 (6.48), histidine 251 (6.52) and asparagine 254 (6.55) are involved in ligand binding. Modeling studies could confirm the influence of the formerly named amino acids and suggested that leucine 88 (3.33) and threonine 277 (7.42) play an additional role in the ligand binding and the recognition of A_1R specific agonists [73].

Mutations of single amino acids in the A_1R sequence can help to reveal their role in ligand binding and recognition and thus lead to more structural insight concerning receptor function. In previous studies a number of mutational analysis was performed for the A_1R using radioligand binding which confirmed the previously described effects [27][74][75][76][77][78][79].

6

It is known that certain amino acids have a distinct influence on ligand affinity and thus are likely to affect ligand binding behavior in the A_1R. A mutation in which leucine in position 88 (3.33) was exchanged to an alanine led to a decrease in agonist and antagonist affinity [73]. A decrease in agonist and antagonist affinity was also seen when threonine in position 91 (3.36) was mutated into an alanine [73]. Decreased antagonist affinity was observed when histidine in position 251 (6.52) was exchanged to a leucine [74]. When threonine in position 277 (7.42) was mutated into an alanine or a serine agonist affinity was decreased [75][77].

Because of their influence in ligand binding affinity the formerly named amino acids represent interesting tools for further investigation leading to a better understanding of A_1R structure and function. Another opportunity to gain more knowledge concerning A_1R was provided with the first crystal structure of the adenosine receptor family, namely the $A_{2A}R$ co-crystallized with the antagonist ZM241385 [25]. It revealed the amino acids which form the ligand binding pocket (compare figure 1.1) and thus are likely to have an impact on ligand binding in the $A_{2A}R$. Another crystal structure of the $A_{2A}R$ was the basis for modeling studies in the A_1R where the ribose-modified adenosine derivative 5'-N-Ethylcarboxamidoadenosine (NECA) was docked into an A_1R model based on the agonist UK-432097 bound crystal structure of the $A_{2A}R$ [43] and suggested more amino acids that are likely to be involved in ligand binding [80], such as histidine in position 251 (6.52), threonine 91 (3.36) and threonine 277 (7.42). All the previous findings of amino acids that were found to have an influence in ligand binding in the A_1R are summarized in table 1.2.

To gain more insight into the functional role of eight amino acids that are known to have a particular impact in ligand binding from former studies in the A_1R and the $A_{2A}R$ these distinct amino acids were investigated via mutational analysis in the A_1R. The crystal structure of $A_{2A}R$ and its sequence were the basis to find amino acids in the A_1R that are in the same spatial position as in the $A_{2A}R$ and the impact on the ligand binding process of these single amino acids was investigated using mutational analysis. The amino acids investigated here were isoleucine 69 (2.64) that was mutated to a valine, leucine 88 (3.33) mutated to an alanine, threonine 91 (3.36) mutated to an alanine, tryptophan 247 (6.48) to an alanine, histidine 251 (6.52) to an alanine, asparagine 254 (6.55) to an alanine, histidine 264 (6.66) to an alanine and threonine 277 (7.42) to an alanine or a serine. As previously mentioned, some of these mutations were earlier examined at the A_1R via radioligand binding studies or their impact in ligand binding was found with the help of modeling studies. These

receptor mutants were now probed using fluorescent tags that were able to elucidate conformational movements of receptor upon ligand binding in living cells.

Amino acid	Effect	Method
L88 (3.33)	involved in ligand binding	homology modeling, mutational analysis [73]
T91 (3.36)	involved in ligand binding	homology modeling [70], mutational analysis [73]
W247 (6.48)	involved in agonist binding	homology modeling [70]
H251 (6.52)	involved in ligand binding	homology modeling [70], mutational analysis [74]
N254 (6.55)	involved in agonist binding	homology modeling [70]
T277 (7.42)	involved in agonist binding	homology modeling [73], mutational analysis [75][77]

Table 1.2: Amino acids in the A_1R with known impact on ligand binding, investigated in previous studies with molecular modeling or mutational analysis

1.2 Receptor ligand interactions

1.2.1 Dynamic receptor movement upon ligand binding

When an agonist binds to a GPCR the receptor transmembrane regions undergo a conformational change that mediates the intracellular signal-transduction. It is thought that agonists either disrupt the intramolecular stabilizing interactions of a receptor or that their appearance enables new interactions between the transmembrane regions which leads to the active state of receptor [81]. The model classically employed for the description of the behavior of a GPCR upon ligand binding is the ternary complex model [82]. In the past years the model was extended to adjust it to the current scientific knowledge and the further developed extended ternary complex model [83] was followed by the cubic ternary complex model [84].

A more simple model for GPCR behavior is the binding and activation model that was first investigated in the context of enzymes [85]. Two affinity forms regarding GPCRs are present: The receptor (R) and ligand (L) form the receptor ligand bound state (RL) that can change into a high affinity receptor ligand bound state (RL*) which is able to mediate signal cascades inside cells. The two state model [86]

describes the following affinity states:

$$R + L \rightleftharpoons RL \rightleftharpoons RL^* \tag{1.1}$$

Models like the formerly named are helpful for dismantling the complex ligand receptor binding process down to the concrete events. However, models also display only parts of the truth because it is widely known that proteins can undergo multiple conformations [87] and thus are not fully explainable by models with just a few conformational states. These models represent a good approximation on processes that happen at receptors upon ligand binding. With the help of crystal structures it is also not feasible to determine the complete dynamical behavior of a receptor because in most cases there are just active and inactive state snapshots of receptor movements available. Dynamical simulations of $A_{2A}R$ revealed that turnover from one conformational state into another includes more than 2^{10} intermediate steps [51]. Thus it would be desirable to get more insight into the overall receptor dynamical movement that occurs upon ligand binding.

Mutagenic studies of adenosine receptors revealed that the transmembrane domains (TM) 3, 5, 6 and 7 are important for ligand binding and recognition in adenosine receptors [27]. Previously performed dynamical simulations confirmed the involvement of TM 1, 2 and 7 when the receptor structure transforms from the inactive into the active conformation [51]. Class A GPCRs in general share some common structures, so called microswitches, which cause a structural change during receptor activation [51]. These structural elements are the DRY, the CWxP and the NPxxY motif [88][89]. For the $A_{2A}R$ it was previously shown that the ionic lock of the DRY motif has to be disturbed to convert receptor from the inactive to the active state [51].

The crystal structures reveal the endpoint of movements that receptors undergo when they bind to an agonist or antagonist. As $A_{2A}R$ was crystallized with antagonists [25][39][41][40] as well as with agonists [43][90][46][45] both dynamical states of this receptor, the inactive and the active state, were available and could be compared to each other. This comparison revealed that helix III, V, and VI move during agonist binding. There were also movements of helix VII and the extracellular loop (EL) 3 that seemed to be specific for the activation process in $A_{2A}R$ [43].

1.2.2 Requirements for effective drugs at receptors

As demonstrated in the previous section it is still a big challenge to investigate drugs that target a distinct member of the adenosine receptor family with high specificity and efficacy. Efficacy describes the extent of effect that is evoked on a receptor when it is exposed to a particular ligand in a distinct environment and was first described by Stephenson [91]. The term efficacy was further developed to intrinsic efficacy which describes the effect of a drug at the receptor itself without regarding the environment [92]. To develop drugs with high efficacy the dissociation constant K_d and the half maximal effective concentration EC_{50} were examined for a specific ligand receptor interaction under equilibrium conditions. Physiological conditions are however non-equilibrium conditions. Therefore, it would be really important to investigate the time that a ligand spends at a receptor and thus is able to mediate its effects under physiological conditions. This time period is named residence time (t_R) and is defined as the reciprocal of the dissociation constant of a receptor ligand complex (k_{off}) [93][94][95]. It was shown that long drug target residence time can be beneficial for higher in vivo efficacy in drugs and that there is a direct correlation between residence time and in vivo efficacy [93][96]. Furthermore, knowledge and therefor modulation of residence time could lead to drugs with less side effects, because the longer a drug acts in the body the higher the probability that it interferes with structures other than the target structure [94]. For the A_1R there was a previous examination where the structure of ligands and the residence time was successfully characterized and modified due to their binding kinetics [97].

In the last years there were several approaches for the examination of residence time [98]. One opportunity to investigate receptor ligand binding kinetics and therefor residence time is fluorophore tagged receptors in combination with fluorescent ligands. In the case of the $A_{2A}R$ a high throughput assay became available that investigates interaction of fluorescent ligands with a fluorescence tagged receptor [99][98]. There were also attempts to optimize chemical properties of newly synthesized antagonists at the $A_{2A}R$ with classical pharmacological methods as well as with kinetic investigations that led to the examination of residence time [100]. Previously performed investigations with $A_{2A}R$ selective agonists were also able to link the efficacy of ligands to their residence time [101].

These previously published results represent a very promising starting point for further development of this field of research.

10

1.3 Fluorescence, description of fluorophores used and fluorescence - based techniques

1.3.1 Fluorescent proteins developed from GFP and other fluorescent molecules for protein labeling

The term fluorescence evolved from fluorspar where this phenomenon was observed and first termed [102]. Fluorescence itself was first reported by F.W. Herschel [103]. To be fluorescent a molecule has to be rigid and needs to contain a system of conjugated free π-electrons.

Green fluorescent protein (GFP) of the jellyfish Aequorea victoria [104] was the starting point for many fluorescent proteins known today. The mutational analysis and further improvement of initial GFP [105] led to fluorescent proteins of a broad variety of colors in the range of visible light [106][107][108]. Therefore developed fluorescent proteins could be cloned into biogenic structures to elucidate biological processes in living organisms [109]. One example of a GFP derived fluorescent protein is the cyan fluorescent protein (CFP) which was further modified concerning quantum yield. This modification led to Enhanced CFP (ECFP) [107]. ECFP was used during this study but will be named CFP throughout the text. mTurquoise2, a further developed mutated form of ECFP [110] and Venus [111], a derivative of the yellow fluorescent protein (YFP), were also used within the scope of this work. The GFP based fluorophores have the advantage that they provide less photo-toxicity compared to other organic fluorophores [112] but one limitation of this powerful imaging technique is the size of fluorescent proteins which is about 250 amino acids, 30 kDa. This difficulty led to the invention of smaller fluorescent molecules to label proteins. One of these fluorophores invented is the small biarsenic fluorescent molecule named Fluorescein Arsenical Hairpin Binder, abbreviated FlAsH [113]. With 0.7 kDa, FlAsH is much smaller than GFP and its derivatives. The small molecule is bound to the protein of interest just before measurement within a labeling procedure and has an enhanced affinity for an amino acid sequence containing four neighboring cysteine residues (C) that are interrupted by two other amino acids (X) in the middle of the binding motif: CCXXCC [114]. The discontinuous tetracysteine binding motif CCPGCC was found to be most suitable for FlAsH binding [115] and is very unlikely to be present in native proteins. Therefore specific labeling should be possible [116]. For the FlAsH derivative Resorufin Arsenical Hair-

pin Binder (ReAsH) [115] it was shown that the small molecule binds very tightly to amino acids and thus follows the smallest movement of the receptor [117] which makes it likely that FlAsH behaves the same manner. The fluorophore properties of FlAsH and YFP are very similar concerning excitation and emission spectra so that experimental settings at the microscopes do not have to be changed. The smaller size of FlAsH compared to YFP contributes to the fact that FlAsH was found to influence receptor downstream signaling less than YFP in the $A_{2A}R$ [118]. Moreover CFP in combination with FlAsH caused bigger changes in FRET ratio compared to the CFP/YFP FRET pair [118] which could be due to different orientation of CFP and FlAsH compared to CFP and YFP. Despite the disadvantage that FlAsH undergoes faster photobleaching than YFP [118], it represents an attractive tool for monitoring protein movements and thus observation of GPCR movements upon ligand binding [119].

1.3.2 The principle of SNAP and CLIP

SNAP was first investigated and developed on base of the 20 kDa DNA repair enzyme O^6-alkylguanine-DNA alkyltransferase (AGT) [120]. SNAP has a specificity for O^6-benzylguanine-derivatives which can be linked to a fluorescent molecule. SNAP-substrates containing a fluorescent dye were used in the context of this work. SNAP has an approximately 50 times higher activity for O^6-benzylguanine-derivatives than naturally occurring AGT [121], thus labeling with SNAP is very specific [122][123]. During the labeling reaction the activated benzyl-group of the O^6-benzylguanine-derivative bearing the fluorophore is covalently linked to SNAP [120][122][123] and can be visualized via light of a wavelength within the range of emission maximum of the certain fluorophore used.

For CLIP, a further investigated variant of SNAP, the basal structure for development was also AGT [124]. Mutation of the former named SNAP tag in 8 positions led to a variation of AGT with an enhanced specificity regarding O^2-benzylcytosine-derivatives [124].

As SNAP and CLIP tag have different substrate specificity it is possible to express them together in the same cellular system, label them simultaneously and visualize two different biological structures, for example receptors, at the same time.

12

1.3.3 Fluorescence and Fluorescence Resonance Energy Transfer

When a fluorophore absorbs a photon it can be excited to a higher energetic level. In detail, the molecule is elevated from its ground singlet state S_0 to a higher energetic state S_1. The first molecules' energy decreases to the lowest vibrational energy level (ν) of S_1 without emission of photons. This loss of energy contributes to the fact that excitation of a fluorophore occurs with higher energetic light than emission of the same fluorophore and is called Stokes shift [125]. Relaxation from high- to low-energetic state can take place via emission of photons and is named luminescence. The Jablonski diagram [126] illustrates the various energy levels including their vibrational energy levels that can be occupied by a molecule. Figure 1.2 shows a simplified Jablonski diagram (modified from [127]). If relaxation occurs without the reversion of an electron-spin ongoing process is named fluorescence where relaxation process takes about 10^{-9} s. But there is also the possibility of inter system crossing that leads to reversion of electron-spin and thus transition of the molecule to the triplet state (T_1). From this state energy is released via phosphorescence.
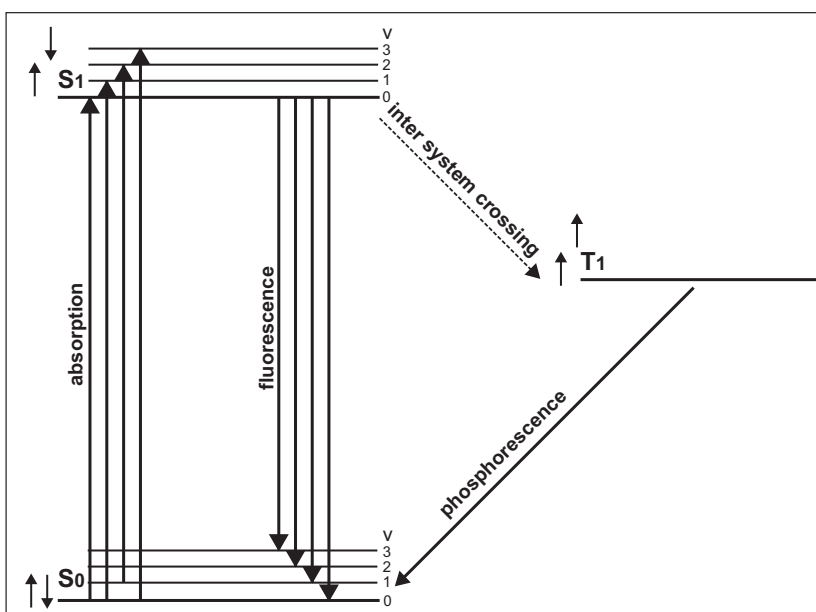
Figure 1.2: Simplified Jablonski diagram, modified from [127]. Principle of light-absorption of a chromophore and fluorescence, inter system crossing or phosphorescence as possibilities of relaxation from high-energy states starting and ending at various vibrational energy levels (ν 0-3)

The Förster Resonance Energy Transfer [128] is another opportunity for energy transfer from an excited molecule so that it can decrease its energy level. As the

method employed here is solely performed with fluorescent reaction partners the term *Fluorescence* Resonance Energy Transfer (FRET) will be used from now on. In this kind of energy transfer energy from a donor in an excited energetic state is released to an acceptor fluorophore without emission of a photon. Figure 1.3 shows the principle of FRET.
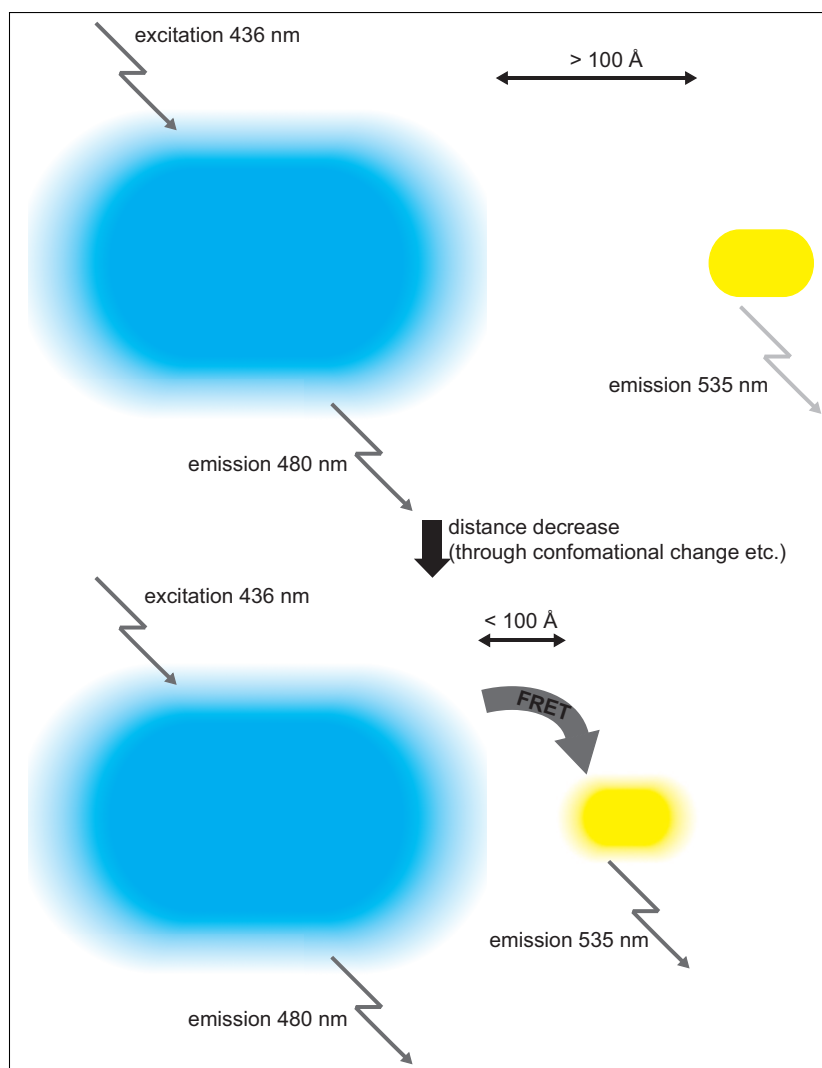
Figure 1.3: Principle of FRET

The energy donor itself is excited with light of a distinct wavelength in the range of its maximal excitation. Now the energy donor is elevated to a higher energetic state which can be visualized in the Jablonski diagram (see figure 1.2). Furthermore, the excited energy donor transfers energy to the acceptor fluorophore. There are some conditions for the occurrence of this non-radiative energy-transfer [129]. First,

emission spectrum of energy donor has to overlap at least 30 % with the excitation spectrum of acceptor [130]. Therefore, the most important step is the choice of fluorophores for the FRET pair. Overlap of the emission spectrum of the energy donor and the excitation spectrum of the energy acceptor leads to the occurrence of energy transfer. The energy donor has to provide a sufficient quantum yield and the two fluorophores have to be ordered in an appropriate angle so that the emission dipole and the absorption dipole are optimally in parallel to each other [131]. In order that FRET can occur the distance between both fluorophores has to be $\leq$ 100 Å [128].

Förster radius (R_0) is dependent of the FRET pair investigated and is usually between 3 to 6 nm [128]. It describes the distance between fluorophores where FRET efficiency (E), the energy transfer between donor and acceptor molecule of a FRET pair, is 50 %. FRET efficiency (E) is inversely proportional to the sixth power of the distance between donor and acceptor fluorophore (r) (equation 1.2) which clarifies the sensitivity and with this the usability of FRET for distance-dependent measurements:

$$E = \frac{1}{1 + (\frac{r}{R_0})^6} \tag{1.2}$$

The FRET pair FlAsH and CFP fulfills the previously described criteria. Figure 1.3 shows the principle of FRET with the two fluorophores CFP and FlAsH. CFP serves as energy donor and is excited with 436 nm and its emission is detected at 480 nm. Because the emission and excitation spectra of the two fluorophores are close to each other, FlAsH the energy acceptor, is additionally cross-excited to a small extent, but there is no energy transfer between the two fluorophores because the distance is $\geq$ 100 Å. When the distance between the two fluorophores is decreased and therefore $\leq$ 100 Å, the energy transfer between energy donor from its excited energy state and acceptor takes place and the emission of FlAsH can be monitored at 535 nm. Figure 1.4 shows excitation and emission spectra of all fluorophores used throughout this work.
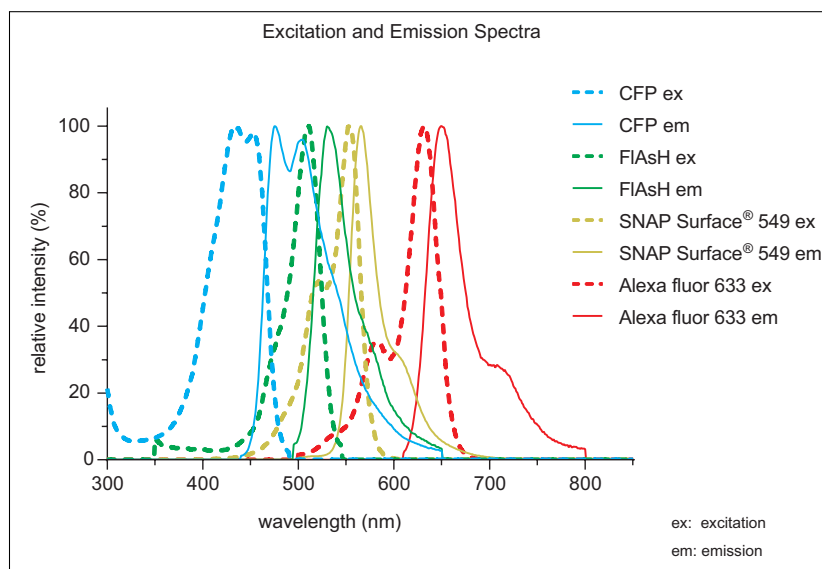
Figure 1.4: Excitation and emission spectra of all fluorophores applied

1.4 Fluorescence based approaches to monitor receptor dynamics and receptor ligand interactions

The most important method for many years for investigating the properties of ligands at GPCRs of interest were radioligand binding studies [132]. There are approaches to perform binding with radioactive labeled ligands in whole cells, but the major part of known drug properties is derived from the receptor ligand interaction that is derived from purified membranes containing the receptor of interest. However, during the last years some new methods were established that provided new insights into receptor ligand interaction with a different approach. One of these techniques invented were fluorescence tagged receptor sensors that avoid radioactivity and allow to do experiments in whole living cells expressing the receptor of interest. Thus conditions during experiments are more physiological as in cell lysates. FRET measurements in fluorescently tagged receptor sensors are a helpful technique to monitor the conformational changes of a receptor that occur when a ligand binds to it [133][134][135]. This approach enables the investigation of receptor dynamics in living cells [136][119][137]. A large range of intramolecular fluorescence based receptor biosensors that enabled the opportunity to perform FRET in GPCRs have

16

been developed during the last 10 to 15 years which allowed for a broad insight into dynamical receptor movements and revealed ligand binding properties for multiple receptors and ligands [138][118][139][140][141]. With these receptor sensors it became possible to investigate ligand concentration dependent response curves of various ligands at one receptor [140]. Comparison of these curves regarding ligand binding affinity and height of FRET signals is feasible when referring all measurements to a standard ligand. It was previously shown that partial agonists led to overall smaller and slower changes in FRET ratio when they were compared to full agonists at the particular receptor [142].

FRET sensors were not only established to elucidate receptor movements, there were also fluorescent G protein sensors developed that allowed to monitor G protein activation regarding a distinct receptor upon ligand binding. When a receptor is activated it causes a conformational change at the G protein which results in an exchange of GDP to GTP bound to the G_α subunit. This causes a dissociation of the $G_{\alpha\beta\gamma}$ trimer into an activated G_α and $G_{\beta\gamma}$ subunit which can mediate further cellular signals until the catalytic site of the G protein α subunit catalyzes GTP to GDP again which leads to a reassembly and thus inactivation of the $G_{\alpha\beta\gamma}$ trimer [143][144]. A successful approach that was previously invented enabled the measurement of FRET at a G_s protein in living cells of the D. discoideum amoebae between a CFP tagged G_α and and a YFP tagged $G_{\beta\gamma}$ subunit upon cAMP stimulation of cells [145]. Further investigation led to a G_i protein FRET sensor that brought insight into G protein signaling in mammalian cells with the help of YFP tagged G_α and and a CFP tagged $G_{\beta\gamma}$ subunit. Thus, it became possible to measure protein activation within millisecond resolution [146]. Further development of such G protein sensors led to a G_q FRET sensor containing the protein of interest including a CFP tagged G_α and a YFP tagged $G_{\beta\gamma}$ subunit in one plasmid which increased the usability of the FRET sensor due to quantitative co-expression of G protein subunits [147]. This newly developed G_q FRET sensor was the starting point for the development of a fluorescent G_i FRET sensor that includes a mTurquoise2 tagged G_α and and a Venus tagged $G_{\beta\gamma}$ subunit in one plasmid (not published yet). This G_i FRET sensor was a kind gift of Dr. J. Goedhart and was employed within the scope of this work.

All methods discussed so far in this section monitor the movement of the receptor or G protein formation resulting from ligand binding. A distinct research approach invented during the past years is the development of fluorophore tagged ligands.

17

The first receptor ligands attached to a fluorophore were invented about 40 years ago [148]. Fluorophore tagged ligands exhibit the advantage that they allow radioactive free receptor characterization regarding ligand binding affinities that can be examined in living organisms or whole tissue. But the fluorophore itself and the sometimes used linker that attaches a fluorophore and a ligand can influence the properties of the ligand [149][150][151]. Nevertheless, it immediately became clear that fluorophore tagged ligands in combination with confocal microscopy represent a powerful tool to elucidate receptor ligand interactions [149]. As they enable the direct observation of receptor ligand interaction fluorescent ligands are suitable for kinetic measurements and visual conformation of receptor localization [131]. Fluorescent antagonists can be utilized to monitor receptor distribution in cells and fluorescent agonists can additionally help to elucidate receptor internalization [152]. FRET between a SNAP tagged receptor and a fluorescent ligand was previously successful examined [99].

In case of the adenosine receptor family a lot of fluorescent ligands were developed during the past years [153][152]. The first fluorescent ligands for this receptor family were investigated in 1987 [154] and were the starting point for further developments. A very promising approach was the confocal visualization of the co-localization of the fluorescence tagged A_1R and fluorescence tagged agonists based on adenosine derivatives [155]. For the A_3R a competition binding assay with fluorescent ligands was invented which was performed with help of a high content automated optical detection system where ligand affinities could be directly correlated to fluorescence intensity in cells [156]. Ligand binding behavior of the $A_{2A}R$ was previously investigated either with a C-terminally CFP tagged receptor where internalization behavior of the $A_{2A}R$ could be monitored over time [157] or with a N-terminally CFP tagged $A_{2A}R$ that was exposed to a fluorescent ligand [158]. Here the association of the fluorescent ligand could be examined and compared to the absence of receptor when a non-fluorescent $A_{2A}R$ antagonist was present, allowing the performance of a competitive binding assay. Fluorescent ligands represent a powerful tool for the investigation of receptor ligand interactions and could replace radioligand binding studies in the future or reveal even more information about GPCR behavior upon ligand binding.

In general fluorescent molecules attached to receptors or to ligands have developed to be valuable tools for visualizing receptors and their dynamical and spatial behavior and will be a further emergent research area in the future.

2 Motivation

Adenosine receptors mediate numerous effects in the human body which makes these receptors valuable targets for drugs. But until now, structural knowledge of adenosine receptors is limited.

One powerful tool for gaining more insight into receptor function in living cells is the approach with intramolecular FRET receptor sensors. This technique was investigated about 10 years ago and enables to elucidate differences in receptor dynamical movements regarding different ligands or different receptor subtypes of a receptor family. Within this work the FRET pair CFP and FlAsH should help to examine differences between two members of the adenosine receptor family, namely the A_1R and the $A_{2A}R$. The fluorescent $A_{2A}R$ sensor was previously investigated and an A_1R sensor should be developed in this work. The A_1R sensor should, like the $A_{2A}R$ sensor, be C-terminally tagged with the energy donor CFP and the binding motif of the energy acceptor molecule FlAsH should be placed in the third intracellular receptor loop. Within the scope of FRET experiments dynamical differences between the two adenosine receptor subtypes should be investigated with the application of different ligands with distinct affinities regarding A_1R and $A_{2A}R$.

In the past both receptors were mainly characterized via radioligand binding studies and detailed structural knowledge for the $A_{2A}R$ became available with numerous crystal structures published during the last years. These approaches revealed amino acids that are important in the ligand binding process. Therefore it would be of great interest to see if the previously mentioned A_1R FRET sensor was able to show the influence of these particular amino acids regarding receptor dynamical movements upon ligand binding. Thus amino acids should be transferred from $A_{2A}R$ to A_1R sequence and investigated via mutational analysis.

This approach should bring more insight into receptor dynamic movements of A_1R as well as $A_{2A}R$ with the help of fluorescence tagged receptors via confocal analysis and FRET experiments.

3 Material and methods

3.1 Material

3.1.1 cDNA

human adenosine A_1 receptor (GenBank entry BC026340)
human adenosine A_{2A} receptor (GenBank entry P29274)

3.1.2 DNA

Primers for construct cloning (MWG Biotech GmbH, Ebersberg, Germany)
All sequencing of DNA was done by Eurofin (Eurofin Genomics, Ebersberg, Germany)

All receptors used are human receptors

A_1 FlAsH3 CFP in pcDNA3 (This work; Zabel U.)
A_1 FlAsH3 CFP I69V in pcDNA3 (This work; Zabel U.)
A_1 FlAsH3 CFP L88A in pcDNA3 (This work; Zabel U.)
A_1 FlAsH3 CFP T91A in pcDNA3 (This work; Zabel U.)
A_1 FlAsH3 CFP W247A in pcDNA3 (This work; Zabel U.)
A_1 FlAsH3 CFP H251A in pcDNA3 (This work; Zabel U.)
A_1 FlAsH3 CFP N254A in pcDNA3 (This work; Zabel U.)
A_1 FlAsH3 CFP H264A in pcDNA3 (This work; Zabel U.)
A_1 FlAsH3 CFP T277A in pcDNA3 (This work; Zabel U.)
A_1 FlAsH3 CFP T277S in pcDNA3 (This work; Zabel U.)
A_1 in pcDNA3 (This work; Zabel U.)
A_1 W247A in pcDNA3 (This work; Zabel U.)
A_1 H251A in pcDNA3 (This work; Zabel U.)

CLIP A_1 in pcDNA3 (This work; Zabel U., Stumpf A.D.)

SNAP A_1 in pcDNA3 (This work; Zabel U., Stumpf A.D.)

Flag CLIP A_1 in pcDNA3 (This work; Zabel U., Stumpf A.D.)

Flag SNAP A_1 in pcDNA3 (This work; Zabel U., Stumpf A.D.)

SNAP A_1 FlAsH3 CFP in pcDNA3 (This work; Zabel U.)

A_{2A} FlAsH3 CFP in pcDNA3 (Hoffmann C.)

Flag CLIP A_{2A} in pcDNA3 (This work; Zabel U., Stumpf A.D.)

Flag SNAP A_{2A} in pcDNA3 (This work; Zabel U., Stumpf A.D.)

SNAP A_{2A} FlAsH3 CFP in pcDNA3 (This work; Zabel U.)

pGβ-2A-YFP-Gγ2-IRES-Gαi1-mTq2 in pEGFP-C1 (Goedhart J.)

Deoxynucleotides (dNTPs) (New England Biolabs, Frankfurt am Main, Germany)

3.1.3 Cell lines

HEK 293

HEK 293 CLIP A_1 (This work)

HEK 293 A_1 FlAsH3 CFP (This work)

HEK 293 A_1 FlAsH3 CFP I69V (This work)

HEK 293 A_1 FlAsH3 CFP L88A (This work)

HEK 293 A_1 FlAsH3 CFP T91A (This work)

HEK 293 A_1 FlAsH3 CFP W247A(This work)

HEK 293 A_1 FlAsH3 CFP H251A (This work)

HEK 293 A_1 FlAsH3 CFP N254A (This work)

HEK 293 A_1 FlAsH3 CFP H264A (This work)

HEK 293 A_1 FlAsH3 CFP T277A (This work)

HEK 293 A_1 FlAsH3 CFP T277S (This work)

HEK 293 SNAP A_1 (This work)

HEK 293 SNAP A_1 FlAsH3 CFP (This work)

HEK 293 CLIP A_{2A} (This work)

HEK 293 A_{2A} FlAsH3 CFP (Hoffmann C.)

HEK 293 SNAP A$_{2A}$ (This work)

HEK 293 SNAP A$_{2A}$ FlAsH3 CFP (This work)

3.1.4 Fluorescent proteins and dyes

CFP (ECFP from BD Bioscience Clontech, Heidelberg, Germany)

CLIP-Cell^{TM} TMR Star (New England Biolabs, Frankfurt am Main, Germany)

CLIP-Surface^{TM} 547 (New England Biolabs, Frankfurt am Main, Germany)

CLIP-Surface^{TM} 647 (New England Biolabs, Frankfurt am Main, Germany)

SNAP-Cell$^{®}$ TMR Star (New England Biolabs, Frankfurt am Main, Germany)

SNAP-Surface$^{®}$ 549 (New England Biolabs, Frankfurt am Main, Germany)

SNAP-Surface$^{®}$ 647 (New England Biolabs, Frankfurt am Main, Germany)

3.1.5 Enzymes

Creatine kinase was purchased from Roche Diagnostics, Mannheim, Germany. If not stated otherwise all other polymerases, ligases and restriction enzymes used, including their appropriate buffers, DNA-dyes and DNA-ladders were purchased from New England Biolabs, Frankfurt am Main, Germany.

3.1.6 Bacteria

E. coli DH5 α (Invitrogen, Darmstadt, Germany)

3.1.7 Plasmids

pcDNA3 vector (Invitrogen, Karlsruhe, Germany)

pcDNA3.1 vector (Invitrogen, Karlsruhe, Germany)

Both plasmids carry the resistance gen for ampicillin which is necessary for clonal selection.

3.1.8 Chemicals

All chemicals used had the purity level pro analysi (p.a.) or higher.

A3-633-AN (Kind gift of Hill S.J.)

A-633-AG (Kind gift of Hill S.J.)

Adenosine (Sigma-Aldrich, Taufkirchen, Germany)

Adenosine Deaminase (ADA), emulsion with ammonium sulfate (Roche Diagnostics, Mannheim, Germany)

Adenosine Desaminase (ADA), glycerol-solution (Roche Diagnostics, Mannheim, Germany)

Agar (Applichem, Darmstadt, Germany)

Aluminumoxide (Sigma-Aldrich, Taufkirchen, Germany)

Ampicillin-Na (Sigma-Aldrich, Taufkirchen, Germany)

ATP (Sigma-Aldrich, Taufkirchen, Germany)

BAL (Fluka- Sigma-Aldrich, Taufkirchen, Germany)

BSA (New England Biolabs, Frankfurt am Main, Germany)

$CaCl_2$ (Applichem, Darmstadt, Germany)

cAMP (Sigma-Aldrich, Taufkirchen, Germany)

CCPA (Tocris, via R&D Systems, Wiesbaden-Nordenstadt, Germany)

CPA (Tocris, via R&D Systems, Wiesbaden-Nordenstadt, Germany)

CLIP-tag (New England Biolabs, Frankfurt am Main, Germany)

DMSO (BioChemica/ Applichem, Darmstadt, Germany)

Dowex®-1X2 Chloride form 2-200 mesh (Sigma-Aldrich, Taufkirchen, Germany)

EDT (Fluka- Sigma-Aldrich, Taufkirchen, Germany)

EDTA (Applichem, Darmstadt, Germany)

EHNA∗HCl (Tocris, via R&D Systems, Wiesbaden-Nordenstadt, Germany)

Ethidiumbromide (Applichem, Darmstadt, Germany)

Ethanol (Roth, Karlsruhe, Germany)

FlAsH (Dr. E. Heller, Universitiy of Würzburg)

Forskolin (Tocris, via R&D Systems, Wiesbaden-Nordenstadt, Germany)

G418 (Geneticin Sulphate) (Gibco Life Technologies Eggenstein, Germany)

Glucose, anhydrous (Applichem, Darmstadt, Germany)

GTP (Sigma-Aldrich, Taufkirchen, Germany)

[^{3}H] CCPA (PerkinElmer GmbH, Rodgau, Germany)

[^{3}H] NECA (Hartmann Analytic GmbH, Braunschweig, Germany)

HEPES (Applichem, Darmstadt, Germany)

H_2O_2, 30 % (Applichem, Darmstadt, Germany)

Immersion oil for microscopy (Applichem, Darmstadt, Germany)

Isopropanol (Sigma-Aldrich, Taufkirchen, Germany)

KCl (Applichem, Darmstadt, Germany)

KH_2PO_4 (Applichem, Darmstadt, Germany)

L-Glutamine 200 mM (Sigma-Aldrich, Taufkirchen, Germany)

Loading dye blue, 6x (New England Biolabs, Frankfurt am Main, Germany)

Methanol (Sigma-Aldrich, Taufkirchen, Germany)

$MgCl_2*6H_2O$ (Applichem, Darmstadt, Germany)

Midori green advance (Intas, Göttingen, Germany)

NaCl (Applichem, Darmstadt, Germany)

Na_2CO_3 (Merck Millipore, Darmstadt, Germany)

Na_2HPO_4 (Applichem, Darmstadt, Germany)

NaOH (Applichem, Darmstadt, Germany)

NECA (Tocris, via R&D Systems, Wiesbaden-Nordenstadt, Germany)

^{32}P α-ATP (Hartmann Analytic GmbH, Braunschweig, Germany)

Penicillin G 10000 U/ml, Streptomycin sulfate 10 mg/ml (Sigma-Aldrich, Taufkirchen, Germany)

Pepton from casein (Applichem, Darmstadt, Germany)

Phosphocreatine (Roche Diagnostics, Mannheim, Germany)

Poly-D-Lysine hydrobromate (MP Biomedicals, Eschwege, Germany

PEG 3000 (Applichem, Darmstadt, Germany)

RO-20-1724 (Sigma-Aldrich, Taufkirchen, Germany)

R-PIA (Sigma-Aldrich, Taufkirchen, Germany)

SNAP-tag (New England Biolabs, Frankfurt am Main, Germany)

SDS Sodium dodecyl sulfate (Applichem, Darmstadt, Germany)

Theophylline (Sigma-Aldrich, Taufkirchen, Germany)

TRIS-acetate (Applichem, Darmstadt, Germany)

TRIS*HCl (Applichem, Darmstadt, Germany)

Tryptone (Applichem, Darmstadt, Germany)

Universalagarose (Peqlab, Erlangen, Germany)

Yeast-extract (Applichem, Darmstadt, Germany)

$ZnAc_2$ (Merck Millipore, Darmstadt, Germany)

Structural formula of the ligands that were used throughout this work are listed in the chapter ligand-structures.

3.1.9 Reagents for cell culture

3.1.9.1 Eucariotic cell culture

DMEM+++: Dulbecco's modified eagle medium with 4.5 g/l glucose (PAN-Biotech Aidenbach, Germany) containing 2 mM L-Glutamine, 0.1 U/l Penicillin G, 0.1 g/l Streptomycin sulfate (both Sigma-Aldrich, Taufkirchen, Germany) and 10 % FCS (Biochrom AG, Berlin, Germany), for HEK 293 cells.

DMEM+++ +0.2 g/l G418: Dulbecco's modified eagle medium with 4.5 g/l glucose containing 2 mM L-Glutamine, 0.1 U/l, Penicillin G, 0.1 g/l Streptomycin sulfate, 10 % FCS and 0.2 g/l G418 as medium for HEK cells stably expressing a plasmid containing a receptor of interest.

DMEM+++ +0.8 g/l G418: Dulbecco's modified eagle medium with 4.5 g/l glucose containing 2 mM L-Glutamine, 0.1 U/l Penicillin G, 0.1 g/l Streptomycin sulfate, 10 % FCS, 0.8 g/l G418 sulfate as selection medium for HEK cells stably expressing a plasmid containing a receptor of interest.

DMEM cell freezing medium: Dulbecco's modified eagle medium with 4.5 g/l glucose containing 2 mM L-Glutamine, 0.1 U/l Penicillin G, 0.1 g/l Streptomycin sulfate, 10 % FCS and 10 % DMSO as freezing medium for HEK 293 cells and HEK 293 cells stably expressing a plasmid containing a receptor of interest.

DPBS (Dulbecco's phosphate buffered saline) (Sigma-Aldrich, Taufkirchen, Germany)
Poly-D-Lysine hydrobromate (MP Biomedicals, Eschwege, Germany) (Solution 1 mg/ml was used)
Trypsine-EDTA Solution 1x (PAN-Biotech Aidenbach, Germany)

3.1.9.2 Procaryotic cell culture

LB-Medium (containing 16 g/l Pepton, 10 g/l Yeast and 5 g/l NaCl)
LB-Medium with Ampicillin (0.08 g/l)
LB-Medium with Agar (8 g/l) for preparation of dishes for bacteria cultivation

3.1.10 Kits

DNA Gel extraction Kit (Merck Millipore, Darmstadt, Germany)
Effectene transfection kit (Qiagen, Hilden, Germany)
Nucleobond Xtra Midi (Macherey and Nagel, Düren, Germany)
Quiagen Plasmid Midi Kit (Qiagen, Hilden, Germany)
Quiagen Plasmid Plus Midi Kit (Qiagen, Hilden, Germany)

3.1.11 Buffers and reagent mixes for assays

Bio-Rad Protein Assay (Bio-Rad, München, Germany)
5/2 Buffer, pH 7.4: 5mM TRIS$*$HCl and 2 mM EDTA
KCM Buffer: 100 mM KCl, 30 mM $CaCl_2$, 50 mM $MgCl_2$
Labeling buffer, pH 7.4: HBSS supplemented with 1 g/l glucose
Measuring buffer, pH 7.3: 2 mM $CaCl_2$, 5.4 mM KCl, 1 mM $MgCl_2$, 140 mM NaCl, 10 mM HEPES
REA-Mix 5x: 0.5 mM cAMP, 1% BSA, 50 μM GTP, 0.5 mM ATP, 5 mM $MgCl_2*6$ H_2O, 750 mM NaCl, 250 mM TRIS$*$HCl pH 7.4, 2.5 mM RO-20-1724
REA-Mix 2x (for 1ml): 400 μl REA-Mix 5x, 5.9 mg Phosphocreatine, 0.8 mg Creatine kinase, ^{32}P α-ATP 4 000 000 (200 000 counts per probe), H_2O ad 1 ml.
TAE Buffer: 40 mM TRIS acetate, 1 mM EDTA
Taq-Polymerase PCR Buffer, 10x (Invitrogen, Darmstadt, Germany)
TM10-Buffer, pH 7.4: 50 mM TRIS$*$HCl, 10 mM $MgCl_2$
TRIS Buffer, 50mM, pH 7.4: 50 mM TRIS$*$HCl
TRIS Buffer, 100 mM, pH 7.4: 100 mM TRIS$*$HCl
TSB: 10 % PEG 3000, 5 % DMSO and 20 mM $CaCl_2$ in LB-Medium

3.1.12 Expendable materials and other subjects used

"Attofluor" Cell chamber (Molecular Probes, Leiden, the Netherlands)

Cell culture dishes (Nunc Fisher Scientific, Schwerte, Germany)

Cell scraper (Hartenstein Laborbedarf GmbH, Würzburg, Germany)

Coverslips 24 mm (Hartenstein Laborbedarf GmbH, Würzburg, Germany)

Cryo-Tubes (Nunc Fisher Scientific, Schwerte, Germany)

Cuvettes, 2x optical, layer thickness 10 mm, Polystyrene (Sarstedt AG & Co., Nümbrecht, Germany)

Falcon tubes (BD Biosciences, Heidelberg, Germany)

Multiwellplates (Nunc Fisher Scientific, Schwerte and Sarstedt, Nümbrecht, Germany)

Pipet-tips (Eppendorf, Hamburg, Germany)

Poly-Prep Chromatography Columns (0.8 x 4 cm) (Bio-Rad, California, USA)

Tubes (Eppendorf, Hamburg, Germany)

96 well glass fiber filter plates (Multiscreen FC 1.2 μm glass fiber Typ C filter, Millipore, Darmstadt, Germany)

3.1.13 Microscopes

Axiovert 200 inverse microscope (Zeiss, Jena, Germany)

Leica TCS SP5 confocal microscope (Leica, Wetzlar, Germany)

Leica TCS SP8 confocal microscope (Leica, Wetzlar, Germany)

3.1.14 Software

Adobe CS 6 (Adobe Systems, California, USA)

Axon Scope 10.3 (Molecular Devices, Sunnyvale, USA)

Graph pad Prism 6 (Graphpad, California, USA)

Leica LAS AF (Leica, Wetzlar, Germany)

Origin 9.1 (Origin labs, Northampton, USA)

3.2 Methods

3.2.1 Cell culture

All working steps with cells were done under sterile conditions at a laminar air flow hood. HEK 293 cells [159] were maintained in appropriate media at 37 °C and 7 % CO_2. HEK 293 cells stably expressing a receptor were cultivated in medium for cells that stably express a receptor of interest which was described above.

Cells were split when they were 70 % confluent. Medium was aspirated, the dishes and cells were washed with 2 ml DPBS per 100 mm dish then DPBS was aspirated, too. Now cells were washed over with 1 ml trypsine-EDTA and detached from the dish by gently tapping against the bottom of the dish after the trypsine-EDTA supernatant was aspirated. Detached cells were now suspended in an appropriate amount of suitable cell culture medium and the appropriate amount of cell suspension was pipetted to a new 100 mm dish containing 10 ml of fresh cell culture medium.

3.2.1.1 Preparation of cells for microscopic analysis

For microscopic analysis single 24 mm cover-slips were placed in 6 well plates and coated with 200 μl Poly-D-Lysine hydrobromate 1 mg/ml per well. After incubation for at least 20 min at 37 °C and 7 % CO_2, Poly-D-Lysine hydrobromate was aspirated and cover-slips were washed with 1 ml DBPS. Cells were seeded on cover-slips in appropriate medium in a density that they reached 50 % confluence until experiments were carried out.

3.2.1.2 Freezing cells

Cells were frozen for intermediate storage at -80 °C or long-term storage in liquid nitrogen. Cells were grown on cell culture dishes in the appropriate cell culture medium as described in the section before. When cells were 70 % confluent, cell culture medium was aspirated from the dishes and dishes were washed with DPBS and detached with help of trypsine-EDTA-solution 1x. After that cells were suspended in DMEM cell freezing medium and aliquoted in Cryo-tubes which were stored at -20 °C for at least 3 h before they were stored at -80 °C or liquid nitrogen.

3.2.1.3 Thawing cells

Cells that were stored at liquid nitrogen or at -80 °C were thawed at room temperature. 1 ml of gently homogenized cell suspension was transferred to a 100 mm cell culture dish containing 10 ml DMEM+++. After 3 h of incubation at 37 °C and 7 % CO_2 cell culture medium was changed to avoid toxic effects of DMSO on the cells coming from DMEM cell freezing medium.

3.2.1.4 Mycoplasm test for eucaryotic cell lines

Possible contamination of cells with mycoplasms was routinely tested with PCR [160]. 100 μl of cell culture medium supernatant of the appropriate cells and 100 μl of a positive-control cell culture medium supernatant were heated for 5 min at 95 °C, tubes were centrifuged afterwards (1 min, 13000 rpm, RT) and 2 μl of supernatant were taken as PCR-template for the PCR-Mix:

Taq-Polymerase PCR Buffer, 10x	2.5 μl
dNTPs (2 mM)	2.5 μl
$MgCl_2$ (50 mM)	1.0 μl
Primer GPO (50 pM)	0.25 μl
Primer MGSO (50 pM)	0.25 μl
Taq-Polymerase	0.25 μl
H_2O	18.3 μl

GPO-Primer: 5' actcctacgggaggcagcagt 3' (MWG Biotech GmbH, Ebersberg, Germany)
MGSO-Primer: 5' tgcaccatctgtcactctgttaacctc 3'(MWG Biotech GmbH, Ebersberg, Germany)

Polymerase chain reaction was now carried out following an appropriate protocol:

1. 95 °C   5 min
2. 95 °C   20 s
3. 60 °C   30 s
4. 72 °C   1 min
5. 72 °C   5 min
6. 4 °C ∞

Step 2.-4. of the PCR protocol were repeated 30 times. After finishing the PCR protocol, 3 μl DNA-Loading Dye Blue were added to each sample and gel electrophoresis with a gel containing 1 % agarose and $6*10^{-6}$ % Midori green advance was carried out as described in the appropriate section.

3.2.1.5 Transfection of HEK 293 cells

As the only adenosine receptor that HEK 293 cells express endogenously is the A_{2B} receptor [161] they were used as the host cell system for the receptor sensors developed and used in the context of this work.

Effectene transfection kit from Quiagen was used for transfecting HEK 293 cells. 24 h before transfection cells were seeded on cover-slips in six wells as described in the former section. Transfection was done when cells were 50 % confluent. The following amounts were used for one well. 0.17 μg of appropriate receptor sensor and if needed for experiments 0.5 μg of the G_i FRET sensor, 50 μl TE buffer and 3.2 μl Enhancer were mixed in a tube an incubated at room temperature for 5 min. After that, 7 μl Effectene were added to the tube and mixed sample was incubated for 20 min at room temperature. Now 100 μl DMEM+++ were pipetted to transfection-mix and the whole solution was added to the well containing HEK 293 cells in freshly appended DMEM+++. Cells were grown at 37 °C and 7 % CO_2. 24 h after transfection medium was replaced and cells were incubated for 24 h more until experiments were carried out.

Transfection of HEK 293 cells in a way that they express the receptor of interest permanently was also carried out with Effectene transfection kit from Quiagen. 24 h before transfection cells were seeded on 100 mm cell culture dishes. Transfection was done when cells were 50 % confluent. As a control one dish containing only HEK 293 cells was always treated the same way as the transfected cells. HEK 293 cells were transfected with the following protocol:

3 μg of appropriate receptor sensor were pipetted in 300 μl EC buffer and 16 μl enhancer were added. After 5 min incubation at room temperature 35 μl Effectene were added and 10 min after that 500 μl DMEM+++ were added to the tube including the transfection mixture. This complete mixture was pipetted on the dish. After 24 h, for selection of stably transfected cells, medium was changed and cells were exposed to DMEM+++ +0.8 mg/l G418.

Cells were microscopically examined every day and medium was changed every day. When there were individual cell colonies visible and no more cells were dying, the

medium was completely removed and the individual colonies were picked with a pipette. Each individual colony was suspended in a well of a 24 well plate with DMEM+++ +0.2 g/l G418. When the single clones were grown in the 24 well plates they were suspended in DMEM+++ +G418 +0.2 g/l and seeded on six well plates. After that they were seeded on cover-slips for confocal analysis.

The colonies remaining on the dish were suspended in 10 ml DMEM+++ +0.2 g/l G418 and placed onto a new dish. This dish contained the cells that expressed the plasmid of interest heterogeneously. When the cells on the dish were 70 % confluent they were seeded on cover-slips like described in the previous section and analyzed with help of a confocal microscope.

3.2.2 Labeling of living cells

3.2.2.1 FlAsH labeling

Figure 3.1 shows the principle of the FlAsH labeling procedure.

FlAsH labeling was performed similar to the method previously published [162]. Briefly, HEK 293 cells stably or transiently expressing the fluorescent receptor sensor of interest were washed with labeling buffer two times. After addition of labeling buffer containing 12.5 μM EDT and 0.5 μM FlAsH cells were incubated for 60 min at 37 °C and 7 % CO_2. Then cells were washed twice with labeling buffer, labeling buffer supplemented with 250 μM EDT was added and cells were again incubated for 10 min at 37 °C and 7 % CO_2. Once again cells were washed twice with labeling buffer and fresh DMEM+++ was added to cells. Cells were incubated at 37°C and 7 % CO_2 until experiments were carried out.
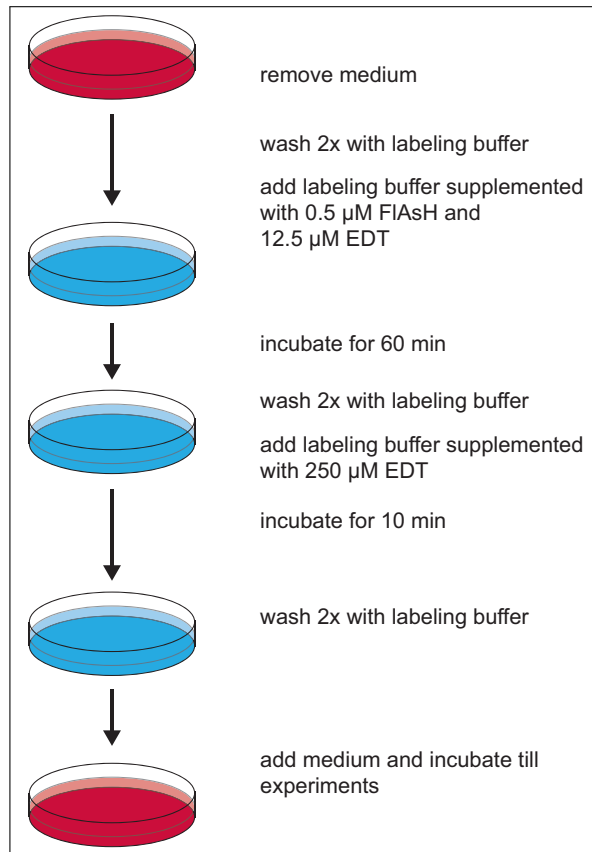
Figure 3.1: Schematic depiction of FlAsH labeling Procedure

3.2.2.2 SNAP and CLIP labeling

Figure 3.2 shows the principle of SNAP and CLIP labeling procedure. HEK 293 cells expressing the receptor sensor of interest that was N-terminally tagged with either SNAP- or CLIP-tag were washed with DMEM+++ and supplemented with DMEM+++ containing 0.5 μM of a benzyl-guanine-linked dye for SNAP-tagged receptors or a benzyl-cytosine-linked dye for CLIP-tagged receptors. Cells were incubated at 37 °C and 7 % CO_2 for 30 min if they expressed SNAP-tagged receptors or for 60 min if they expressed CLIP-tagged receptors. After the particular incubation time cells were washed twice with DMEM+++ and retained in fresh DMEM+++ at 37 °C and 7 % CO_2 until experiments were carried out. As a control non-transfected HEK 293 cells were labeled the same way each time to show that there was no unspecific binding of SNAP and CLIP dyes.
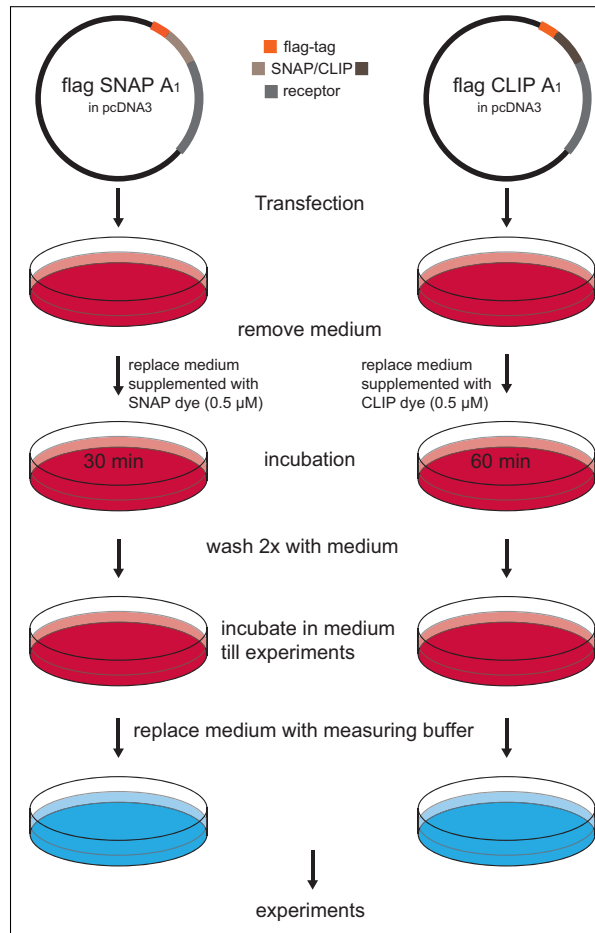
Figure 3.2: Schematic depiction of SNAP- and CLIP labeling procedure using the example of flag SNAP A_1 and flag CLIP A_1 receptor sensor

3.2.3 FRET measurement

FRET experiments were carried out with HEK 293 cells expressing the construct of interest either stable or transient and labeled with FlAsH if needed, experiments were carried out like previously described [118][138]. For experiments cells were seeded on cover-slips as described in the earlier section. Cells containing an adenosine receptor were incubated with ADA-emulsion concentrated 1 U/ml for 1 h before FRET measurement to compare these so treated cells to non-treated cells for testing the influence of endogenous released adenosine from HEK 293 cells. To examine the effects of endogenous released adenosine from HEK 293 cells furthermore, they were supplemented with measuring buffer containing 2 U/ml ADA-emulsion.

Cell-containing cover-slips were placed on an inverted microscope (Zeiss Axiovert 200) with help of an "Attofluor" cell chamber. Cells were supplemented with mea-

suring buffer during experiments and investigated with help of a 63x oil immersion objective.

CFP or mTurquoise2 as donor fluorophores were excited with 436 nm (436 +/- 10 nm with a dichroic long-pass beam splitter (DCLP) 460 nm). Light source was a polychrome IV (TILL photonics, Gräfelfing, Germany). Illumination of samples was set at 40 out of 100 ms to reduce photobleaching of fluorophores. Emission of energy donor (CFP or mTurquoise2) and acceptor (FlAsH or Venus) was detected using a dual emission photometric system from TILL photonics. Donor signal was detected at 480 +/- 20 nm (F_{480}) and acceptor signal was detected at 535 +/- 15 nm (F_{535}) (beam splitter DCLP 505 nm) with a frequency of 10 Hz.

For further corrections emission of direct excitation of energy donor at 490 nm was determined for each experiment. The emission ratio was additionally corrected by the spill-over of CFP into the 535 nm channel (spill-over of FlAsH into the 480 nm channel was negligible) to give a corrected FRET ratio F^*_{ratio}:

$$F^*_{ratio} = \frac{F^*_{535}}{F^*_{480}} \tag{3.1}$$

During experiment cells were constantly superfused with measuring buffer if they were not superfused with agonist or antagonist diluted in measuring buffer. This was done with help of a computer assisted solenoid valve-controlled pressurized perfusion system (ALA-VM8 from ALA scientific Instruments, Farmingdale, USA). Detected signals were digitized with help of an analog/digital converter (Axon Digidata 1440A from Molecular Devices, Sunnyvale, USA) and recorded with Clampex 10.3 software (Molecular Devices). After each ligand exposure cells were superfused with measuring buffer until the signal reached baseline again.

3.2.3.1 FRET efficiency

Determination of FRET efficiency was previously described [118][163]. For determination of FRET efficiency FlAsH labeled HEK 293 cells expressing the receptor sensor of interest were seeded on cover-slips and the cover-slip bathed with measuring buffer was mounted to an inverted microscope like described in the section before. Instead of a ligand BAL was added manually so that its final concentration was 5 mM and FRET efficiency was calculated with the following equation:

$$FRET_{efficiency} = \frac{(CFP_{max} - CFP_{start})}{CFP_{start}} \tag{3.2}$$

3.2.4 Confocal microscopy

Confocal analysis were performed using a Leica TCS SP 5 or SP 8 confocal microscope. For confocal images cover-slips with the fluorescent probe of interest were placed on an inverted microscope on top of a 63x oil immersion objective with help of an "Attofluor" cell chamber. During experiments cells were maintained in measuring buffer. Fluorophores were excited with manufacturer's predefined settings. CFP was excited with a 442 nm laser line from a diode laser and FlAsH with a 514 nm Argon laser line. SNAP-surface® 549 and CLIP-surface® 547 were excited with the 561 nm line of a DPSS laser, whereas SNAP-surface® 647, CLIP-surface® 647 and the fluorescent ligands A3-633-AN and A-633-AG were excited with a 633 nm helium-neon laser line. CFP emission was detected with a hybrid-photo detector at a wavelength range from 460-505 nm and FlAsH emission was detected with a photo-multiplier at 525-600 nm. The red fluorescent ligands A3-633-AN and A-633-AG and SNAP-surface® 647 and CLIP-surface® 647 were detected with help of a photo-multiplier in a wavelength range of 676-754 nm. The green fluorescent dyes SNAP-surface® 549 and CLIP-surface® 547 were detected with help of a hybrid-photo detector within a range of 589-619 nm. Image size was kept constant at 512x512 pixel, images were recorded with line accumulation of 2 and frame average of 4. All other settings were kept constant for all experiments. For time series an image was recorded every 30 s over the appropriate period of time depending on the experiment. Time series were started with manual addition of ligand.

For reasons of visibility some of the confocal pictures were adapted concerning brightness and contrast using either Photo Shop CS 6 or Leica LAS AF lite 3.3 software. Quantitative analysis was only performed on original images.

3.2.5 Generation of competent bacteria

Competent bacteria were generated with help of E. coli DH5 α cells. 20 μl of competent bacteria were plated on 100 mm dishes containing 15 ml of solid LB-medium and were grown for 24 h at 37 °C. The so derived bacteria-colonies were transferred into 50 ml liquid LB-medium and shaken for another 24 h at 37 °C. The concentrated bacteria-suspension was now diluted in 250 ml LB-medium that was again shaken at 37 °C until optic density reached 0.5 (595 nm). Optic density was examined with help of the Nanodrop nanophotometer (Nanodrop 2000c, Peqlab, Erlangen, Germany) in a polystyrene cuvette. Bacteria were now separated from

LB-medium (10 min, 5000 rpm, 4 °C) and pellet was resuspended in 25 ml TSB. The bacteria suspension was now aliquoted, incubated on ice for 90 min, aliquots were then frozen in liquid N_2 and stored at -80 °C.

3.2.6 Purification, amplification and processing of plasmid DNA

3.2.6.1 Amplifying DNA

The first step of multiplying DNA was to transform the plasmid with help of competent bacteria. 100 μl of competent bacteria that were generated like described in the previous section were suspended in 100 μl KCM, 1 μg of Plasmid containing the DNA of interest was added and mixture was incubated on ice for 20 min. After additional incubation for 10 min at RT, 1 ml LB-medium was added and bacteria-suspension was mixed for 50 min at 37 °C. Bacteria-suspension was now centrifuged (5 min, 5000 rpm, RT) and resulting pellet was resuspended in 100 μl LB-medium and plated on 100 mm dishes containing 15 ml of solid LB-medium and the selective antibiotic of the plasmid of interest. After growing colonies for 24 h at 37 °C, they were separately picked and grown in liquid LB-medium. Further steps, depending on the protocol applied, followed.

Quiagen Plasmid Midi Kit
For Quiagen Plasmid Midi Kit colonies were shaken at 37 °C for 15 h in 250 ml LB-medium containing the selective antibiotic of the plasmid used, afterwards bacteria suspension was centrifuged (10 min, 5000 rpm, 4 °C) and supernatant was discarded. Bacteria-pellet was frozen at -20 °C when protocol was interrupted or pellet was immediately resuspended in 5 ml of buffer P1, 5 ml of lysis buffer P2 were added and suspension was incubated for 4 min at RT. After that 5 ml of neutralization buffer P3 were added, mixture was incubated on ice for 20 min and centrifuged (30 min, 20 000 rpm, 4 °C). Supernatant was completely pipetted on associated column containing an anion-exchanger resin which was washed with 5 ml of equilibration buffer before. Now column with the supernatant was washed twice with 5 ml washing buffer. Next, the plasmid was eluted from the column with help of 5 ml elution buffer. Plasmid was precipitated with 7.5 ml isopropanol. After this step, plasmid-containing solution was centrifuged (30 min, 4000 rpm, 4°C) and supernatant was discarded. As a second washing step, pellet was resuspended in 2 ml ethanol 70 % and centrifuged again (60 min, 4000 rpm, 4°C), supernatant was

discarded once more and dried pellet was diluted in 100 μl H$_2$O. After examining the concentration of DNA in the probe and adjusting it to 1 μg/μl via dilution with H$_2$O, plasmids were stored at -20 °C.

Quiagen Plasmid Plus Midi Kit

For this faster plasmid-preparation protocol compared to Quiagen Plasmid Midi Kit pre-cultures including one bacteria colony and 5 ml of LB-medium with the appropriate antibiotic were shaken for 8 h at 37 °C. After that bacteria-suspension was diluted with 30 ml of LB-medium including the appropriate antibiotic and shaken at 37 °C for 15 h. Afterwards bacteria-suspension was centrifuged (10 min, 5000 rpm, 4 °C) and supernatant was discarded. Pellet was resuspended in 4 ml of buffer P1, 4 ml of lysis buffer P2 were added and mixture was incubated for 4 min at RT. After that 4 ml of buffer S3 were added and lysate was immediately pipetted on appropriate columns containing anion-exchanger resin. Lysate was forced through column with help of a stamp after incubation for 10 min. 2 ml BB buffer were added to eluate and it was gently inverted six times. Eluate was now pipetted in the associated spin columns and aspirated with ~300 mbar. Now columns were washed with 700 μl ETR buffer, 700 μl PE buffer and were centrifuged (1 min, 10 000 rpm). After 1 min incubation time at RT the plasmid was eluted with 150 μl EB buffer during a second centrifugation step (1 min, 10 000 rpm).

After examining the concentration of plasmid in the probe and adjusting it to 1 μg/μl via dilution with H$_2$O, plasmids were stored at -20 °C.

Nucleobond Xtra Midi

For Nucleobond Xtra Midi Kit colonies were shaken at 37 °C for about 15 h in 200 ml LB-medium containing the selective antibiotic of the plasmid used, afterward optical density of bacteria suspension was examined at 600 nm (OD$_{600}$) to calculate the sufficient amount of bacteria-suspension with the following equation:

$$V(ml) = \frac{400}{OD_{600}} \tag{3.3}$$

Bacteria-suspension was centrifuged (10 min, 4500 rpm, 4 °C) and supernatant was discarded. Bacteria-pellet was resuspended in 8 ml of buffer RES+RNase A and lyzed with 8 ml of buffer LYS. Mixture was inverted 5 times and incubated for 5 min at RT. Solution was now pipetted on associated column containing an anion-

exchanger resin and a preceding filter that was washed with 12 ml of equilibration buffer before. Now analyte containing column was washed with 5 ml buffer EQU and filter in column was discarded. In the following washing step 8 ml buffer WASH were pipetted to column and DNA was eluted with 5 ml buffer ELU. Plasmid was precipitated with 3.5 ml isopropanol, centrifuged (30 min, 4500 rpm, 4 °C) and supernatant was discarded. Pellet was resuspended in 2 ml ethanol 70 % as a second precipitation step and centrifuged again (5 min, 4500 rpm, 4 °C), supernatant was discarded once more and desiccated pellet was diluted in 100 μl H_2O. After examining the concentration of plasmid in the probe and adjusting it to 1 μg/μl via dilution with H_2O, plasmids were stored at -20 °C.

3.2.6.2 Gel electrophoresis with agarose gels

Gel electrophoresis with agarose gels was used for separating and characterizing DNA. Gels were prepared with TAE-buffer $6*10^{-6}$ % Midori green advance and 1 % agarose. 1 kb DNA ladder was pipetted to gels for characterization of the DNA bands in the gel. Separation of DNA was done in an electrical field in TAE-buffer using a voltage of 80 V and an amperage of 60 mA. Time of run depended on how long it took the marker band to reach two-thirds of the gel. Then electric field was switched off and Midori green advance that has intercalated into DNA was excited using UV-light (365 nm). DNA-fragments and markers became visible at approximately 500 nm. Concentration and size of DNA fragments could be estimated with help of the 1 kb DNA ladder.

3.2.6.3 Purification of DNA from agarose gels

When DNA fragments were needed for further experiments they were identified with help of the 1 kb DNA ladder and cut out with a scalpel. DNA fragment purification was done with DNA Gel Extraction Kit from Millipore. The piece of gel containing the DNA of interest was given to the gel nebulizer that was on top of a sample filter cup which was in a vial. Vial was now centrifuged (10 min, 5000 g) and DNA fragment, solved in TAE-Buffer, was filtered into the vial. Now DNA was ready for use in following experiments.

3.2.6.4 Digestion of plasmids

To assure that the amplified plasmid was the plasmid containing the DNA of interest, or for preparation of a ligation with another DNA fragment, plasmid was digested with specific enzymes that should lead to specific fragments of the plasmid.

Usually the plasmid was digested with two enzymes. As a control original plasmid was also digested with these enzymes. The approach was done as follows:

DNA	1 μg
Enzyme-buffer	2 μl
10x BSA	2 μl
Enzyme A	1 μl
Enzyme B	1 μl
H$_2$O	13 μl

Mixture was now digested for 1 h at 37 °C and shaken with 300 rpm. After that DNA was supplemented with 3 μl DNA loading dye blue and pipetted into the gel-chambers of the 1 % agarose gel as described in the previous section.

3.2.6.5 Ligation of DNA fragments

Ligation of DNA-fragments was done at 16 °C over night in a total volume of 20 μl. Ligation mixture consisted of 3 ng DNA fragment of interest and 30 ng vector, both digested with appropriate enzymes before. 1 μl T4 DNA-ligase with 2 μl of corresponding buffer (10 x ligase-buffer) were used. Improvement of successful ligation was done via transformation of competent bacteria, purification of DNA from the resulting bacteria-colonies, preparation of DNA and digestion of DNA as it was described in the appropriate sections. After all these analyzing steps DNA sequence was analyzed (by MWG Biolabs) to fully confirm identity of the plasmid.

3.2.6.6 Examining the amount of DNA

Amount of DNA was examined with help of a UV/VIS-spectrophotometer (Nanodrop 2000c, Peqlab, Erlangen, Germany) where absorption of DNA was measured at 260 nm. Concentration of 1 μl DNA was measured by pipetting it on the measurement pedestal and concentration of DNA was adjusted at 1 μg/μl via dilution with H$_2$O.

3.2.6.7 Polymerase chain reaction

Polymerase chain reaction was used to amplify a DNA fragment of interest with the overlapping PCR-technique [160]. This was done with specific primers that had the complementary sequence of the sequence of interest, one forward-primer and one backward-primer. Both primers consisted of not more than 30 bases and had about the same melting temperature so that an equal annealing of both primers was possible. PCR mix was done using following conditions:

DNA fragment	100 ng
Forward-primer (20 μM)	2.5 μl
Backward-primer (20 μM)	2.5 μl
Polymerase buffer (10 x)	10 μl
dNTPs (10 mM)	2 μl
DNA polymerase	1 μl

Polymerase chain reaction was now carried out in a thermocycler following an appropriate protocol:

1. 95 °C   3 min
2. 95 °C   30 s
3. 60 °C   1 s
4. 72 °C   3 min
5. 72 °C   5 min
6. 4 °C ∞

First and second step were the steps where DNA was denatured, primer annealing took place in the third step and elongation in the fourth and fifth step. Step 2.-4. of the PCR protocol were repeated 30 times and temperature of step 3., 4. and 5. depended on the exact composition of primers.

3.2.7 Inhibitory adenylate cyclase assay

At the day when the assay was performed, membranes were prepared from freshly grown HEK 293 cells expressing the receptor of interest, which was the A_1R. All the membrane preparation steps were performed on ice if not otherwise stated. Cell culture dishes were washed with DBPS two times and cells were scraped off with 4 ml 5/2 buffer per 150 mm dish. The cell suspension was now homogenized twice for

5 s with help of an Ultraturrax, centrifuged (27000 rpm, 20 min, 4 °C) and the so gained pellet was resuspended in TRIS∗HCl 50 mM and homogenized with a glass potter and a syringe. Concentration of protein was examined with help of Bradford assay as described in the appropriate section. Membrane dilutions were adjusted to a membrane concentration of 1 μg/μl. ADA solution was added to membrane dilution with a final concentration of 0.2 U/ml just before experiments were carried out.

In the first step of inhibitory adenylate cyclase assay 10 μl of CCPA 10 μM, 10 μl of forskolin 100 μM, 30 μl of freshly prepared membrane dilution containing the receptor of interest and 50 μl REA-Mix 2x were mixed in a tube. Absolute activation of adenylate cyclase was examined with 10 μl H_2O instead of CCPA, basal activity of probes was examined with 20 μl H_2O instead of CCPA and forskolin and blank value was examined with 30 μl H_2O instead of membrane dilution. Mixtures were incubated at 37 °C for 20 min. After that the tubes were replaced on ice and 400 μl of a $ZnAc_2$ solution 125 mM and 600 μl of a Na_2CO_3 solution 144 mM were added to tubes. Probes were mixed and incubated on ice for 10 min. Accumulated $ZnCO_3$ was precipitated after a centrifugation step (10000 rpm, 5 min, RT). 800 μl of the supernatant were pipetted into a Polyprep Chromatography Column filled with Aluminumoxide. Aluminumoxide columns were washed two times with 5 ml TRIS∗HCl 100 mM per column. Elution was done with 2 ml TRIS∗HCl 100 mM for two times. Eluate was counted in a liquid scintillation analyzer (Tri Carb 2910 TR from Perkin Elmer, Rodgau, Germany). Each value was examined in triplicate.

3.2.7.1 Purification of ^{32}P α-ATP

For inhibitory adenylate cyclase assay purification of ^{32}P α-ATP was necessary. A Polyprep Chromatography column was filled with a saturated Dowex®-1X2 Chloride from 2-200 mesh and washed with 5 ml water. After that ^{32}P α-ATP was pipetted to the column. Column was now washed twice with 5 ml HCl 0.136 M and after that with 150 μl HCl 0.25 M. Elution was done with HCl 0.25 M. 3 ml were eluted and 3 μl ATP 10 mM were added. pH was adjusted to 7. Activity of ^{32}P α-ATP was counted with help of a liquid scintillation analyzer (Tri Carb 2910 TR from Perkin Elmer, Rodgau, Germany).

3.2.8 Membrane preparation

If not otherwise stated all of the following steps for membrane preparation were done on ice. Frozen cell culture dishes (Ø150 mm) containing HEK 293 cells stably expressing the construct of interest were thawed and scraped off with 4 ml ice-cold 5/2 buffer per plate. Cell suspension was collected and homogenized with help of an Ultra-turrax (Ika, Staufen, Germany). After a first centrifugation step (10 min, 1000 g, 4 °C) supernatant was centrifuged a second time (40 min, 100000 g, 4 °C) to get a pellet that contained cell membranes with the receptor of interest. Pellet was then resuspended with a sufficient amount of TRIS∗HCl 50 mM to get a total protein concentration of 1-2 mg/ml and was homogenized with a glass potter and a syringe. Concentration of protein was examined with help of Bradford assay as described in the appropriate section. If the receptor examined belonged to the Adenosine receptor family ADA solution was added to membrane dilution with a final concentration of 0.2 U/ml just before experiments were carried out.

3.2.9 Determination of protein concentration with help of Bradford assay

For determination of protein concentration Bradford assay was applied [164]. Aqueous protein solution was compared to a calibration curve. Bradford reagent-mix was bought as a ready-to-use solution (Bio-Rad Protein Assay) and BSA was taken as an internal standard. Every concentration investigated was examined in duplicate. Probes and reagents were prepared in polystyrene cuvettes as follows:

Concentration (μg/μl)	BSA (0.2μg/μl)	H$_2$O (μl)	Bradford-reagent-mix (μl)
0	0	800	200
2	10	790	200
4	20	780	200
6	30	770	200
8	40	760	200
10	50	750	200

After 5 min incubation at RT, calibration curve and protein concentrations were investigated with a photometer (NanoDrop 2000c) at 595 nm. Bradford reagent-mix and water, without BSA served as blank value.

3.2.10 Radioligand saturation binding assay

Saturation binding experiments were performed on 96 well glass fiber (1.2 μm) filter plates like previously published [67]. The assay buffer used for binding experiments was TRIS*HCl 50 mM for A_1R or TM 10 for $A_{2A}R$. Theophylline with final concentration of 4 mM was used to determine nonspecific binding in A_1R and R-PIA 100 μM was used for detection of nonspecific binding regarding the $A_{2A}R$. Applied agonists, $[^3H]CCPA$ for A_1R or $[^3H]NECA$ for $A_{2A}R$ were used at increasing concentrations in a total volume of 200 μl per well containing 0.2 U/ml ADA and 100 μg protein. After 3 h incubation of the pre-mixed plates at room temperature wells were filtered and washed three times with 200 μl ice-cold appropriate assay buffer per well. Then 20 μl of scintillation liquid were added at each dried well before total and nonspecific binding were counted in a liquid scintillation counter (1450 Micro-Beta Trilux Counter from Perkin Elmer, Rodgau, Germany). Each concentration was examined in duplicate per experiment.

3.2.11 Data analysis

Single cell FRET measurements were analyzed and corrected with Origin 9.1. EC_{50} values were obtained with help of FRET measurements as previously described [140]. Changes in FRET ratio and the resulting signal amplitude correlated with the ligand and its applied concentrations. Signal amplitude measurement for each ligand concentration examined was done with inclusion of a standard (1 mM adenosine) and data were shown as change in FRET ratio (%) correlated to the standard. With help of these concentration dependent signal amplitudes investigation of of a concentration dependent response curve was possible. Ligand concentration plotted at logarithmic abscissa was correlated to appropriate signal amplitude at the ordinate (given in % of signal amplitude of the standard) and curve was fitted with a log dose response nonlinear regression curve fit with Prism 6.
Association- and dissociation-kinetics of the different ligands used where examined with help of Clampfit 10.3. Each ligand-induced change in FRET ratio, either the association- (k_{on}) or the dissociation movement (k_{off}) were fitted to the function best suitable which was a standard exponential function

$$f(t) = \sum_{i=1}^{n} *A_i * e^{-t/\tau_i} + C \tag{3.4}$$

and τ- values which refer to the association- and dissociation kinetics (given in ms) were examined.

IC_{50}-values of antagonists (theophylline) were determined with the antagonist induced inhibition of agonist (adenosine) induced FRET signals where agonist induced FRET signals decreased with increasing concentrations of antagonist. For these inhibitory concentration response curves agonist concentration was set at approximately 80 % of the EC_{50} value of the particularly measured receptor sensor. In experiments cells were superfused with a constant concentration of agonist including increasing concentrations of antagonist. Inhibition curves were investigated via correlation of signal height of FRET signals caused by antagonist and agonist with the signal height of agonist alone. Data were shown as change in FRET ratio (%) correlated to the standard. Values were analyzed and fitted with help of Prism 6. K_i values were calculated using the examined IC_{50}-values and Cheng-Prusoff equation [165].

When performing confocal analysis image size was kept constant at 512x512 pixel and images were recorded with line accumulation of 2 and frame average of 4. Only for optical reasons contrast of images depicted was adjusted, but for analysis unmodified confocal images were taken. If not otherwise stated white bars in the cell-images refer to 20 μm.

Data from binding experiments and inhibitory cyclase assay were also analyzed using Prism 6. In FRET experiments data are shown as mean +/- s.e.m., data for each measuring point were examined at least n= 10 carried out on at least 3 different experimental days. If not otherwise stated confocal analysis, radioligand binding and inhibitory cyclase assay were examined at least n= 3 on at least 3 different experimental days.

4 Results

4.1 Development of A$_1$ Fl3 CFP and comparison to A$_{2A}$ Fl3 CFP

4.1.1 Generation of A$_1$ Fl3 CFP receptor sensor

In 2008 [25] and 2011 [43] the first antagonist (ZM241385)- and agonist (UK-432097)-bound crystal structures of the A$_{2A}$R were published and gave a static insight into receptor ligand interaction. The A$_{2A}$ FlAsH3 CFP (A$_{2A}$ Fl3 CFP) receptor sensor that was previously published [118] revealed further insight into behavior of receptor upon ligand binding ans was the base for development of the human A$_1$R FRET sensor. Both fluorescent receptor sensors, A$_1$ Fl3 CFP and A$_{2A}$ Fl3 CFP, contain the FlAsH binding motif, consisting of *CCPGCC*, in the third intracellular loop and the CFP encoding sequence at the C-terminus of receptor (figure 4.1 A and B), whereas C-terminus of the A$_{2A}$R sensor was truncated due to distance between the two fluorophores (figure 4.1 A).

The fluorescent A$_1$R probe was designed on base of the human ADORA1 wild type receptor. CFP was fused C-terminally to the human A$_1$R and the discontinuous tetracysteine binding motif of FlAsH, *CCPGCC*, was inserted into the third intracellular loop of the receptor between D221 and P222 (figure 4.1 B). The receptor sensor was cloned via overlapping PCR [160] and was inserted into pcDNA3 vector. The so obtained fluorescent A$_1$R sensor was called A$_1$ FlAsH3 CFP and will be abbreviated A$_1$ Fl3 CFP throughout this work for ease of reading.

For investigation of G protein activation with help of a trimeric G$_i$ FRET-sensor A$_1$R was cloned into pcDNA3 plasmid without insertion of fluorophores or their binding sequence. The correct sequence of receptor sensor was confirmed via sequencing.

The trimeric G$_i$ FRET sensor was a kind gift of Dr. Goedhart where a modified G$_{\alpha i}$ Turquoise [166][167][110][168], named G$_{\alpha i}$-mTurquoise2-δ 9, was used to replace

$G_{\alpha q}$-mTurquoise-$\delta6$ in a FRET based sensor [147]. Thus $G_{\alpha i}1$-mTurquoise2-$\delta9$, G_{β} and cpV6-$G_{\gamma}2$ were co-expressed in one plasmid which was used as a FRET based biosensor for examination of G_i protein activation. This sensor will be abbreviated G_i FRET sensor throughout this work.
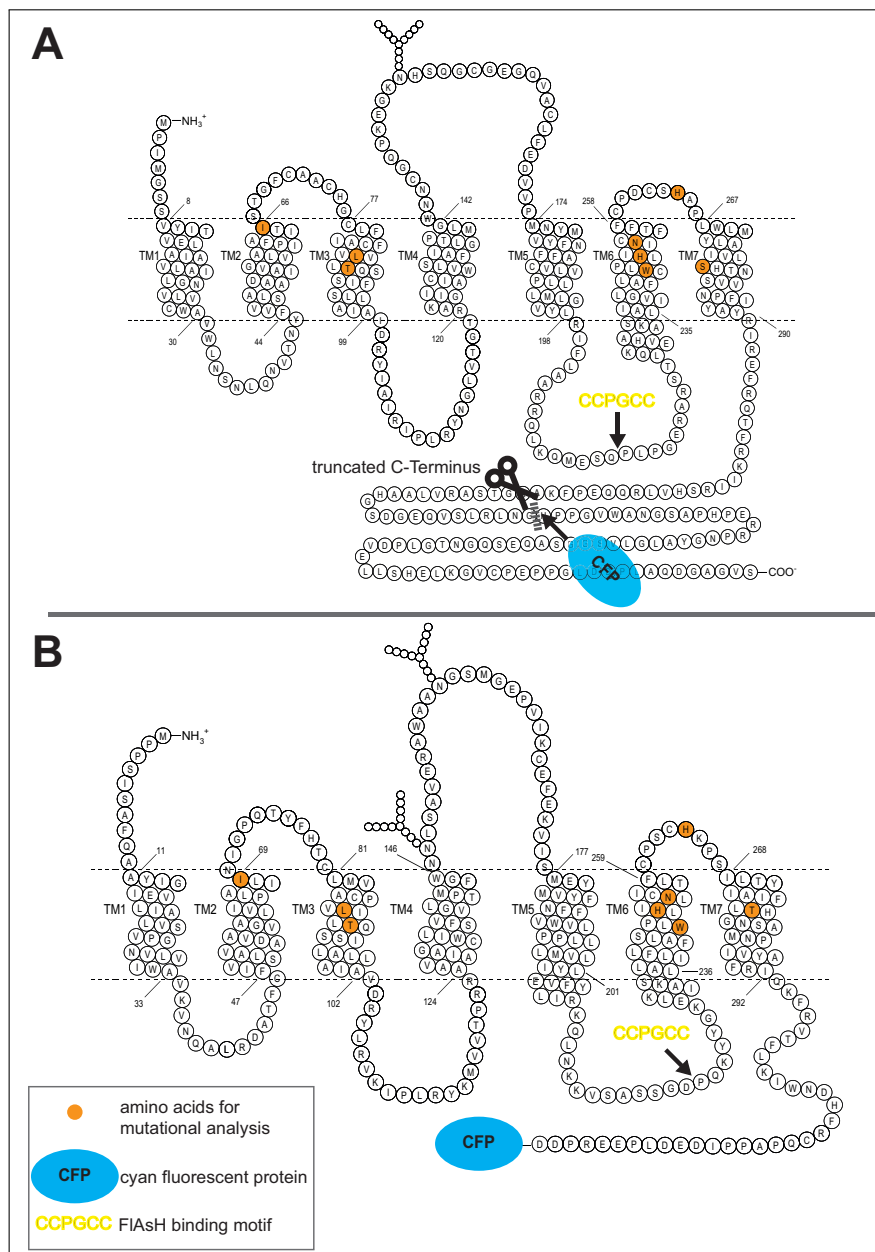
Figure 4.1: Snakeplots of **(A)** $A_{2A}R$ and **(B)** A_1R with positions of mutated amino acids and insertion positions for fluorophores used

4.1.2 Characterization of A_1 Fl3 CFP receptor sensor

A_1 Fl3 CFP receptor sensor was properly expressed in the plasma membrane of HEK 293 cells which could be confirmed via confocal analysis (image in figure 4.2 A). The same held true for A_{2A} Fl3 CFP receptor sensor (figure 4.2 B). Both receptor sensors were suitable for FRET measurements as shown in figure 4.2 A and B (representative FRET experiments). At the A_1 Fl3 CFP receptor sensor FRET ratio increased upon stimulation with agonist (figure 4.2 A) whereas it decreased regarding agonist stimulated A_{2A} Fl3 CFP receptor sensor (figure 4.2 B).
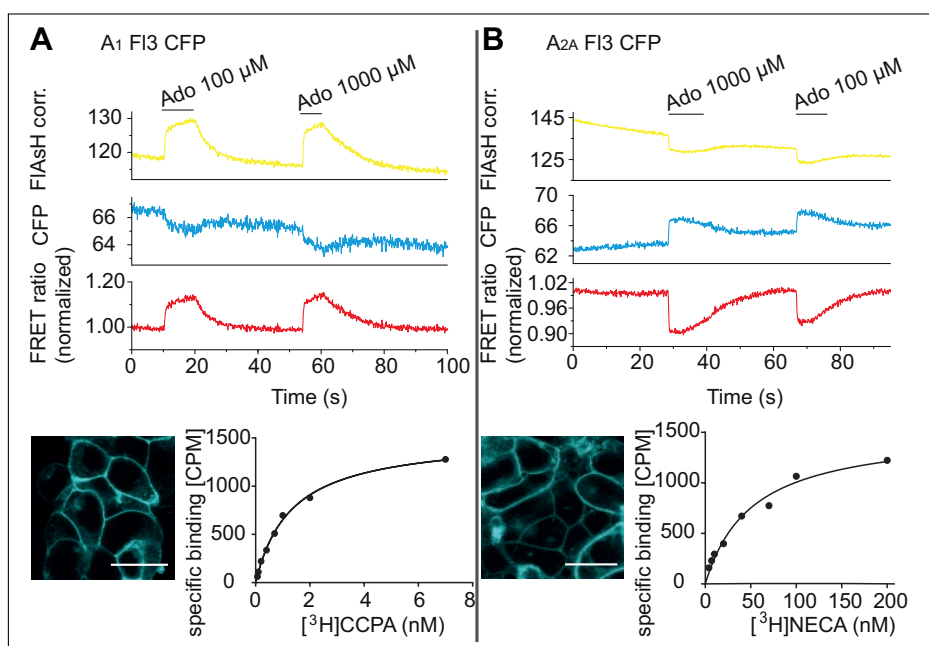
Figure 4.2: The A_1 Fl3 CFP **(A)** and A_{2A} Fl3 CFP **(B)** receptor sensor were functional concerning localization in the plasma membrane (confocal images, white bar corresponds to 20 μm), receptor sensors could be saturated with appropriate amounts of radioligand as wild type A_1R and $A_{2A}R$ and FRET experiments are feasible with both of receptor sensors.

4.1.2.1 Saturation binding experiments with A_1 Fl3 CFP receptor sensor

For characterization of A_1R sensor developed here and for the purpose of linking the pharmacological properties of this receptor sensor to existing data in the adenosine receptor field [67] saturation binding experiments were carried out with radioactive [^{3}H] labeled ligands (4.2 A, specific binding is depicted).

[^{3}H] CCPA, an adenosine receptor agonist with high affinity for the A_1R [169] was used for the A_1 Fl3 CFP receptor sensor. Experiments showed that A_1R sensor was

functional and the average K_d-value of 4.4 nm was in the same dimension as K_d-value of wild type A_1R where a K_d-value of 0.61 nm was investigated [67]. Previously investigated saturation radioligand binding experiments at the A_{2A} Fl3 CFP receptor sensor showed that it is also functional concerning the binding properties of [³H] NECA (K_d= 59.3 nm) [118] compared to unmutated $A_{2A}R$ (K_d= 20.1 nm) [67] (figure 4.2 B, specific binding is depicted).

4.1.2.2 Adenylate cyclase is inhibited via G_i protein of A_1 Fl3 CFP

Radioactivity based inhibitory cyclase assay was carried out for G_i coupled A_1 Fl3 CFP receptor (figure 4.3). Stimulation of adenylate cyclase with 10 μM forskolin and inhibition of adenylate cyclase with 1 μM CCPA was successful which can be seen in figure 4.3 where signal of stimulated adenylate cyclase (black, 100 %) is higher than signal of inhibited adenylate cyclase (gray, 49 %).
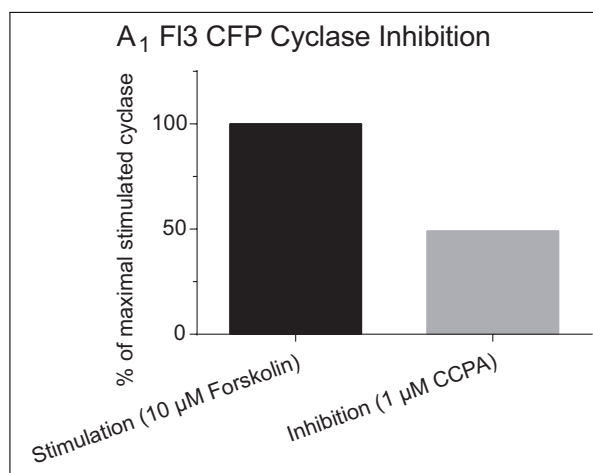
Figure 4.3: Inhibitory adenylate cyclase assay with A_1 Fl3 CFP. Forskolin stimulated adenylate cyclase (black column) can be inhibited through G_i protein via receptor activation with the A_1R selective agonist CCPA (gray column). Data show outcome of one experiment performed in triplicate

4.1.3 FRET experiments at A_1 Fl3 CFP and A_{2A} Fl3 CFP - comparison regarding signal amplitudes and kinetics

As A_{2A} Fl3 CFP receptor sensor was the base for design of A_1 Fl3 CFP sensor it was of great interest to see if there were differences in receptor dynamical movements when both receptor sensors are exposed to various ligands during FRET experiments

(figure 4.4 shows representative FRET experiments). Characterization of A_{2A} Fl3 CFP and its mutants was part of previous work [170].
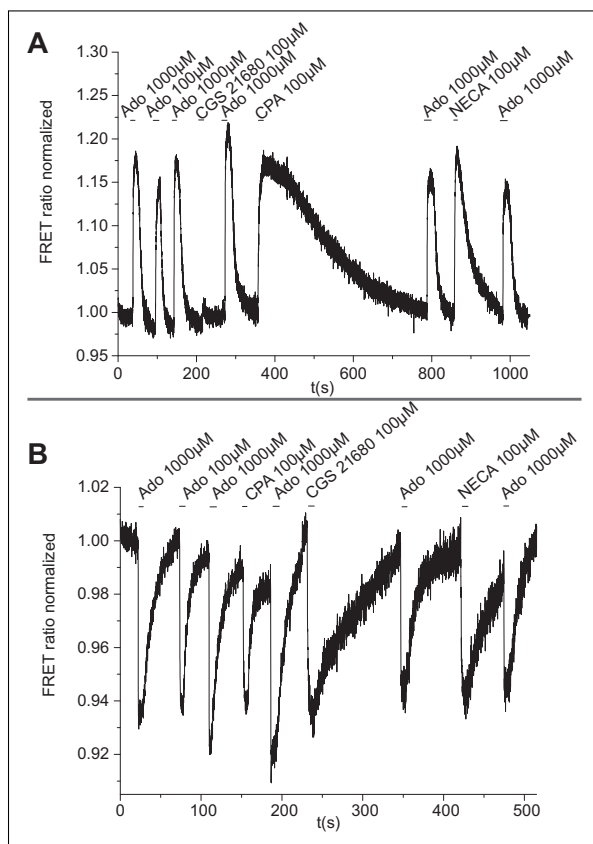
Figure 4.4: Representative FRET experiments with **(A)** A_1 Fl3 CFP where FRET ratio increased upon agonist binding and **(B)** A_{2A} Fl3 CFP where FRET ratio decreased upon agonist binding. Both receptor sensors are exposed to various ligands at saturating concentrations. Investigated ligands in detail are adenosine, CPA, CGS 21680 and NECA each concentrated 100 μM, adenosine 1000 μM was taken as reference to correlate signal heights of ligands

The ligands investigated are adenosine which is the physiological agonist of all adenosine receptors, NECA (N- ethylcarboxamidoadenosine) an unspecific agonist on all adenosine receptors which has a higher affinity for the receptors than adenosine [67], CGS 21680 (2 -p-(2 -Carboxyethyl)phenetylamino- 5'-N-ethylcarboxamidoadenosine) that has a higher specificity for the A_{2A}R and CPA (N^6- Cyclopentyladenosine) which has an increased affinity for the A_1R. CGS 21680 is a well-known agonist at the A_{2A}R [57] which has recently been modeled into the A_{2A}R- agonist bound structure [171] and crystal structural data bound to A_{2A}R recently became available [46].
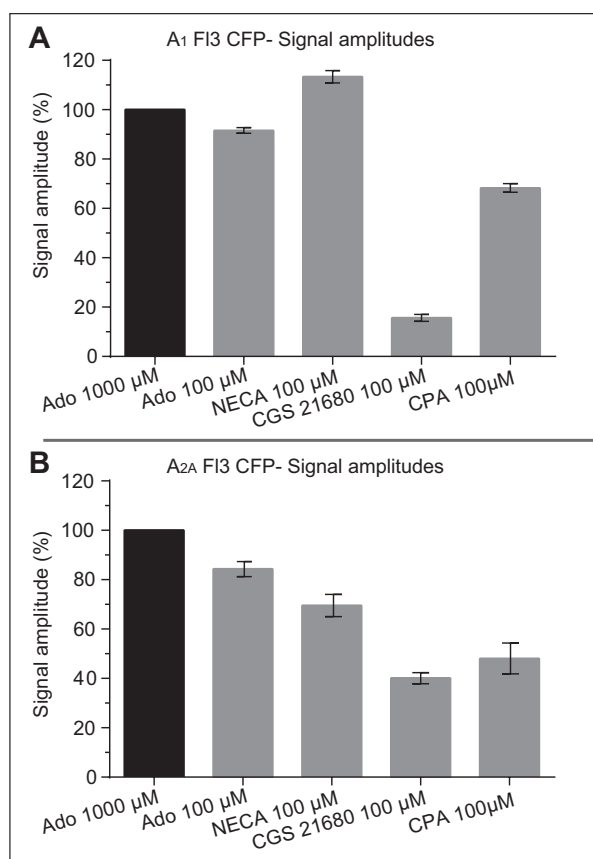
Figure 4.5: Signal amplitudes of adenosine, CPA, CGS 21680 and NECA each 100 μM (gray column) examined at the **(A)** A_1 Fl3 CFP and **(B)** A_{2A} Fl3 CFP receptor sensor in FRET experiments. Adenosine 1000 μM (black column) was taken as reference to correlate signal amplitudes of various ligands. Columns show the mean of 10 to 15 single FRET experiments investigated at 3 days, errors are depicted as S.E.M.

All ligands were investigated at saturating concentrations of 100 μM, adenosine 1000 μM was taken as reference substance and was set at 100 %. Figure 4.4 A shows a representative FRET experiment where A_1R sensor was exposed to various ligands. For investigation of the influence of intracellular adenosine cells were preincubated with medium or buffer containing the enzyme ADA. However, the pretreated cells did not show differences in the outcome of FRET experiments if they were compared to not pretreated cells. Panel A of figure 4.5 shows the relative signal amplitudes that former named ligands caused at the A_1 Fl3 CFP receptor sensor. Black column shows the reference ligand adenosine 1000 μM that was set at 100 %. Gray columns from left to right show signal amplitudes of adenosine 100 μM (92 %), NECA 100 μM (113 %), CGS 21680 100 μM (16 %) and CPA 100 μM (68 %) correlated to the

standard substance. NECA induced the biggest change in FRET ratio at the A_1 Fl3 CFP receptor sensor.

FRET experiments with the same ligands were conducted at A_{2A} Fl3 CFP (figure 4.4 B). All ligands investigated were again correlated to adenosine 1000 μM (black column). Signal amplitudes of ligands (gray columns, from left to right) led to following results: Adenosine 100 μM caused a signal amplitude of 84 %, NECA 100 μM caused 70 %, CGS 21680 100 μM caused 40 % and CPA 100 μM led to a signal amplitude of 48 %.

In comparison (see figure 4.4), signal amplitude of adenosine 100 μM is slightly higher at the A_1R sensor compared to A_{2A}R sensor, whereas signal amplitude of NECA exhibited the biggest difference between these two receptor subtypes. NECA 100 μM induced the highest signal at A_1 Fl3 CFP, even higher as the reference, but only the third highest signal at A_{2A} Fl3 CFP. CGS 21680 100 μM led to the smallest signal amplitude regarding both receptor sensors, but its signal amplitude at A_1 Fl3 CFP was smaller (16 %) than its signal amplitude of A_{2A} Fl3 CFP (40 %). CPA 100 μM induced a higher signal at the A_1R sensor compared to the A_{2A}R sensor.

During experiments it became visible that the various ligands investigated had different association- and dissociation-times at the two adenosine receptor subtypes investigated. To explore this fact further association- and dissociation-times (τ_{on} and τ_{off}) of ligands in FRET experiments were analyzed (figure 4.6). Values are given as mean of single FRET experiments and as normalized values correlated to adenosine 1000 μM which was set as 1.

Figure 4.6 A shows normalized τ values of the ligands tested at the A_1 Fl3 CFP receptor sensor. The left diagram shows association kinetics where adenosine 1000 μM (black column) has the smallest value (1) and therefor the fastest association kinetic. Following ligands were correlated to adenosine 1000 μM (gray columns): adenosine 100 μM (1.5), NECA 100 μM (1.8) and CPA 100 μM (1.8). The A_{2A} selective ligand CGS 21680 100 μM was also probed at the A_1R sensor. Upon ligand stimulation there was a change in FRET ratio observable (see figure 4.5 A), but it was very small and thus not evaluable (compare figure 4.4 A). The right diagram of figure 4.6 A shows dissociation kinetics of ligands at the A_1 Fl3 CFP receptor sensor. The τ_{off} values of NECA 100 μM were equal with the reference ligand adenosine 1000 μM (black column) which was set as 1, a faster dissociation rate was observed for adenosine 100 μM (0.7), but CPA 100 μM (5.7) had a markedly longer τ_{off} value than all other ligands tested at this receptor subtype. Due to the small change in

FRET ratio evoked by CGS 21680 100 μM evaluation of dissociation kinetic values was not feasible for this ligand. Figure 4.6 B shows kinetic values of the ligands previously mentioned tested at the A$_{2A}$ Fl3 CFP receptor sensor. Left diagram shows means of τ_{on} values and right diagram means of τ_{off} values. Adenosine 1000 μM served as reference, was set as 1 and plotted in black bars, whereas ligands correlated to the reference ligand were plotted in gray. Again, for association kinetics, adenosine 1000 μM (1) had the fastest τ_{on} value, adenosine 100 μM (1.7), NECA 100 μM (2.1) and CGS 21680 100 μM (3.9) were slower and CPA 100 μM (3.1) was faster than CGS 21680 100 μM at the A$_{2A}$R sensor.
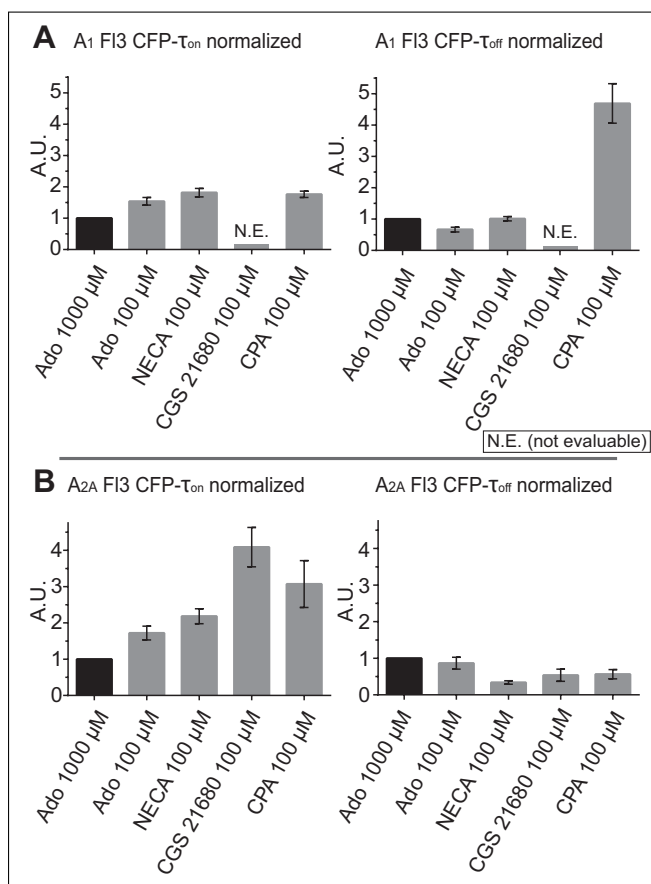
Figure 4.6: Association- (τ_{on}) and dissociation-kinetics (τ_{off}) of various ligands used at saturating concentrations at **(A)** A$_1$ Fl3 CFP and **(B)** A$_{2A}$ Fl3 CFP receptor sensor, data for ligands (gray columns) were normalized and correlated to adenosine 1000 μM which was set as 1 (black column). Columns show the mean of 10 to 15 single FRET experiments investigated at 3 days, errors are depicted as S.E.M.

Right diagram of figure 4.6 B shows dissociation kinetics of former named ligands at

the $A_{2A}R$ sensor. Adenosine 1000 μM (1) served as reference ligand, adenosine 100 μM (0.9), NECA 100 μM (0.4), CGS 21680 100 μM (0.5) and CPA 100 μM (0.5) were faster than the reference ligand.

4.1.4 Development of A_1 Fl3 CFP receptor sensor mutants

As explained in a previous section A_{2A} Fl3 CFP receptor sensor [118] was the base for development of human A_1R FRET sensor (A_1 Fl3 CFP). Amino acid sequence of $A_{2A}R$ was taken as template and secured that positions of amino acids that were mutated in the A_1R were in the same position as in the $A_{2A}R$ via sequence alignment with CLUSTAL W (figure 4.7) [172].

```
                   10        20        30        40        50
                   ....|....|....|....|....|....|....|....|....|....|
h-A2A              MP---IMGSSVYITVELAIAVLAILGNVLVCWAVWLNSNLQNVTNYFVVS
h-A1               MPPSISAFQAAYIGIEVLIALVSVPGNVLVIWAVKVNQALRDATFCFIVS
Clustal Consensus  **      .:.** :*: **:::: ***** *** :*. *::.*  *:.**

                   60        70        80        90        100
                   ....|....|....|....|....|....|....|....|....|....|
h-A2A              LAAADIAVGVLAIPFAITISTGFCAACHGCLFIACFVLVLTQSSIFSLLA
h-A1               LAVADVAVGALVIPLAILINIGPQTYFHTCLMVACPVLILTQSSILALLA
Clustal Consensus  **.**:***.*.**:** *. *  :   * **::** **:******::***

                   110       120       130       140       150
                   ....|....|....|....|....|....|....|....|....|....|
h-A2A              IAIDRYIAIRIPLRYNGLVTGTRAKGIIAICWVLSFAIGLTPMLGWNNCG
h-A1               IAVDRYLRVKIPLRYKMVVTPRRAAVAIAGCWILSFVVGLTPMFGWNNLS
Clustal Consensus  **:***: ::*****: :** **  ** **:***.:*****:**** .

                   160       170       180       190       200
                   ....|....|....|....|....|....|....|....|....|....|
h-A2A              QPKEGKNHSQGCGEGQVACLFEDVVPMNYMVYFNFFACVLVPLLLMLGVY
h-A1               AVERAWAANGSMGEPVIKCEFEKVISMEYMVYFNFFVWVLPPLLLMVLIY
Clustal Consensus  :..   . ** : * **.*:.*:********. ** *****: :*

                   210       220       230       240       250
                   ....|....|....|....|....|....|....|....|....|....|
h-A2A              LRIFLAARRQLKQMESQPLPGERARSTLQKEVHAAKSLAIIVGLFALCWL
h-A1               LEVFYLIRKQLNKKVSASS-GD-PQKYYGKELKIAKSLALILFLFALSWL
Clustal Consensus  *.:*   *:**::   * .  *: .:.   **:: *****:*: ****.**

                   260       270       280       290       300
                   ....|....|....|....|....|....|....|....|....|....|
h-A2A              PLHIINCFTFFCPDCSHAPLWLMYLAIVLSHTNSVVNPFIYAYRIREFRQ
h-A1               PLHILNCITLFCPSC-HKPSILTYIAIFLTHGNSAMNPIVYAFRIQKFRV
Clustal Consensus  ****:**:*:***.* * *  * *:**.*:* **.:**::**:**:.:**

                   310       320       330       340       350
                   ....|....|....|....|....|....|....|....|....|....|
h-A2A              TFRKIIRSHVLRQQEPFKAAGTSARVLAAHGSDGEQVSLRLNGHPPGVWA
h-A1               TFLKIWNDHFRCQP----------------------------APP----
Clustal Consensus  ** ** ..*. *                                **

                   360       370       380       390       400
                   ....|....|....|....|....|....|....|....|....|....|
h-A2A              NGSAPHPERRPNGYALGLVSGGSAQESQGNTGLPDVELLSHELKGVCPEP
h-A1               -IDEDLPEERPDD-------------------------------------
Clustal Consensus  .   **.**:.

                   410
                   ....|....|....|
h-A2A              PGLDDPLAQDGAGVS
h-A1               ---------------
Clustal Consensus
```
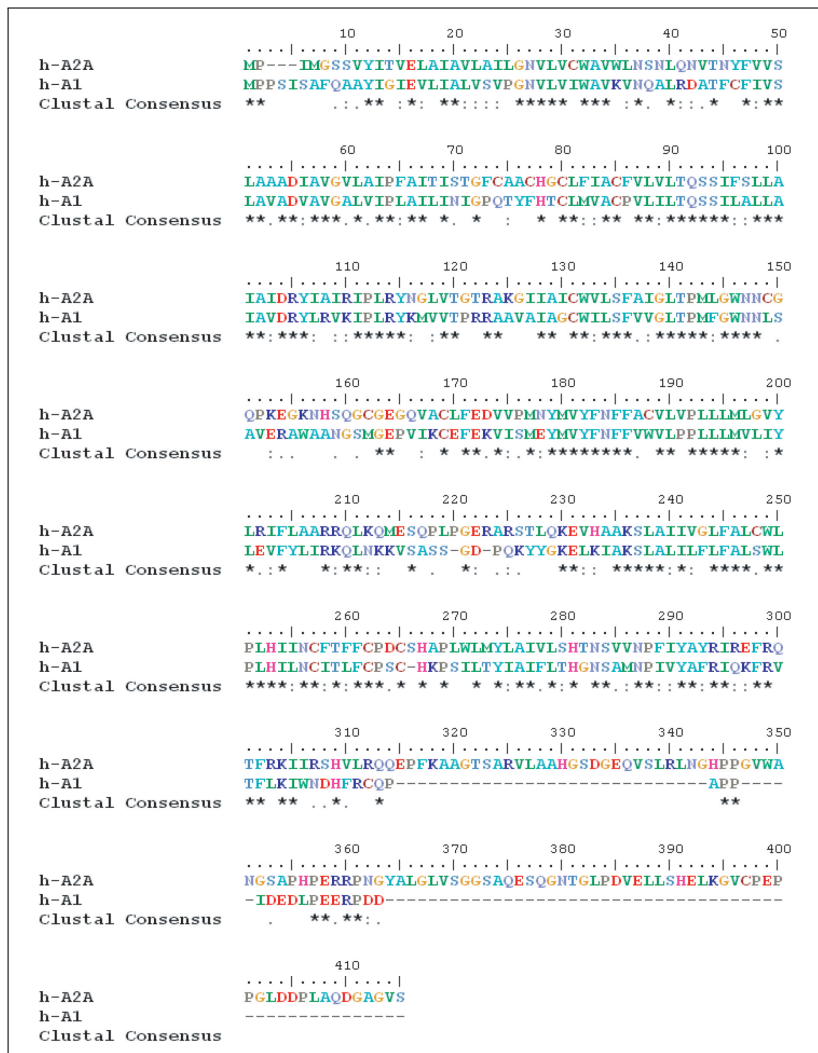
Figure 4.7: Sequence alignment of A_1R and the $A_{2A}R$, obtained with CLUSTAL W [172]

Crystal structure of the $A_{2A}R$ bound to ZM241385 [25] was the base for selection of amino acids that are likely to have an impact on ligand binding in the A_1R and thus were selected for investigation with help of mutational analysis. Figure 4.8 A shows amino acids building the $A_{2A}R$ ligand binding pocket with the physiological agonist adenosine. These amino acids are likely to have an impact on ligand binding because they are in close proximity to the ligand in the binding pocket in the $A_{2A}R$ crystal structure. Thus they were chosen for mutational analysis in the $A_{2A}R$ which was done in previous work [170]. Within this work the effect of these particular amino acids in the A_1R was investigated. Single amino acids positions from the $A_{2A}R$ sequence were transferred to the A_1R sequence via sequence alignment (figure 4.7) as stated before. Figure 4.8 B shows how particular amino acids derived from $A_{2A}R$ ligand binding pocket could form a hypothetical A_1R ligand binding pocket.

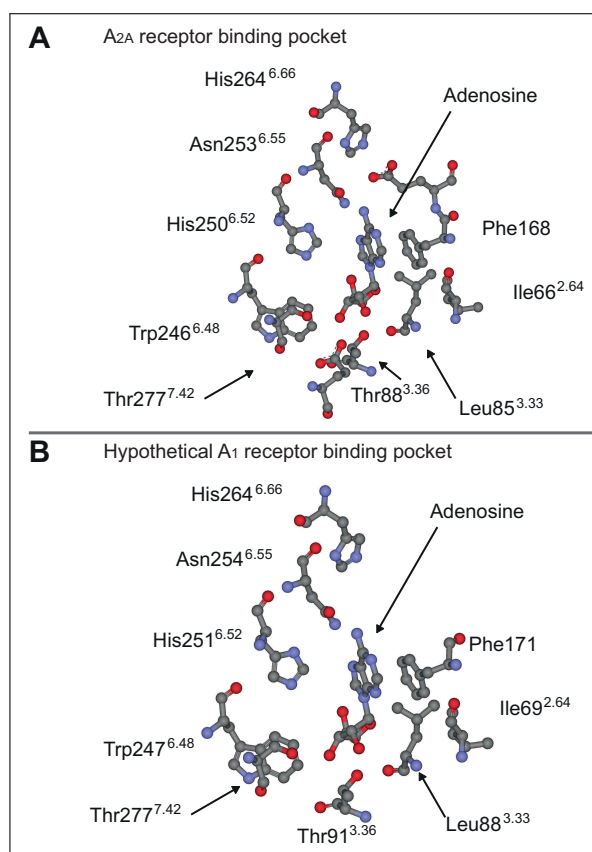**Figure 4.8:** Amino acids forming the binding pocket of **(A)** $A_{2A}R$ **(B)** Hypothetical binding pocket of A_1R. Amino acids in the $A_{2A}R$ were obtained from the crystal structure of this receptor and amino acids forming A_1R binding pocket were deduced from $A_{2A}R$ binding pocket

Table 4.1 shows positions of amino acids that were mutated in the $A_{2A}R$ and the

corresponding mutated amino acids in the A_1R. Numbering of amino acids follows Ballesteros and Weinstein nomenclature [21] and numerical position in the sequence of the appropriate receptor.

The fluorescent receptor mutants were designed on base of the A_1 Fl3 CFP receptor sensor (figure 4.1 B) where CFP was fused C-terminally and the discontinuous tetracysteine binding motif of FlAsH was inserted into the third intracellular loop of the receptor. The nine former named point mutations were introduced into the unmutated receptor sensor sequence with help of overlapping PCR technique [160]. The correct sequence of receptor sensor mutants was confirmed via sequencing.

Because they appeared to have especially interesting behavior during experiments, two mutants, in particular A_1 H251A and A_1 W247A, were additionally investigated concerning G protein activation. This was done with help of the former described trimeric G_i FRET sensor. The particular A_1R mutants were cloned into pcDNA3 plasmid without insertion of fluorophores or their binding sequence. The so developed non-fluorescent receptor mutants in detail are A_1 H251A and A_1 W247A, where histidine in position 251 and tryptophan in position 247 were mutated to an alanine, respectively. Unmutated A_1R co-expressed with trimeric G_i FRET sensor was also investigated and served as control.

Position	A_1R (Location)	$A_{2A}R$ (Location)
2.64	I69V (TM2)	I66V (TM2)
3.33	L88A (TM3)	L85A (TM3)
3.36	T91A (TM3)	T88A (TM3)
6.48	W247A (TM6)	W246A (TM6)
6.52	H251A (TM6)	H250A (TM6)
6.55	N254A (TM6)	N253A (TM6)
6.66	H264A (EL3)	H264A (EL3)
7.42	T277A (TM7)	T277A (TM7)
7.42	T277S (TM7)	T277T (TM7)

Table 4.1: Positions of amino acids that were mutated in the $A_{2A}R$ and positions of corresponding mutated amino acids in the A_1R. Numbering was done using Ballesteros and Weinstein nomenclature and numerical position of the sequence of receptors

4.1.5 Confocal analysis of A_1 Fl3 CFP and its mutants

A_1 Fl3 CFP and its 9 mutants stably expressed in HEK 293 cells were analyzed with a confocal microscope where A_1 Fl3 CFP receptor sensor was properly located in the plasma membrane (figure 4.9).
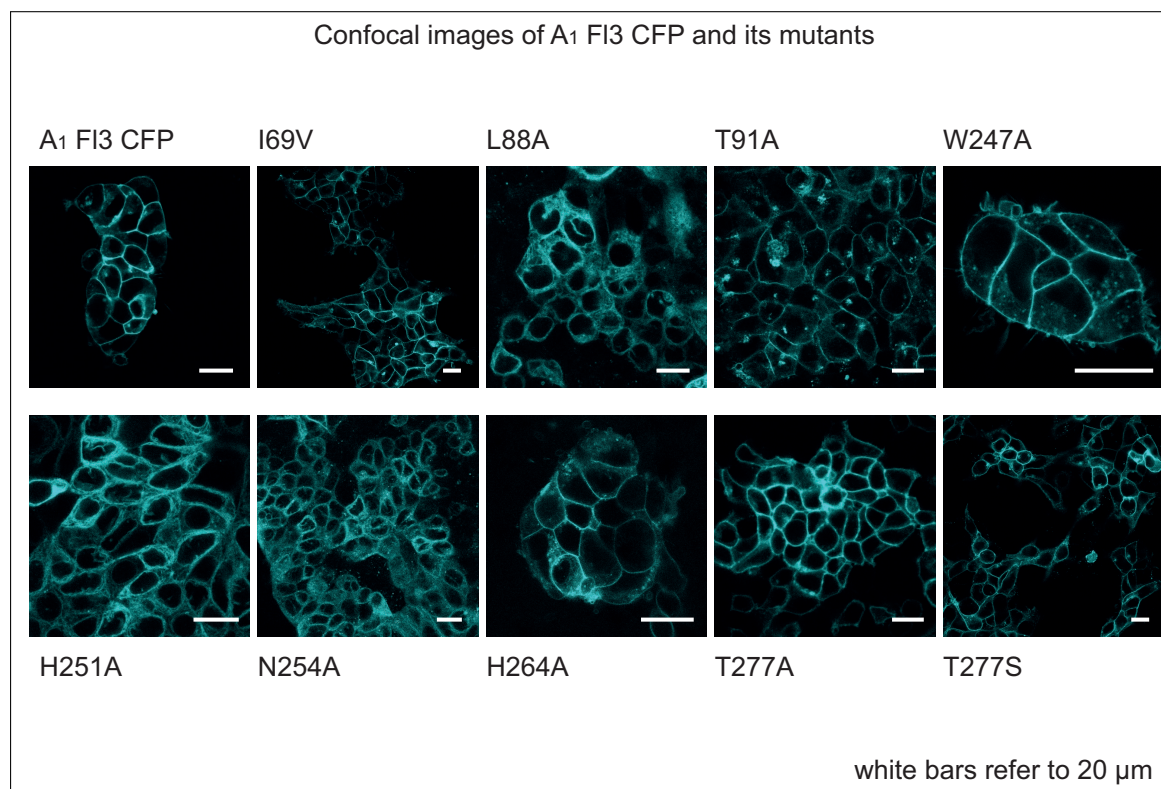

Figure 4.9: Confocal images of A_1 Fl3 CFP and all its mutants investigated here which are (from left to right and from the first to the second row of images) A_1 Fl3 CFP, A_1 Fl3 CFP I69V, L88A, T91A, W247A, H251A, N254A, H264A, T277A and T277S. CFP at receptor sensors was excited and emission was detected to see cellular distribution of receptor sensors. A_1 Fl3 CFP and mutants are located in the plasma membrane, except A_1R sensors that were mutated in position L88A, H251A and N254A. White bars refer to 20 μm

During experiments it turned out that A_1 Fl3 CFP and its mutants showed different cellular receptor distribution (see table 4.2 and figure 4.9). Unlabeled receptor sensors were visualized with help of a confocal microscope via excitation of CFP (442 nm). Whereas unmutated A_1 Fl3 CFP receptor sensor and the mutants I69V, T91A, W247A, H264A, T277A and T277S showed proper plasma membrane expression of receptors (figure 4.9) mutations L88A, H251A and N254A led to a loss of membrane localization of receptors (figure 4.10 A, first row and figure 4.9). This could not be

seen in former confocal analysis of respective mutants in the A_{2A} Fl3 CFP receptor sensor (see table 4.2 and figure 4.10 A, third row).

Position	A_1R	Localization	A_{2A}R	Localization
2.64	I69V	plasma membrane	I66V	plasma membrane
3.33	L88A	intracellular structures	L85A	plasma membrane
3.36	T91A	plasma membrane	T88A	plasma membrane
6.48	W247A	plasma membrane	W246A	plasma membrane
6.52	H251A	intracellular structures	H250A	plasma membrane
6.55	N254A	intracellular structures	N253A	plasma membrane
6.66	H264A	plasma membrane	H264A	plasma membrane
7.42	T277A	plasma membrane	S277A	plasma membrane
7.42	T277S	plasma membrane	S277T	plasma membrane

Table 4.2: Cellular localization of A_1 Fl3 CFP and A_{2A} Fl3 CFP receptor sensors and their mutants in confocal analysis

It was previously stated that the correct folding of receptors is assisted by small molecules, so called chaperones [173] and that pharmacological ligands are also able to act as chaperones that assure correct folding and localization of receptor [174], or even enhance efficacy for ligands at a distinct receptor [175]. Additionally, Zhang and co-workers showed that small ligands, if available in cell culture medium, can help to stabilize receptor in the plasma membrane of cells [176]. To investigate if cellular receptor distribution of these three mutants could be altered with help of such a chaperone they were exposed to cell culture medium containing theophylline. A_1 Fl3 CFP L88A, A_1 Fl3 CFP H251A and A_1 Fl3 CFP N254A turned to the plasma membrane of HEK 293 cells after 24 h incubation with cell culture medium containing 5 mM of the xanthine-derivative theophylline which is an adenosine receptor antagonist [177][178] (figure 4.10 A, second row). After theophylline treatment receptors were stably expressed in the plasma membrane of HEK 293 cells which could be confirmed via confocal analysis. Thus theophylline is able to act as a chaperone at these receptor mutants.
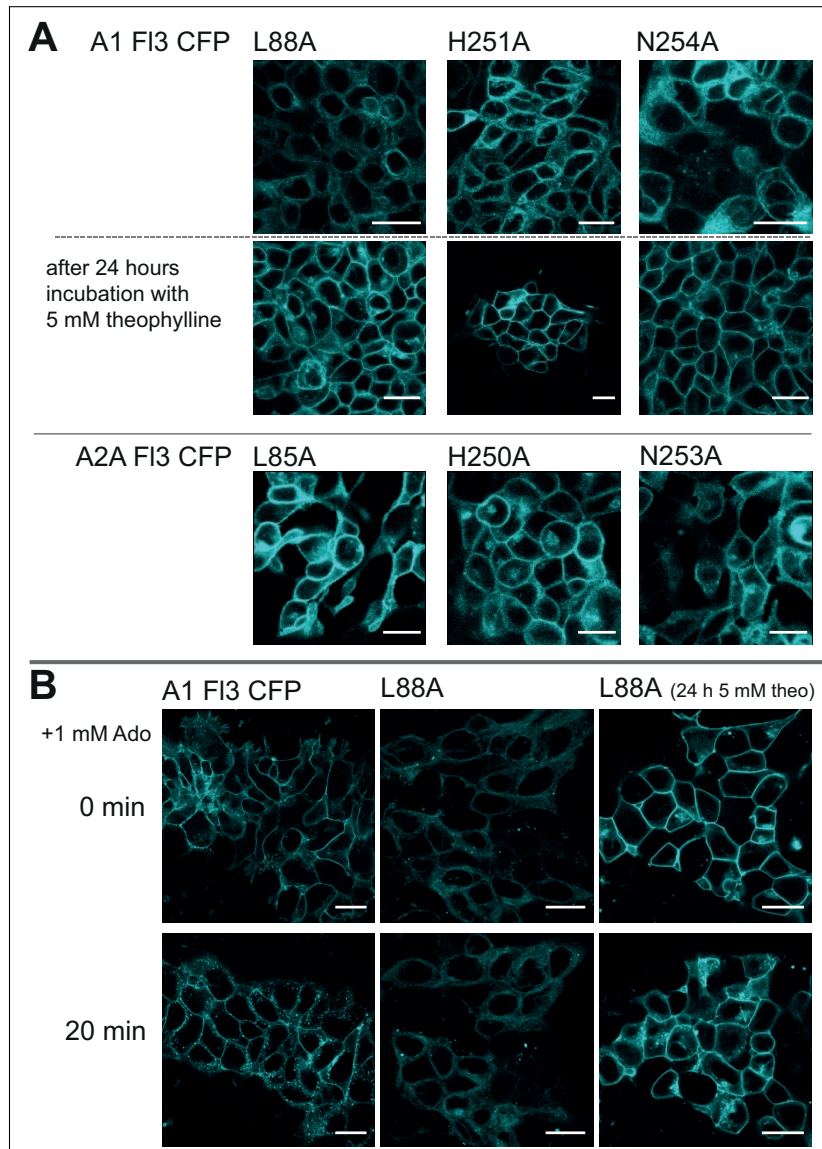
Figure 4.10: **(A)** Confocal images of locally corresponding mutants in the A$_1$ Fl3 CFP and A$_{2A}$ Fl3 CFP receptor sensor, first row shows A$_1$ Fl3 CFP L88A, H251A and N254A before treatment and second row shows L88A, H251A and N254A after 24 h incubation with 5 mM theophylline, locally corresponding mutants in the A$_{2A}$ Fl3 CFP L85A, H250A and N253A are depicted in the third row. **(B)** First row shows the starting images of a 20 min time series where 1 mM adenosine was added to either (from left to right) A$_1$ Fl3 CFP, A$_1$ Fl3 CFP L88A without or A$_1$ Fl3 CFP L88A with theophylline pretreatment. Second row of images shows the endpoints of these time series

To learn more about the transport effect of these appointed mutants in the A$_1$R confocal time series were performed for one mutant of the former described pheno-

type where receptors were not properly expressed in the plasma membrane, A_1 Fl3 CFP L88A. For comparison A_1 Fl3 CFP, A_1 Fl3 CFP L88A without and A_1 Fl3 CFP L88A with theophylline pretreatment were analyzed (figure 4.10 B, from left to right). 1 mM adenosine was added to cells at the beginning of each experiment (figure 4.10 B, first row) and localization of CFP tagged receptors was observed via detection of emission of CFP. Images were taken every 30 s. A_1 Fl3 CFP receptor sensor was located in the plasma membrane at the start of experiment and a clear receptor internalization appearing as small vesicles in the cytoplasm was visible after 20 min (figure 4.10 B, second row, first image). A_1 Fl3 CFP L88A mutant that was not pretreated with 5 mM theophylline did not show any visible alteration concerning receptor distribution throughout experiment, at the beginning of experiment and after 20 min receptor remained intracellular (figure 4.10 B, second row, second image). A_1 Fl3 CFP L88A mutant that was incubated with 5 mM theophylline for 24 h before experiment showed plasma membrane localization at the beginning of experiment and an increase in intracellular fluorescence and thus intracellular receptor after 20 min (figure 4.10 B, second row, third image). Compared to the unmutated A_1 Fl3 CFP intracellular transport of the mutated receptor had a different phenotype which will be an interesting point for further investigations in the future.

4.1.6 FRET measurements of A_1 Fl3 CFP and its mutants

With help of radioligand saturation binding experiments (figure 4.2 A) and inhibitory adenylate cyclase assays (figure 4.3) it was shown that the A_1 Fl3 CFP receptor sensor was functional compared to wild type A_1R. Mutants of the A_1 Fl3 CFP receptor sensor were characterized regarding their FRET efficiency which provides information of correct protein folding.

4.1.6.1 Investigation of the FRET efficiency of A_1 Fl3 CFP receptor sensor and its mutants

Ability of receptor sensors to perform FRET was examined with help of investigating FRET efficiency [118][163] for A_1 Fl3 CFP receptor sensor and its mutants (figure 4.11). At the beginning of each single cell FRET measurement FlAsH labeled HEK 293 cells stably containing A_1 Fl3 CFP or one of its mutants were supplemented with BAL (figure 4.11 B shows a representative FRET trace). BAL

displaced FlAsH, the FRET energy acceptor from its binding site. This could be seen in a loss of fluorescence in the FlAsH channel (F_{535}) and a consequential dequenching and thus increase of fluorescence in the CFP donor fluorophore channel (F_{480}). FRET efficiency was calculated like described in the previous chapter (see equation 3.2).

Unmutated A_1 Fl3 CFP and its 9 single amino acid mutants showed FRET efficiencies that were not statistically different from each other (figure 4.11 A) when tested with 1 way ANOVA test.
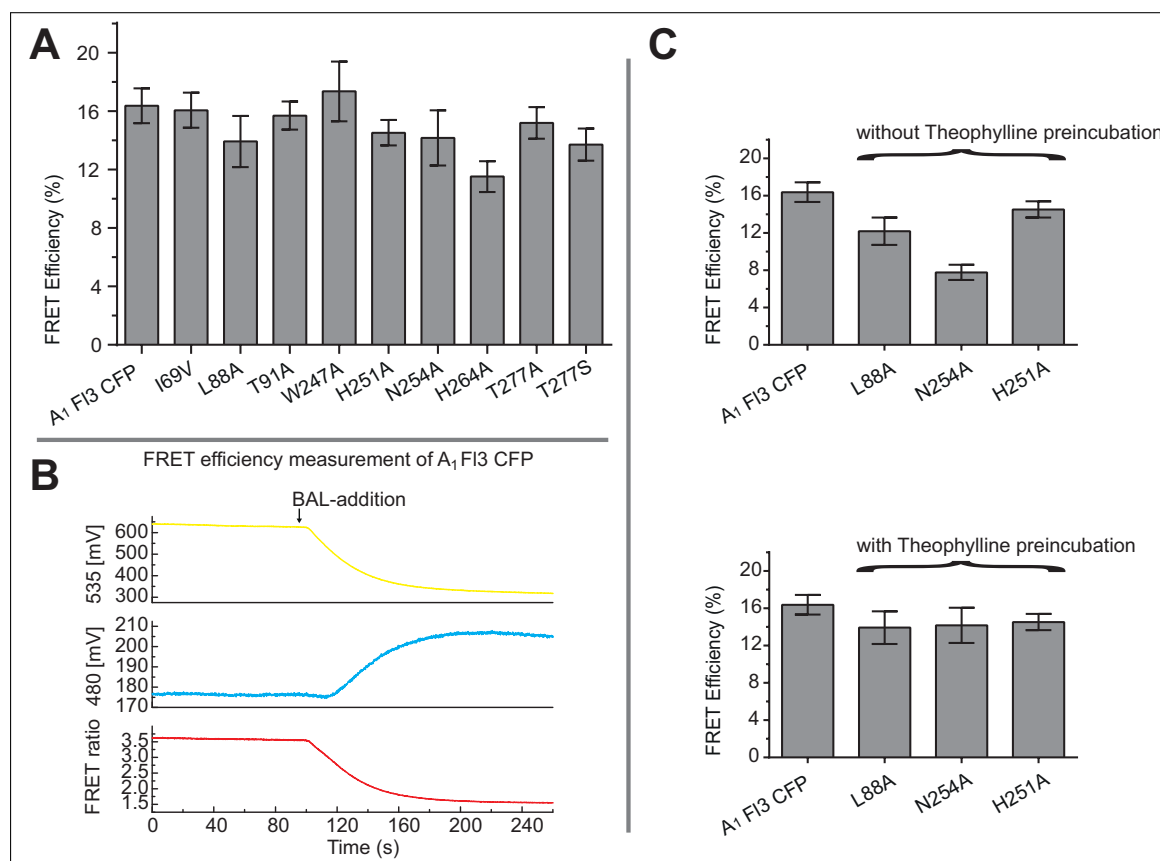

Figure 4.11: FRET efficiency measurements of A_1 Fl3 CFP and its mutants. **(A)** Average FRET efficiency values of not mutated A_1 Fl3 CFP receptor sensor and its mutants. **(B)** Representative FRET trace of a FRET efficiency measurement at the A_1 Fl3 CFP receptor sensor. **(C)** FRET efficiency values of A_1 Fl3 CFP L88A, N254A and H251A compared to unmutated receptor sensor without 24 h theophylline (5 mM) preincubation (upper diagram) and with 24 h theophylline (5 mM) preincubation (lower diagram) before experiment. Columns show the mean of 10 to 15 single FRET experiments investigated at 3 days, errors are depicted as S.E.M.

In figure 4.11 A, from the left to the right, FRET efficiency values given in (%)

are 16 (A_1 Fl3 CFP), 16 (A_1 Fl3 CFP I69V), 14 (A_1 Fl3 CFP L88A), 16 (A_1 Fl3 CFP T91A), 17 (A_1 Fl3 CFP W247A), 15 (A_1 Fl3 CFP H251A), 14 (A_1 Fl3 CFP N254A), 12 (A_1 Fl3 CFP H264A), 15 (A_1 Fl3 CFP T277A) and 14 (A_1 Fl3 CFP T277S). Thus all receptor sensors established were able to perform FRET and this ability was not disturbed via an amino acid mutation.

For mutations A_1 Fl3 CFP L88A, A_1 Fl3 CFP H251A and A_1 Fl3 CFP N254A 24 h preincubation with cell culture medium containing 5 mM theophylline was necessary before experiment to obtain former stated FRET efficiency values. Lower diagram of figure 4.11 C shows FRET efficacy values of these particular mutants in comparison to A_1 Fl3 CFP with theophylline pretreatment (figure 4.11 C, lower diagram) and without this pretreatment (figure 4.11 C, upper diagram). FRET efficiency measurements without theophylline pretreatment led to following values (given in %): 12 (A_1 Fl3 CFP L88A) and 8 (A_1 Fl3 CFP N254A). The value of A_1 Fl3 CFP H251A (15 %) was not distinct from the value examined after theophylline pretreatment.

As elucidated in the sections before, the fluorescent receptor sensor A_1 Fl3 CFP was investigated for the purpose of examining receptor movements that occur in the ligand binding process. Like shown in a previous section FRET measurements with the physiological agonist adenosine were successful where exposure of receptor sensor to adenosine led to a change in FRET ratio. While FRET ratio increased for A_1 Fl3 CFP receptor sensor upon agonist stimulation it decreased for the former investigated A_{2A} Fl3 CFP receptor sensor [118] (see figure 4.2 A). Introduced A_1 Fl3 CFP receptor sensor single amino acid mutations were also probed regarding their ability to perform FRET upon stimulation with adenosine to elucidate their influence in ligand binding process. NECA and CPA as further agonists and theophylline as an antagonist were also tested. Outcome of these FRET measurements will be reported in the following sections. Table 4.3 gives an overview of EC_{50}- and K_i-values investigated at the A_1 Fl3 CFP receptor sensor and its mutants.

A$_1$ Fl3 CFP	Adenosine EC$_{50}$ [μM] (95 % CI)	fold Shift	CPA EC$_{50}$ [μM] (95 % CI)	fold Shift	NECA EC$_{50}$ [μM] (95 % CI)	fold Shift	Theophylline K$_i$ [μM] (95 % CI)	fold Shift
wt	6.4 (4.2-9.7)		3.9 (2.6-6.1)		2.6 (1.2-3.4)		7.2 (5.8-8.9)	
I69V (2.64)	48.7 (42.4-56)	8	40.9 (20.3-80.3)	11	11.4 (8.6-15.1)	4	7.6 (6.1-9.5)	1
L88A (3.33)	107.8 (82.7-140.5)	17	15.4 (6.7-35.3)	4	71.6 (57.2-89.7)	28	77.7 (50.6-119.4)	11
T91A (3.36)	>1000	>1000	>100	>100	>100	>100	ND	ND
W247A (6.48)	12.6 (8.9-17.6)	2	1.1 (0.4-2.7)	0.3	14.7 (7.0-30.9)	6	1.3 (0.7-2.4)	0.2
H251A (6.52)	19.8 (13.1-130.1)	3	4.3 (1.8-10.6)	1	NE	NE	25.4 (19.0-34.0)	4
N254A (6.55)	>1000	>1000	13.7 (8.0-23.4)	3	>100	>100	ND	ND
H264A (6.66)	12.1 (9.3-15.7)	2	0.7 (0.4-1.3)	0.2	1.1 (0.7-1.9)	0.4	15.9 (12.1-20.2)	2
T277A (7.42)	>1000	>1000	>100	>100	>100	>100	ND	ND
T277S (7.42)	16.4 (12.0-22.4)	3	2.2 (1.2-4.2)	0.6	2.7 (2.0-3.8)	1	8.8 (7.2-10.6)	1

Table 4.3: K$_i$- and EC$_{50}$-values investigated at A$_1$ Fl3 CFP receptor sensor and its mutants (ND: not determined; NE: not evaluable)

4.1.6.2 Comparison of adenosine affinity for locally corresponding mutations in the A$_1$ Fl3 CFP and A$_{2A}$ Fl3 CFP receptor sensor

Agonist concentration dependent alteration in FRET ratio with the physiological agonist adenosine showed differences between mutation of the locally corresponding amino acids in the A$_1$ Fl3 CFP compared to mutations in the A$_{2A}$ Fl3 CFP receptor sensor.
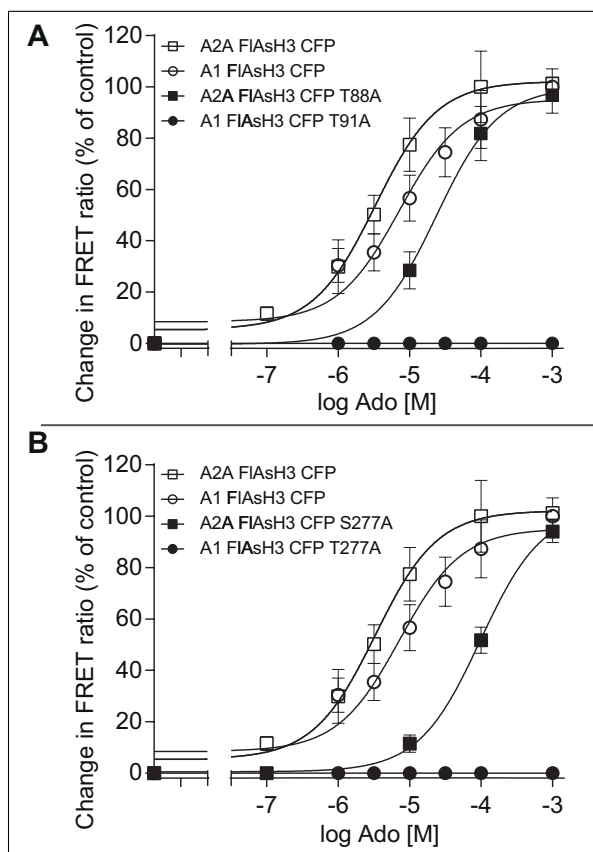

Figure 4.12: Comparison of adenosine affinity derived from FRET measurements with adenosine. Concentrations of adenosine (given as log of adenosine [M]) are related to the change in FRET ratio that is given in % change of control, 1 mM adenosine was set as 100 %. **(A)** Concentration response curves of A$_1$ Fl3 CFP (open circles), A$_1$ Fl3 CFP T91A (filled circles), A$_{2A}$ Fl3 CFP (open squares) and A$_{2A}$ Fl3 CFP T88A (filled squares). **(B)** Concentration response curves of A$_1$ Fl3 CFP (open circles), A$_1$ Fl3 CFP T277A (filled circles), A$_{2A}$ Fl3 CFP (open squares) and A$_{2A}$ Fl3 CFP T277A (filled squares). Data points show the mean of 10 to 15 single FRET experiments investigated at 3 days, errors are depicted as S.E.M.

The change in FRET ratio, given in % change of control (1000 μM adenosine was set as 100 %), was observed in relation to different concentrations of adenosine (given

as log of adenosine [M]). In detail there was a comparison of the outcomes of FRET experiments with adenosine at A_1 Fl3 CFP, A_1 Fl3 CFP T91A, A_1 Fl3 CFP T277A and A_{2A} Fl3 CFP, A_{2A} Fl3 CFP T88A and A_{2A} Fl3 CFP S277A.

The A_{2A} Fl3 CFP receptor sensor had a slightly higher affinity for adenosine (EC_{50}= 2 μM) (open squares, figure 4.12 A) than the A_1 Fl3 CFP (EC_{50}= 6.4 μM) (open circles, figure 4.12 A). The A_{2A} Fl3 CFP T88A mutant (EC_{50}= 23.7 μM) (filled squares, figure 4.12 A) had a 12 fold shift in ligand affinity compared to A_{2A} Fl3 CFP. But for the corresponding mutation in A_1 Fl3 CFP which is T91A (filled circles, figure 4.12 A) there was no change in FRET ratio detectable up to concentrations of 1000 μM adenosine. Hence, there was a more than 1000 fold decrease in ligand affinity for the mutant in the A_1 Fl3 CFP compared to the not mutated receptor sensor (figure 4.12 A). There were other mutants that showed the same phenomenon. A_{2A} Fl3 CFP S277A mutant (filled squares, figure 4.12 B) had a 43 fold loss in ligand affinity compared to not mutated A_{2A} Fl3 CFP receptor sensor. For mutation of the same numerical position in A_1 Fl3 CFP, namely T277A (filled circles, figure 4.12 B) there was no change in FRET ratio detectable up to concentrations of 1000 μM adenosine. Further FRET measurements with the ribose-modified adenosine derivative NECA and the N^6-adenine-modified adenosine derivative CPA at A_1 Fl3 CFP, A_1 Fl3 CFP T91A and A_1 Fl3 CFP T277A led to the same results. Up to concentrations of 100 μM CPA or NECA there was no change in FRET ratio detectable, neither for A_1 Fl3 CFP T91A nor for A_1 Fl3 CFP T277A. Thus ligand affinity of A_1 Fl3 CFP T91A and A_1 Fl3 CFP T277A was decreased more than 100 fold for NECA and CPA when compared to affinity of these ligands at A_1 Fl3 CFP (table 4.3).

4.1.6.3 Theophylline pretreatment of A_1 Fl3 CFP L88A, A_1 Fl3 CFP H251A and A_1 Fl3 CFP N254A and the effect on FRET experiments

Confocal analysis that were described in a previous section showed that A_1 Fl3 CFP L88A, A_1 Fl3 CFP H251A and A_1 Fl3 CFP N254A were only properly expressed in plasma membrane of cells when they were preincubated with cell culture medium containing 5 mM theophylline. Now the impact of this pretreatment regarding the outcome of FRET experiments was investigated. The small adenosine receptor antagonist theophylline was added to cells 24 h before experiments were carried out. Theophylline was removed from cells just before measurement through washing steps during the FlAsH labeling procedure [162]. If labeling procedure was not

required theophylline containing medium was replaced through measuring buffer before experiments.

If FRET experiments with these particular mutants were performed without the theophylline pretreatment changes in FRET ratio were not detectable in experiments where up to 1000 μM adenosine and 100 μM CPA or NECA were investigated (compare figure 4.13).
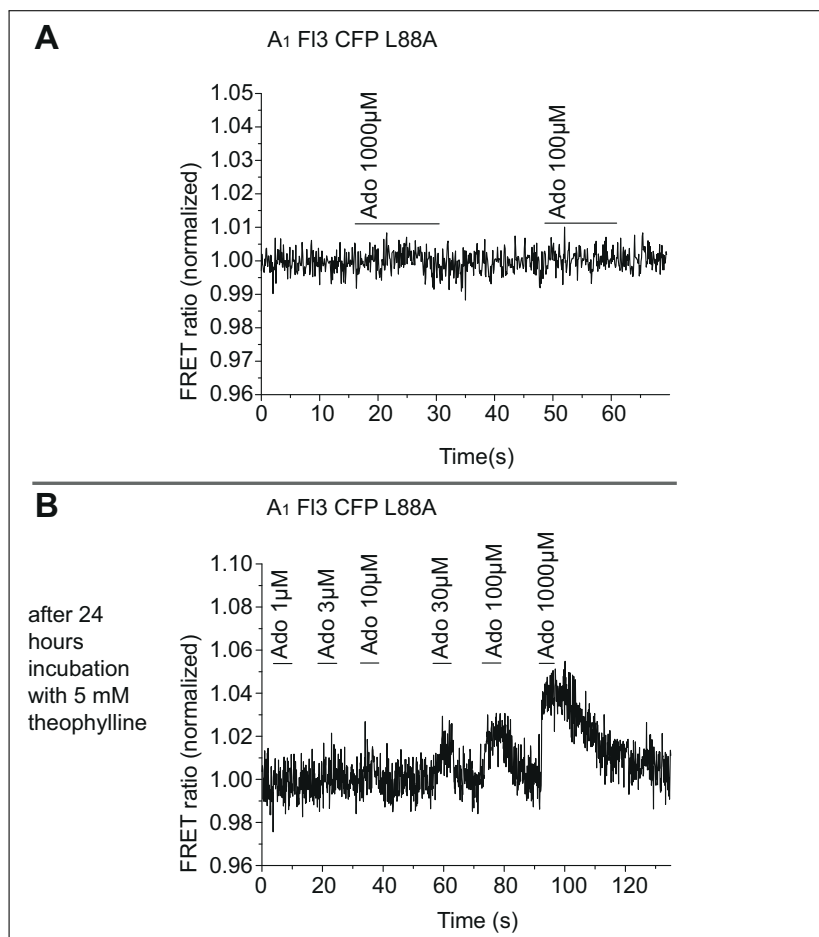

Figure 4.13: Representative single cell FRET measurements with adenosine at A_1 Fl3 CFP L88A. **(A)** Not pretreated A_1 Fl3 CFP L88A did not show a change in FRET ratio when exposed to concentrations up to 1000 μM adenosine. **(B)** A_1 Fl3 CFP L88A preincubated with 5 mM theophylline for 24 h before experiment led to observable changes in FRET ratio

After pretreatment with theophylline a change in FRET ratio could be observed for A_1 Fl3 CFP L88A during FRET measurements (figure 4.13 B). The mutants' ligand affinity for adenosine was 17 fold decreased compared to not mutated A_1 Fl3 CFP receptor sensor (table 4.3), 4 fold decreased for CPA and 28 fold decreased for

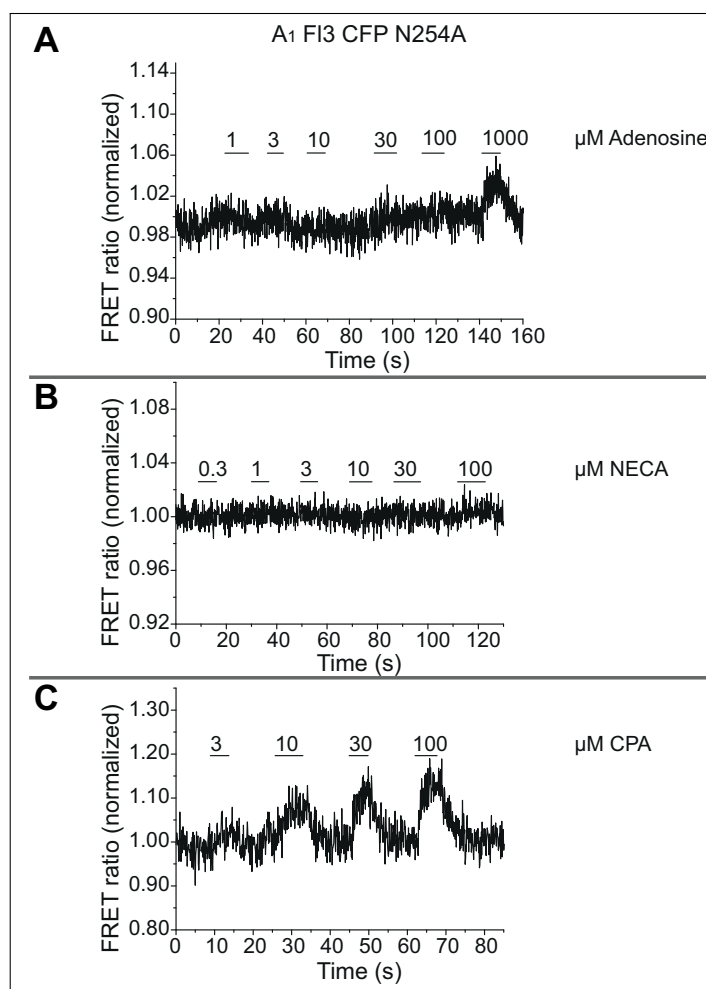NECA if compared to A_1 Fl3 CFP (table 4.3).

Figure 4.14: Comparison of representative single cell FRET experiments with A_1 Fl3 CFP N254A mutant, preincubated with theophylline. **(A)** For adenosine a change in FRET ratio was observable when adenosine concentration reached 1000 μM. **(B)** No change in FRET ratio was detectable when A_1 Fl3 CFP N254A was supplemented with NECA up to concentrations of 100 μM. **(C)** CPA induced changes in FRET ratio at A_1 Fl3 CFP N254A mutant that were detectable from 3 μM CPA on.

For A_1 Fl3 CFP N254A behavior in FRET experiments was different concerning ligand binding affinities, this mutant was also preincubated with theophylline before experiments. For adenosine a change in FRET ratio was observed when agonist concentration reached 1000 μM. Hence, this mutant has an at least 1000 fold decrease in ligand affinity for adenosine compared to unmutated A_1 Fl3 CFP receptor sensor. Regarding NECA a change in FRET ratio was not detectable up to 100 μM so there

was a more than 100 fold decrease in ligand affinity compared to A_1 Fl3 CFP. FRET experiments with the adenosine derivative CPA showed that there was a threefold decrease in ligand affinity ($EC_{50}= 13.7 \ \mu$M) compared to A_1 Fl3 CFP (table 4.3, figure 4.14).
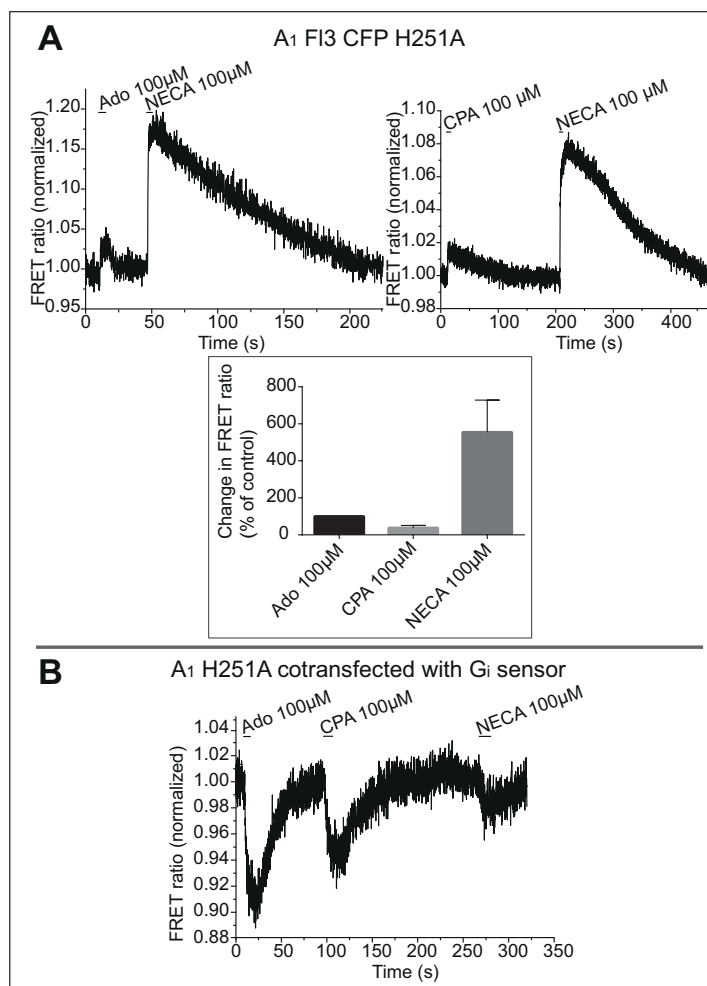

Figure 4.15: Representative FRET experiments of A_1 H251A mutant where cells were pretreated with 5 mM theophylline 24 h before experiments. **(A)** FRET measurement with A_1 Fl3 CFP H251A where change in FRET ratio was examined for adenosine 100 μM and NECA 100 μM (left FRET trace) and CPA 100 μM and NECA 100 μM (right FRET trace). Correlated to adenosine 100 μM that was set at 100 % (black column) CPA 100 μM showed a change in FRET ratio of 38 % and NECA 100 μM showed a change in FRET ratio of 555 % (gray columns). Columns show the mean of 10 to 15 single FRET experiments investigated at 3 days, errors are depicted as S.E.M. **(B)** FRET measurement of A_1 H251A receptor mutant co-transfected with G_i FRET sensor with adenosine 100 μM, CPA 100 μM and NECA 100 μM led to a change in FRET ratio.

A$_1$ Fl3 CFP H251A was the third mutant in this study that needed 24 h preincubation with 5 mM theophylline before experiments to express receptor in the plasma membrane. This mutant had a 3 fold decrease in adenosine affinity (EC$_{50}$= 19.8 μM) compared to A$_1$ Fl3 CFP (table 4.3). For CPA A$_1$ Fl3 CFP H251A had an affinity that was marginally different (EC$_{50}$= 4.3 μM) from that of A$_1$ Fl3 CFP (table 4.3). During FRET experiments it was observed that NECA induced huge changes in FRET ratio and remarkably long off rates compared to adenosine and CPA, the other ligands investigated at A$_1$ Fl3 CFP H251A. As previously described, cells were permanently superfused with measuring buffer or ligand during FRET experiments. The long off rates of H251A mutant would lead to very long experiment times and the liquid volume caused by the permanent flow of the FRET perfusion system would exceed the volume of the "Attofluor" cell chamber used. For this reason it was not feasible to examine a concentration response curve and therefore EC$_{50}$ value for NECA regarding this particular mutant. To investigate this mutant further comparative FRET measurements were performed at A$_1$ Fl3 CFP H251A where adenosine, CPA and NECA were examined, each concentrated 100 μM and the effect caused by the ligands was compared (representative FRET experiments are shown in figure 4.15 A). When changes in FRET ratio evoked by 100 μM adenosine, CPA or NECA were compared to each other for this particular mutant, CPA caused a statistically significant decrease in change in FRET ratio with 38 % correlated to adenosine which was set as 100 % (unpaired t test p < 0.0001). NECA 100 μM caused a statistically significant increase in change of FRET ratio correlated to adenosine 100 μM (unpaired t test p < 0.006) of 555 % at A$_1$ Fl3 CFP H251A when compared to adenosine 100 μM (figure 4.15 A, column diagram).

For investigation of impact on intracellular signaling A$_1$R mutant H251A was co-expressed with G$_i$ FRET sensor and FRET experiments were performed with 100 μM adenosine, CPA or NECA (representative FRET experiment in figure 4.15 B). When changes in FRET ratio of different ligands were compared to each other adenosine and CPA caused clearly visible changes in FRET ratio that did not differ significantly from each other when adenosine 100 μM was set as 100 %. But NECA induced only a change in FRET ratio of 32 % when compared to adenosine. If unmutated A$_1$R sensor was co-expressed with G$_i$ FRET sensor there were only marginal differences concerning change in FRET ratio when comparing ligands adenosine, NECA and CPA, each concentrated 100 μM (figure 4.18 A, left column).

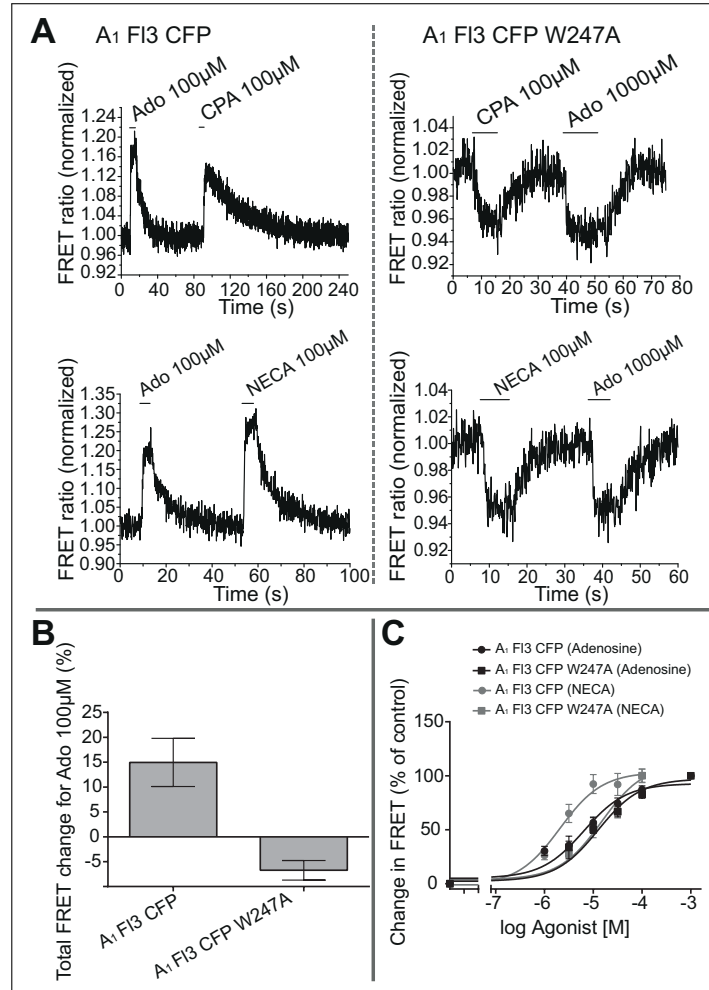### 4.1.6.4 Mutation in A_1R position W247 (6.48) - impact on FRET experiments

Figure 4.16: (A) Representative FRET experiments of A_1 Fl3 CFP and W247A mutant with adenosine, NECA and CPA (each concentrated 100 μM). Left column shows FRET traces with the unmutated A_1 Fl3 CFP receptor sensor and right column shows traces of A_1 Fl3 CFP W247A mutant. First row: FRET measurements with adenosine 100 or 1000μM and CPA 100 μM. Second row: FRET measurements with adenosine 100 μM or 1000 μM and NECA 100μM. **(B)** Comparison of total change in FRET ratio with adenosine 100 μM at A_1 Fl3 CFP and W247A mutant. Columns show the mean of 10 to 15 single FRET experiments investigated at 3 days, errors are depicted as S.E.M. **(C)** Concentration response curves for adenosine at A_1 Fl3 CFP W247A (black squares) and A_1 Fl3 CFP (black circles) and concentration response curves for NECA at A_1 Fl3 CFP W247A (gray squares) and A_1 Fl3 CFP (gray circles).

Comparison of FRET traces derived from different A_1R sensors exhibited striking differences between A_1 Fl3 CFP and A_1 Fl3 CFP W247A. Upon ligand stimulation FRET ratio decreased for A_1 Fl3 CFP W247A mutant instead of an increase as it was could be observed for A_1 Fl3 CFP and all its other mutants during FRET experiments (figure 4.16 A, B). This effect was valid for all agonists tested. The next markedly difference were overall smaller FRET ratio amplitudes that could be observed for A_1 Fl3 CFP W247A mutant compared to unmutated receptor sensor. This phenomenon is elucidated at adenosine where mean absolute value change in FRET ratio was 15 % at A_1 Fl3 CFP and 7 % at A_1 Fl3 CFP W247A which was a statistically smaller amplitude in FRET ratio (unpaired t test p < 0.0001) (figure 4.16 B). Following FRET experiments concentration response curves were investigated for A_1 Fl3 CFP W247A mutant compared to unmutated receptor sensor. The shift in ligand affinity was only 2 fold for adenosine (EC_{50}= 12.6 μM) when A_1 Fl3 CFP W247A (black squares, figure 4.16 C) was compared to A_1 Fl3 CFP (black circles, figure 4.16 C), but for NECA a 6 fold decrease in ligand affinity (EC_{50}= 14.7 μM) was observed at A_1 Fl3 CFP W247A (gray squares, figure 4.16 C) compared to A_1 Fl3 CFP (gray circles, figure 4.16 C). NECA (gray circles, figure 4.16 C) had an about 3 fold increase in ligand affinity compared to adenosine for A_1 Fl3 CFP (black open circles, figure 4.16 C).

In previous studies it was examined that mutation of single amino acids in GPCR structure could lead to constitutive activity of receptor [83][179][180]. FRET based approaches could confirm these findings [181][182]. In these studies it was successfully shown that fluorescent receptor sensors could indicate altered receptor movement through a change in FRET ratio direction. The alteration of FRET ratio direction was found to be indicative for inverse agonism of a distinct ligand at a receptor where direction of FRET ratio changed for the inverse agonist ligand compared to an agonist [181].

Tryptophan in position 6.48 is very conserved among class A GPCRs [183] and involved in formation of the CWxP motif. It was found to act as a rotamer toggle switch for inactive to active state of receptors and to be linked to regulation of constitutive activity [184][180]. As this amino acid was mutated to an alanine in the A_1 Fl3 CFP receptor sensor within this work it was of particular interest for further investigations. Constitutively active receptors are characterized by an enhanced basal activity that could be quantified with increased levels of intracellular second messengers [179]. Thus to get insight into effect of this mutant concerning

downstream signaling of receptor it was investigated with examination of adenylate cyclase activity which is a commonly used method to investigate constitutive activity in G_i-coupled GPCRs [179]. Inhibitory adenylate cyclase assay was performed with A_1 Fl3 CFP and A_1 Fl3 CFP W247A (figure 4.17).
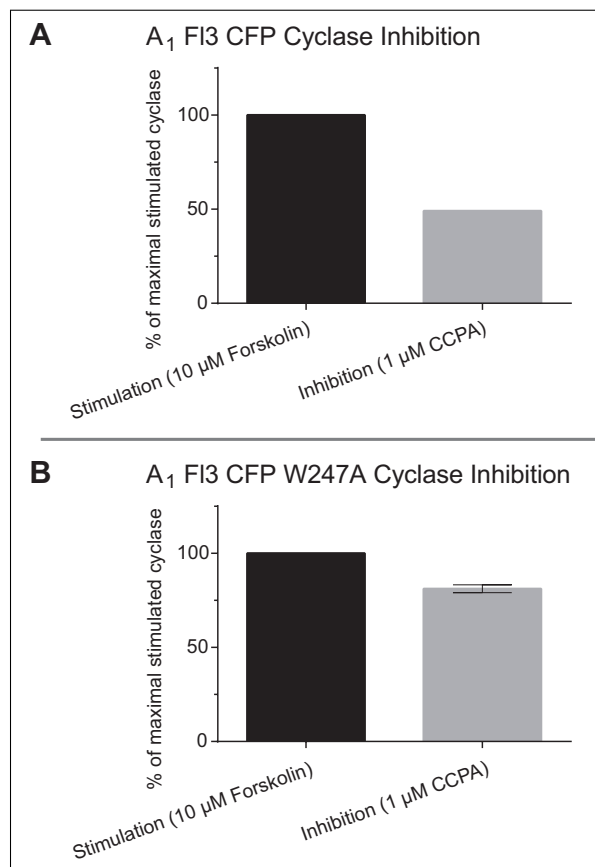

Figure 4.17: Inhibitory adenylate cyclase assay with **(A)** A_1 Fl3 CFP (outcome of one single experiment performed in triplicate) and **(B)** A_1 Fl3 CFP W247A (mean of 3 experiments performed in triplicate). In both cases forskolin-stimulated adenylate cyclase (black column) could be inhibited through G_i-protein via receptor activation with the A_1R-selective agonist CCPA (gray column).

Stimulation of adenylate cyclase with 10 μM forskolin and G_i protein mediated inhibition of adenylate cyclase with 1 μM CCPA was successful for unmutated receptor sensor (figure 4.17 A) where signal of stimulated adenylate cyclase that was set as 100 % (black column) was higher than signal of inhibited adenylate cyclase (gray column, 49 %). For the W247A mutant there was also a decrease in adenylate cyclase activity observable (figure 4.17 B) when stimulated adenylate cyclase (black column, set as 100 %) was compared to inhibited adenylate cyclase (gray column, 78

%). Thus both receptor sensors were functional concerning inhibition of adenylate cyclase and W247A mutant showed no constitutive activity.
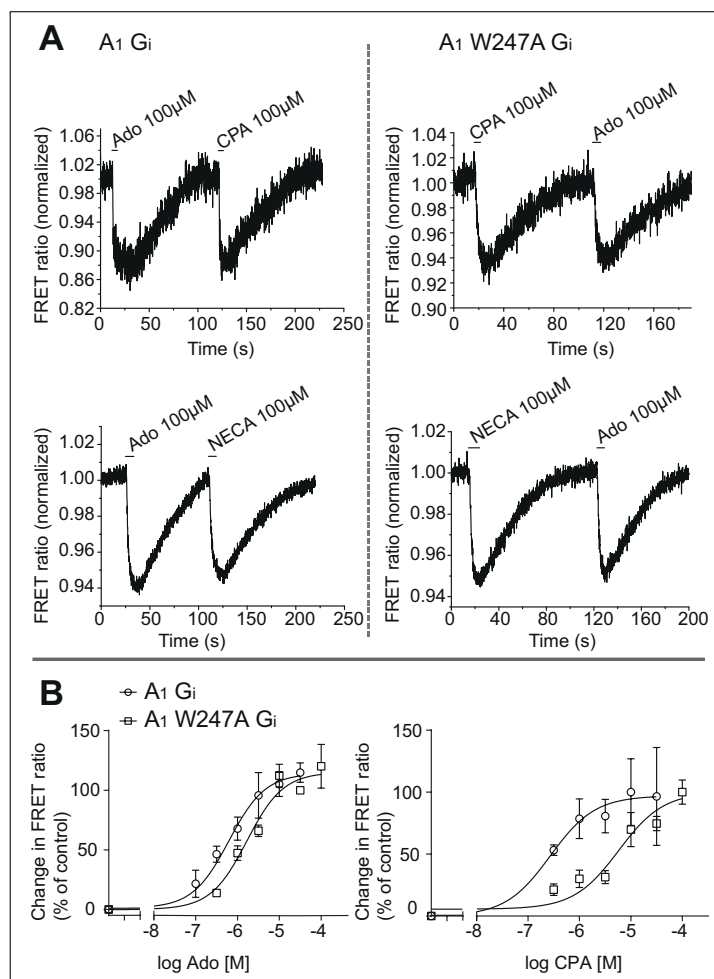

Figure 4.18: Comparison of representative FRET measurements for adenosine, NECA and CPA (100 μM each) and comparison of concentration response curves for adenosine and CPA of A_1R and A_1R W247A mutant each co-transfected with G_i FRET sensor. **(A)** Left column: FRET experiments with A_1R. Right column: FRET experiments with A_1R W247A. First row: FRET experiments with 100 μM adenosine and 100 μM CPA. **(B)** Comparison of concentration response curves (given in log [M]of ligand) of A_1R (open circles) and A_1R W247A (open squares) for adenosine (left curves) and CPA (right curves).

To investigate the effect of this mutant further, intracellular G-protein signaling was examined. A_1R and the A_1R W247A mutant, both without fluorophores, were co-transfected with G_i FRET sensor and FRET experiments were performed with adenosine, NECA and CPA (figure 4.18 A). Both receptors A_1R and A_1R W247A

were functional when they were co-expressed with G_i FRET sensor, changes in FRET ratio were visible for all three ligands tested and FRET ratio went in the same direction for unmutated and W247A-mutated receptor. Investigated EC_{50} values for adenosine were 3 fold decreased (EC_{50}= 1.7 μM) for A_1R W247A (open squares, left curve, figure 4.18 B) compared to A_1R (EC_{50}= 0.6 μM) (open circles, left curve, figure 4.18 B). The A_1R selective agonist CPA was 19 fold decreased in A_1R W247A (EC_{50}= 5.8μM) (open squares, right curve, figure 4.18 B) compared to unmutated A_1R (EC_{50}= 0.3μM) (open circles, left curve, figure 4.18 B).

4.1.6.5 Competitive FRET measurements with theophylline and adenosine at A_1 Fl3 CFP and its mutants - investigation of Ki values

The FlAsH CFP based FRET sensors utilized here elucidate conformational changes in the receptor that, given regular receptor function, only occur when agonists bind to the receptor [182]. Thus for investigation of the impact of an antagonist at these receptor sensors competitive FRET measurements are required. As CPA has a high affinity and slow dissociation times at A_1R it was not suitable for this approach and adenosine was the agonist of choice. EC_{50} values of adenosine for A_1 Fl3 CFP and each of its mutants were taken as a base for calculation. Concentrations in the nearly saturating range of adenosine, about 80 % of the EC_{50} value of the particular receptor sensor, were used for FRET experiments as previously investigated for the A_{2A}R [170]. Only mutants were investigated where EC_{50} value could be investigated in former described FRET measurements. Thus mutations T91A, N254A and T277A of A_1 Fl3 CFP receptor sensor could not be examined in this kind of experiments. Their EC_{50} values where either not determinable under the experimental conditions employed here or the values determined were so huge that ligand concentration resulting for experiments was not suitable for perfusion system used. The remaining mutants were investigated with help of adenosine solutions with following concentrations: 50 μM (A_1 Fl3 CFP, T277S, H264A), 200 μM (I69V, W247A) and 1000 μM (L88A, H251A). As described before mutants A_1 Fl3 CFP L88A and H251A were preincubated for 24 h with 5 mM theophylline before experiments were carried out. These particular adenosine concentrations were then supplemented with increasing concentrations of the xanthine-derivative theophylline until change in FRET ratio induced via adenosine was completely blocked with theophylline (see figure 4.19 A for a representative experiment at the A_1 Fl3 CFP receptor sensor where change in FRET ratio induced through adenosine was totally blocked when theophylline con-

centration reached 3000 μM). With help of these competitive FRET measurements inhibitory concentration response curves for theophylline at A_1 Fl3 CFP and each of the mutants were investigated. The resulting IC_{50} values were the base for the K_i values calculated with help of Cheng-Prusoff equation (see table 4.3) [165].

$$K_i = \frac{IC_{50}}{1 + \frac{[S]}{K_m}} \tag{4.1}$$

Figure 4.19 B shows all inhibitory concentration response curves that were investigated at the A_1 Fl3 CFP receptor sensor and its mutants which were suitable for these experiments.
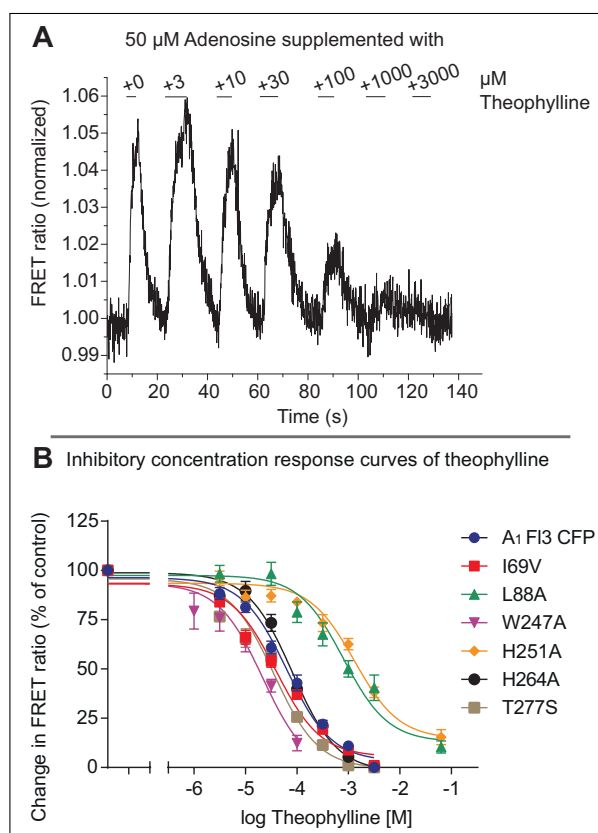

Figure 4.19: **(A)** Representative competitive FRET experiment at A_1 Fl3 CFP with adenosine 50 μM supplemented with increasing concentrations of theophylline. Change in FRET ratio decreased with increasing concentrations of theophylline. **(B)** Overview of inhibitory concentration response curves investigated at A_1 Fl3 CFP and mutants. Data points show the mean of 10 to 25 single FRET experiments investigated at at least 3 days, errors are depicted as S.E.M.

A_1 Fl3 CFP is depicted in blue (IC_{50}= 63.2 μM), I69V in red (IC_{50}= 38.8 μM),

L88A in green (IC_{50}= 798.7 μM), W247A in violet (IC_{50}= 21.6 μM), H251A in yellow (IC_{50}= 1310.0 μM), H264A in black (IC_{50}= 81.4 μM) and T277S in brown (IC_{50}= 35.5 μM). All inhibitory curves were about in the same range except the curves of L88A and H251A mutant that were right shifted compared to the rest. For K_i values calculated see table 4.3, K_i-value for theophylline at A_1R investigated in membrane based binding studies was 7 nM [67].

4.2 Investigation of N-terminally SNAP and CLIP tagged A_1 and A_{2A} receptor sensors

Sensor technique with FlAsH and CFP that was elucidated before is useful to monitor intramolecular dynamical receptor movements, N-terminal SNAP and CLIP labeling technique can help to make extracellular occurrences at receptor visible and help visualizing interactions between the so tagged receptor and other fluorescent targets. Within this work SNAP and CLIP tagged receptor sensors of A_1R and $A_{2A}R$ were developed and the design of these sensors is described hereafter.

First attempt was the development the CLIP A_1R and SNAP A_1R constructs where the SNAP- or CLIP- encoding sequence was placed at the N-terminal end of the A_1R sequence. Receptor sensors were cloned in pcDNA3 plasmid where the human A_1R was N-terminally tagged with the SNAP- or CLIP- encoding sequence. Resulting plasmids contained CLIP and SNAP tagged A_1R receptor sensors. Sensors could be multiplied with help of transformation in competent bacteria and HEK 293 cells stably expressing CLIP A_1R and SNAP A_1R sensor were generated. To investigate the success of transfection and receptor localization cells were labeled with CLIP-Surface^{TM} 547, CLIP-Surface^{TM} 647 or SNAP-Surface$^®$ 647 for confocal analysis. But visualization of receptor sensors via confocal imaging was not possible (figure 4.20, first row) with these not plasma membrane permeable dyes. Thus plasma membrane permeable dyes were used in the following approach that are able to visualize intracellular SNAP or CLIP tagged receptors. CLIP A_1R and SNAP A_1R sensors could be labeled inside cells with CLIP-Cell^{TM}-TMR-Star and SNAP-Cell$^®$-TMR-Star. This could be confirmed with confocal analysis (figure 4.20, second row). As an attempt to increase the amount of membranous receptor a flag export tag encoding the sequence *DYKDDDDK* was introduced between plasmid of either SNAP or CLIP sequence which results in a proper plasma membrane localization of the new developed receptor sensors named flag SNAP A_1 and flag CLIP A_1. This find-

ing could be confirmed via confocal analysis with successful labeling of flag SNAP A_1R and flag CLIP A_1R stably expressed in HEK 293 cells with CLIP-Surface^{TM} 547, SNAP-Surface$^®$ 549 or SNAP-Surface$^®$ 647 (figure 4.20, third row).
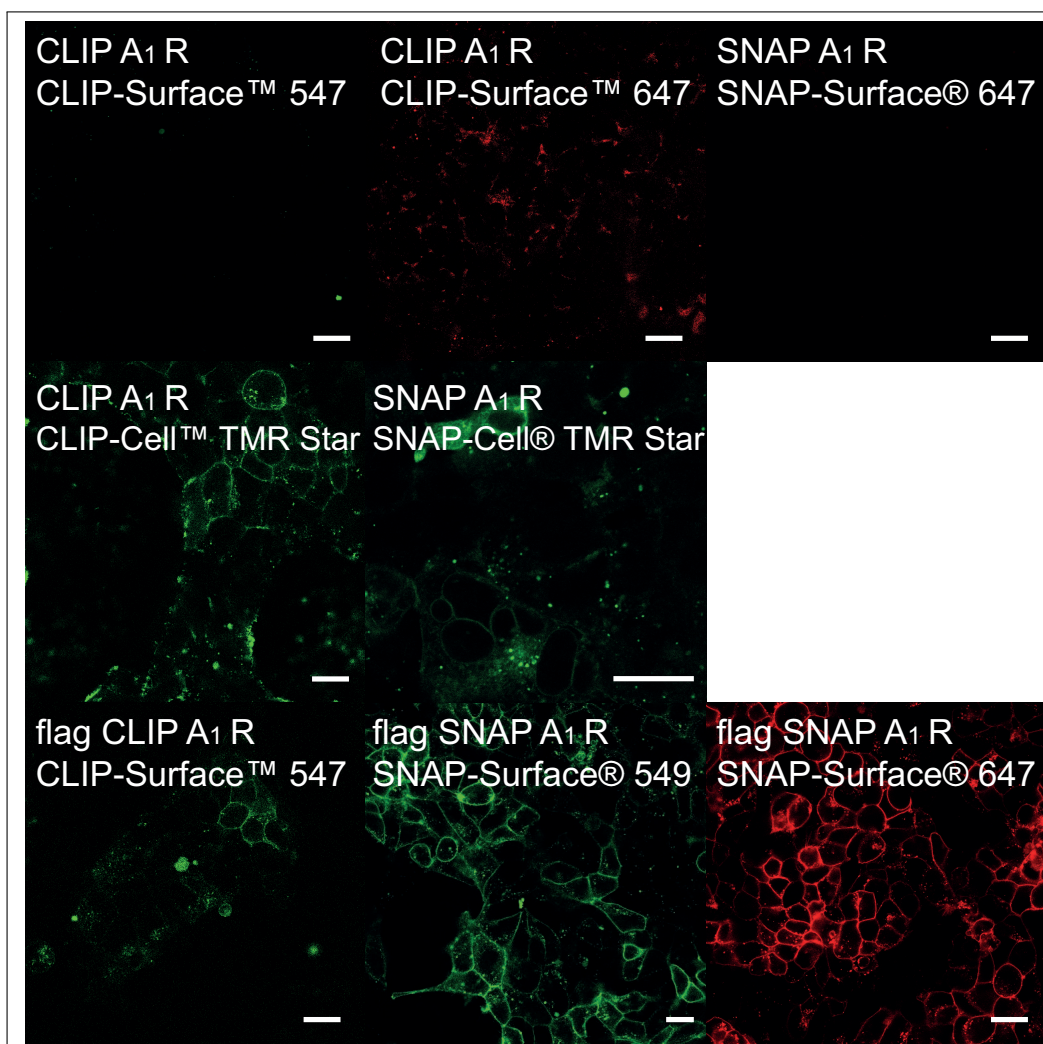

Figure 4.20: Confocal images of HEK 293 cells stably expressing A_1R tagged with CLIP or with SNAP. Images are described from left to right, white bars in the images refer to 20 μm. First row: CLIP A_1R labeled with CLIP-Surface^{TM} 547 and CLIP-Surface^{TM} 647, SNAP A_1R labeled with SNAP-Surface$^®$ 647. Second row: CLIP A_1R labeled with CLIP-Cell^{TM} TMR Star and SNAP A_1R labeled with SNAP-Cell$^®$ TMR Star. Third row: flag CLIP A_1R labeled with CLIP-Surface^{TM} 547 and flag SNAP A_1R labeled with SNAP-Surface$^®$ 549 and SNAP-Surface$^®$ 647.

The flag SNAP A_1R and flag CLIP A_1R sensors were the base of flag CLIP $A_{2A}R$ in pcDNA3 and flag SNAP $A_{2A}R$ in pcDNA3 where the human $A_{2A}R$ was N-terminally

tagged with the SNAP- or CLIP- encoding sequence with an upstream flag export tag that has the sequence *DYKDDDDK*. Flag SNAP A_{2A} and flag CLIP A_{2A} plasmid could be multiplied with help of competent bacteria and receptor sensors could be labeled with CLIP-Surface^{TM} 547, CLIP-Surface^{TM} 647, SNAP-Surface$^{®}$ 549 and SNAP-Surface$^{®}$ 647 as receptor sensors were located in the plasma membrane of HEK 293 cells stably expressing the receptor sensors (figure 4.21).
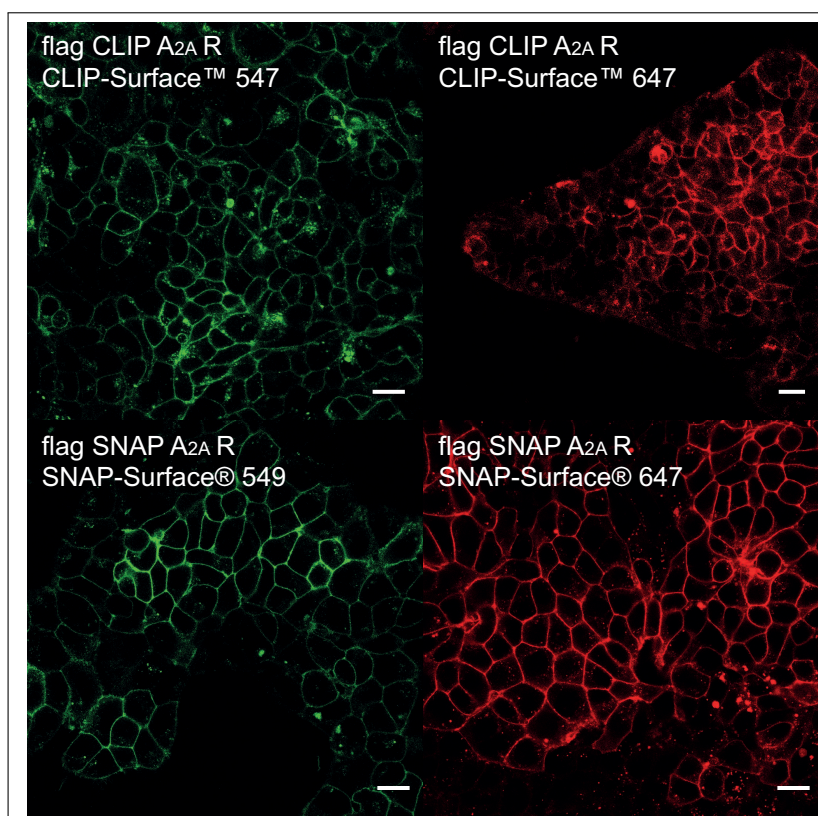

Figure 4.21: Confocal images of HEK 293 cells stably expressing flag A_{2A}R tagged with CLIP or with SNAP. Images are described from left to right, white bars in the images refer to 20 μm. First row: flag CLIP A_{2A}R labeled with CLIP-Surface^{TM} 547 and CLIP-Surface^{TM} 647. Second row: flag SNAP A_{2A}R labeled with SNAP-Surface$^{®}$ 549 and SNAP-Surface$^{®}$ 647.

It was also possible to label HEK 293 cells expressing either flag SNAP A_1R or flag CLIP A_{2A}R simultaneously. For this experiments HEK 293 cells stably expressing flag SNAP A_1R or flag CLIP A_{2A}R were seeded on the same cover-slip. First step was the labeling with CLIP-Surface^{TM} 647 after 30 min incubation SNAP-Surface$^{®}$ 549 labeling solution was added and after additional 30 min labeling solution was aspirated from cover-slips and not bound dye was washed off with cell

culture medium. Final concentration of each dye was 0.5 μM during labeling procedure. Cells expressing flag SNAP A_1R could be imaged through green fluorescence from SNAP-Surface$^{\textregistered}$ 549 and cells expressing flag CLIP A_{2A}R could be visualized through red fluorescence from CLIP-Surface^{TM} 647 (figure 4.22, first and second image). Overlay of both fluorescence detecting channels showed that there is no direct superposition of red and green fluorescence. Thus flag SNAP A_1R and flag CLIP A_{2A}R are separately expressed and specifically labeled (figure 4.22, third image).
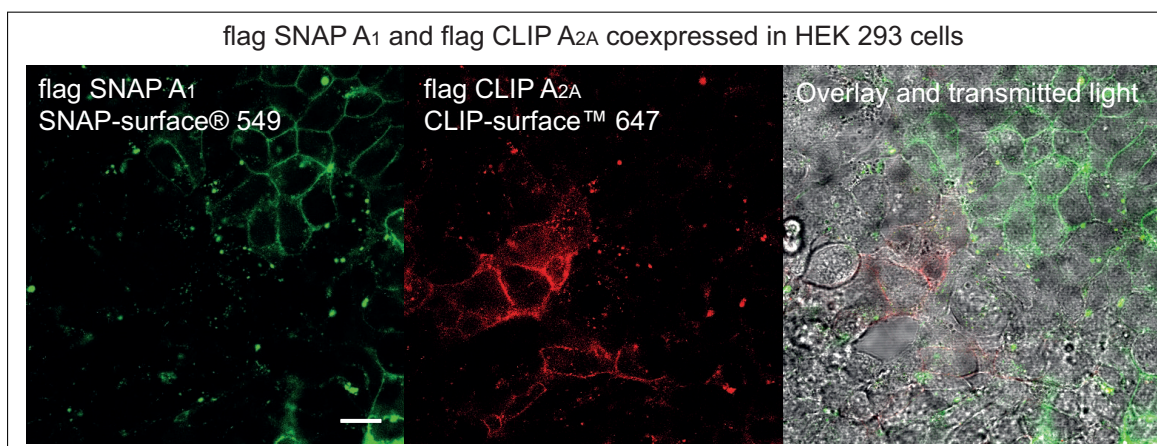

Figure 4.22: Confocal images of HEK 293 cells expressing either flag SNAP A_1R or flag CLIP A_{2A}R. White bar in the image refers to 20 μm. Cells were labeled with SNAP-Surface$^{\textregistered}$ 549 (first image) and CLIP-Surface^{TM} 647 (second image). Third image shows overlay of channels and transmitted light

As SNAP tagged receptors turned out to be more robust throughout experiments SNAP tagged receptor sensors flag SNAP A_1R and flag SNAP A_{2A}R were used for following examinations.

4.2.1 Characterization of flag SNAP A_1R and flag SNAP A_{2A}R

Confocal analysis confirmed that flag SNAP A_1R and flag SNAP A_{2A}R are located in the plasma membrane of cells and thus could be labeled with SNAP-Surface$^{\textregistered}$-dyes (compare figures 4.20, third row and 4.21).
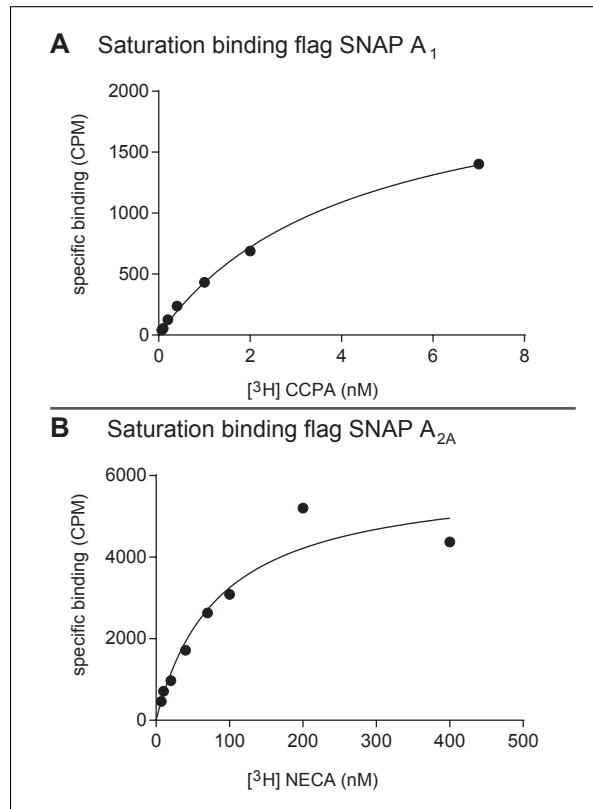
Figure 4.23: Representative saturation binding experiments of **(A)** flag SNAP A_1R with [^{3}H] CCPA and **(B)** of flag SNAP A_{2A}R with [^{3}H] NECA. Specific binding is depicted in both cases

For investigation of receptor sensor function saturation binding experiments with radioactively labeled agonists were performed. Experiments were carried out using the high affinity ligand [^{3}H] CCPA [169] for flag SNAP A_1R (figure 4.23 A). Examination led to an average K_d value of 5.7 nM which was about 10 fold increased regarding the K_d value investigated with membranes of the wild type human A_1R (0.5 nM) [67].

For flag SNAP A_{2A}R the radioactively labeled agonist [^{3}H] NECA was employed for saturation binding experiments (figure 4.23 B). The K_d value investigated was 80.4 nM which is in the range of K_d value (20.1 nM) that was previously published for human wild type A_{2A}R [67].

4.2.2 SNAP-tagged receptor sensors - binding experiments with fluorescent adenosine receptor ligands

As flag SNAP A_1R and flag SNAP $A_{2A}R$ showed localization in the plasma membrane of cells and revealed ligand binding functionality in saturation binding experiments these two receptor sensors were further examined with help of a fluorescence tagged adenosine receptor agonist and an antagonist. Fluorescent ligands were linked to BODIPY 630/650 fluorophore which is a fluorophore emitting light in the near infrared spectra range. Thus it is beneficial for a clear segregation of autofluorescence of amino acids [153]. Furthermore, this fluorophore provides high fluorescence intensity and low photobleaching [185]. The fluorescence-tagged agonist A-633-AG is a NECA derivative that is tagged with a linker and BODIPY 630/650 fluorophore [150][155]. The fluorescent antagonist A3-633-AN is a XAC derivative that is also tagged with a linker and BODIPY 630/650 fluorophore [156]. For structural details see chapter ligands-structures and properties. Figure 4.24 shows the principle of binding of a fluorescent ligand at a SNAP tagged receptor.
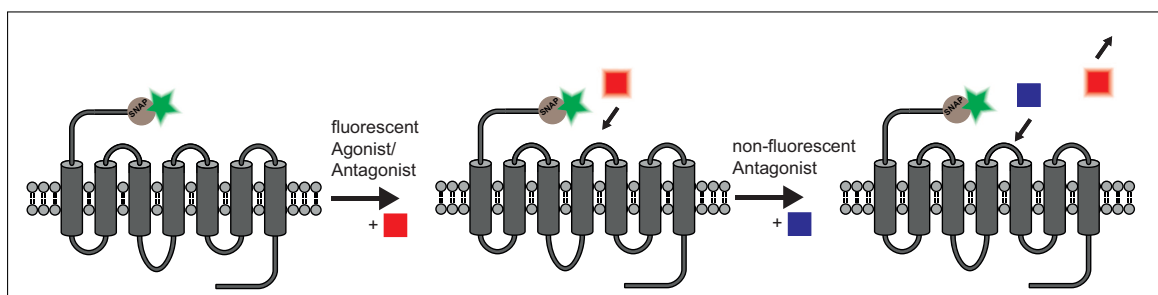

Figure 4.24: Principle of fluorescent ligand binding at a N-terminal SNAP tagged receptor sensor labeled with a green fluorescent dye. Fluorescent ligand that is labeled with a red fluorescent dye is displaced with a non-fluorescent antagonist from receptor sensor
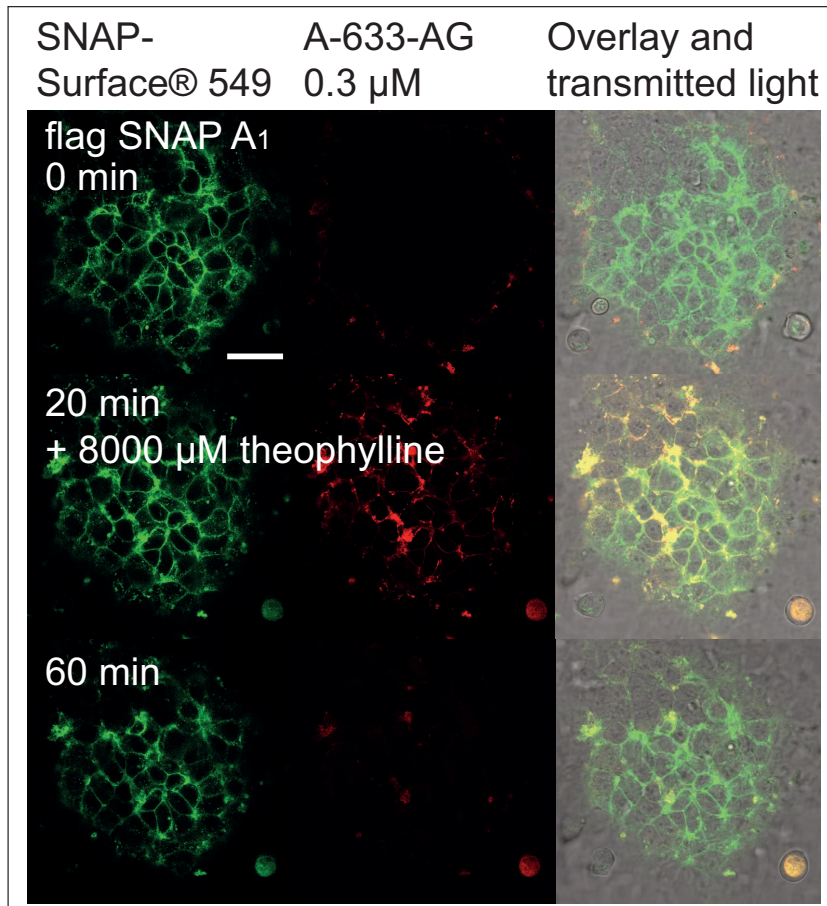
Figure 4.25: flag SNAP A_1R labeled with SNAP-Surface$^®$ 549 and supplemented with 0.3 μM A-633-AG at t= 0 min (first row), addition of 8000 μM theophylline at t= 20 min (second row) and competitive binding of both ligands until t= 60 min (third row). White bar refers to 20 μm

Confocal time series were carried out for flag SNAP A_1R using a final concentration of 0.3 μM A-633-AG that was pipetted to cells at beginning of the time series (figure 4.25). First binding of fluorescent ligand was observed just at the beginning of experiment. At t= 20min, red fluorescence that is indicative for ligand binding was clearly observable and antagonist theophylline with a final concentration of 8000 μM was added. After another 40 min theophylline was partly able to compete A-633-AG from its binding site. But the remaining red fluorescence indicates that not all A-633-AG was displaced from cells.
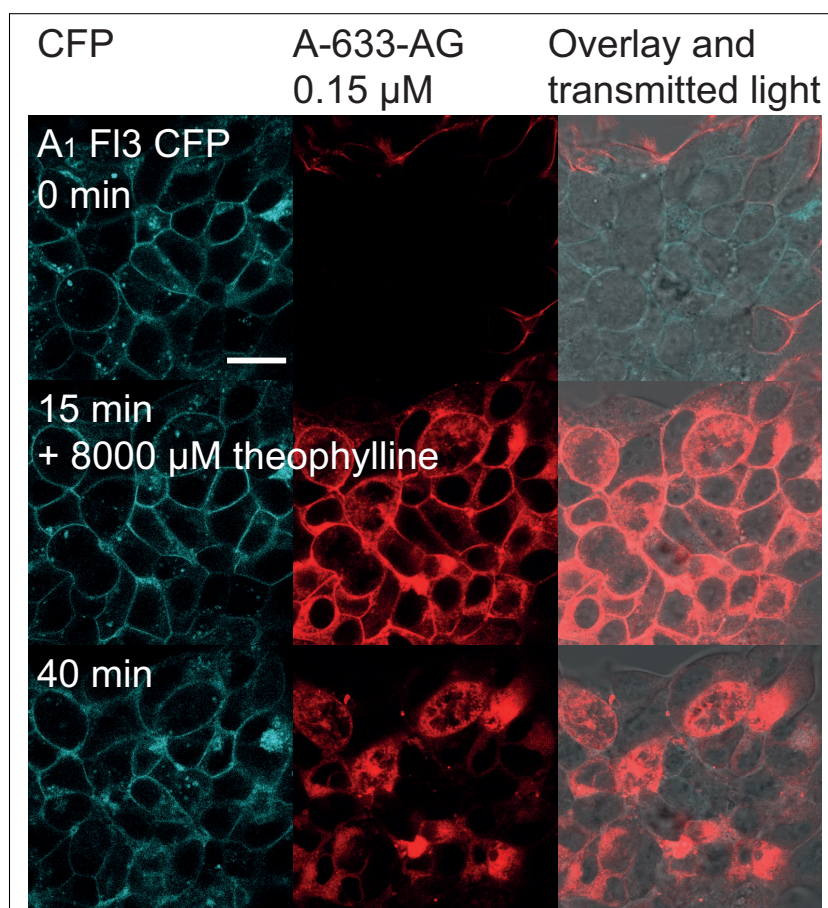
Figure 4.26: A$_1$ Fl3 CFP receptor sensor supplemented with A-633-AG 0.15 μM at t= 0 min (first row), addition of 8000 μM theophylline at t= 15 min (second row) and competitive binding of both ligands until t= 40 min (third row). White bar refers to 20 μm

For further investigation of the ligand binding behavior of the fluorescent agonist at the A$_1$R sensors, time series were performed with A$_1$ Fl3 CFP and A-633-AG. It could be shown that fluorescent ligand binding was successful at A$_1$ Fl3 CFP receptor sensor (figure 4.26). A-633-AG with a final concentration of 0.15 μM was pipetted to cells at t= 0 min. First binding of fluorescent agonist was observed just at beginning of time series. At t= 15 min binding of A-633-AG was distributed equally to all receptors labeled, which could be seen in an increase in red fluorescence from first to second row in figure 4.26. Now antagonist theophylline with a final concentration of 8000 μM was added to cells but was only partly able to displace fluorescent agonist within further 25 min.
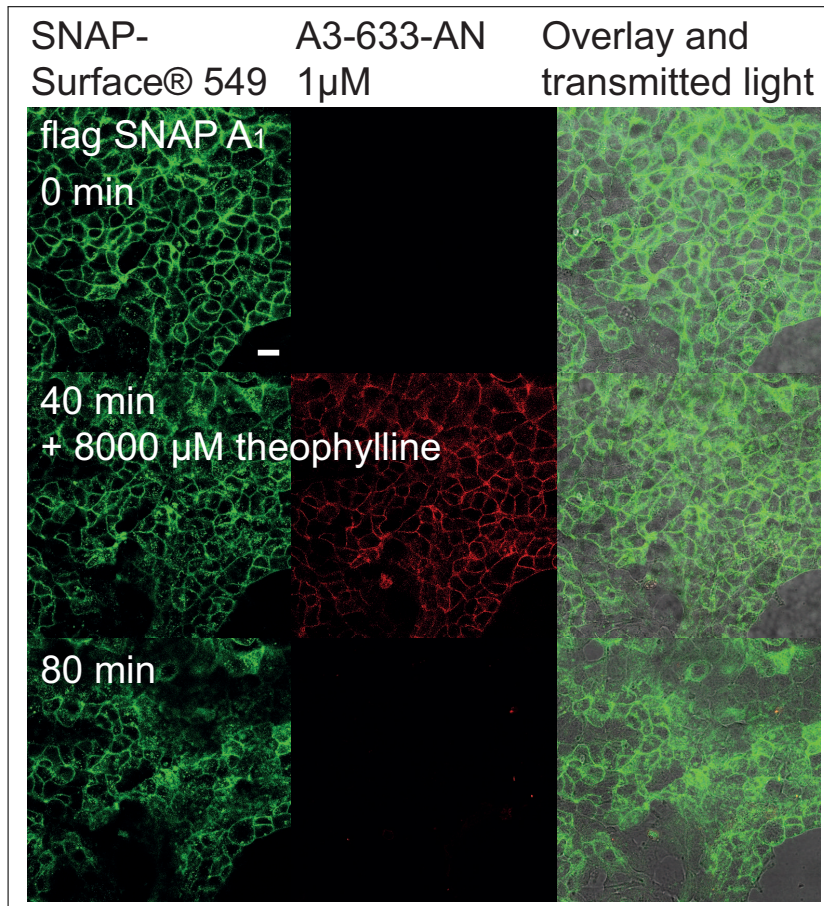
Figure 4.27: flag SNAP A_1R labeled with SNAP-Surface$^{\circledR}$ 549 and supplemented with A3-633-AN 1 μM at t= 0 min (first row), addition of 8000 μM theophylline at t= 40 min (second row) and competitive binding of both ligands until t= 80 min (third row). White bar refers to 20 μm

Fluorescent antagonist A3-633-AN (final concentration 1 μM) was investigated at flag SNAP A_1R and was like before, added to cells at beginning of experiment (figure 4.27). First binding of fluorescent antagonist was observed at t= 5 min. At t= 40min, red fluorescence that is indicative for binding of A3-633-AN was clearly visible at plasma membrane of cells and theophylline with a final concentration of 8000 μM was added. Another 40 min later theophylline was able to compete A-633-AG completely from its binding site.
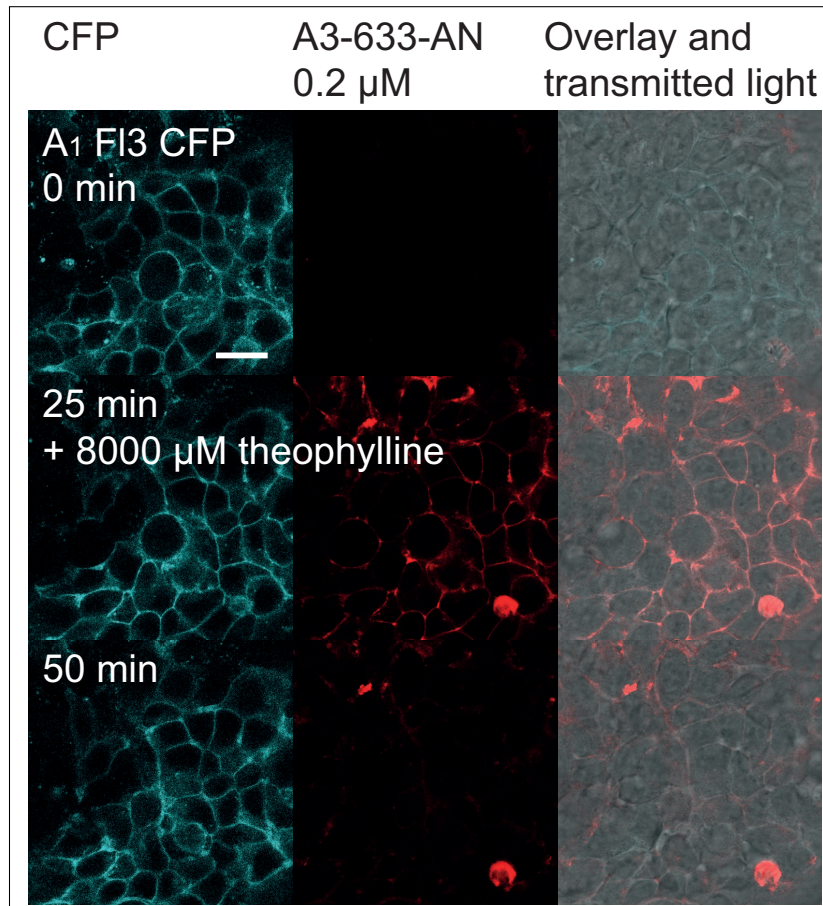
Figure 4.28: A$_1$ Fl3 CFP supplemented with A3-633-AN 0.2 μM at t= 0 min (first row), addition of 8000 μM theophylline at t= 25 min (second row) and competitive binding of both ligands until t= 50 min (third row). White bar refers to 20 μm

Additionally, binding behavior of fluorescent antagonist A3-633-AN was examined at cells expressing A$_1$ Fl3 CFP (figure 4.28). 0.2 μM A3-633-AN were added and first binding of fluorescent antagonist was observed immediately at beginning of time series. At t= 25 min binding of A3-633-AN was distributed equally to all receptors labeled, which could be seen in an increase in red fluorescence from first to second row in figure 4.28. Now antagonist theophylline with a final concentration of 8000 μM was added to cells and was able to displace fluorescent antagonist nearly complete within further 25 min.
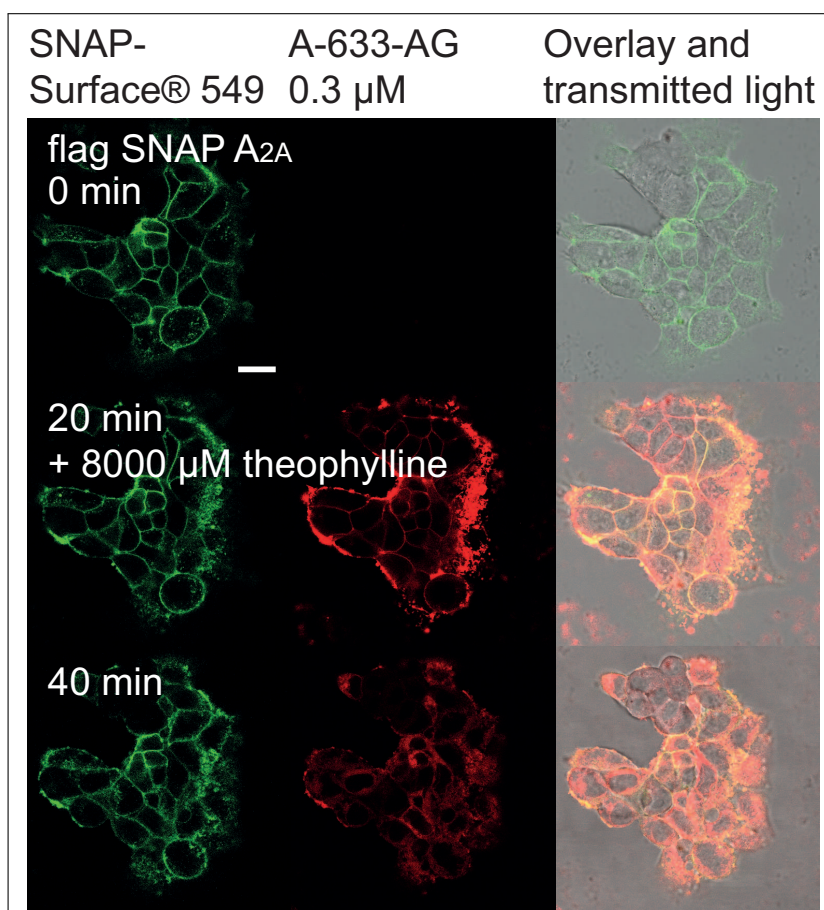
Figure 4.29: flag SNAP A$_{2A}$ labeled with SNAP-Surface$^{\textregistered}$ 549 supplemented with 0.3 μM A-633-AG at t= 0 min (first row), addition of 8000 μM theophylline at t= 20 min (second row) and competitive binding of both ligands until t= 40 min (third row). White bar refers to 20 μm

Fluorescent ligands were now investigated at the fluorescent A$_{2A}$ receptor sensors probed throughout this work. Flag SNAP A$_{2A}$, labeled with SNAP-Surface$^{\textregistered}$ 549, was examined with a final concentration of 0.3 μM A-633-AG that was added to cells at starting point of time series (figure 4.29). First binding was observed at t= 1 min and was clearly visible at t= 20 min. Now theophylline with a final concentration of 8000 μM was added to cells but was not able to displace fluorescent agonist of flag SNAP A$_{2A}$R within further 20 min.
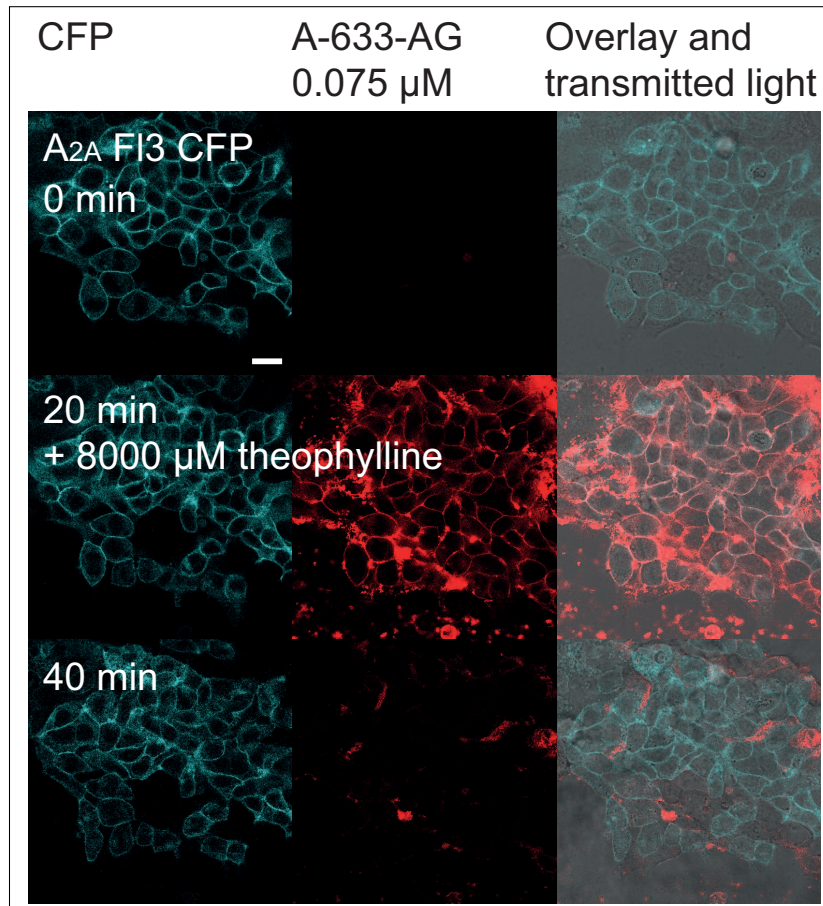
Figure 4.30: A_{2A} Fl3 CFP supplemented with 0.075 μM A-633-AG at t= 0 min (first row), addition of 8000 μM theophylline at t= 20 min (second row) and competitive binding of both ligands until t= 40 min (third row). White bar refers to 20 μm

For further investigation of A-633-AG at the A_{2A}R sensors A_{2A} Fl3 CFP was supplemented with a final concentration of 0.075 μM A-633-AG that was added to cells at the starting point of the time series (figure 4.30). First binding of fluorescent agonist was observed at t= 4 min and was visible at the plasma membrane of cells at t= 20 min. Now theophylline with a final concentration of 8000 μM was added to cells and was almost fully able to displace fluorescent agonist within further 20 min.
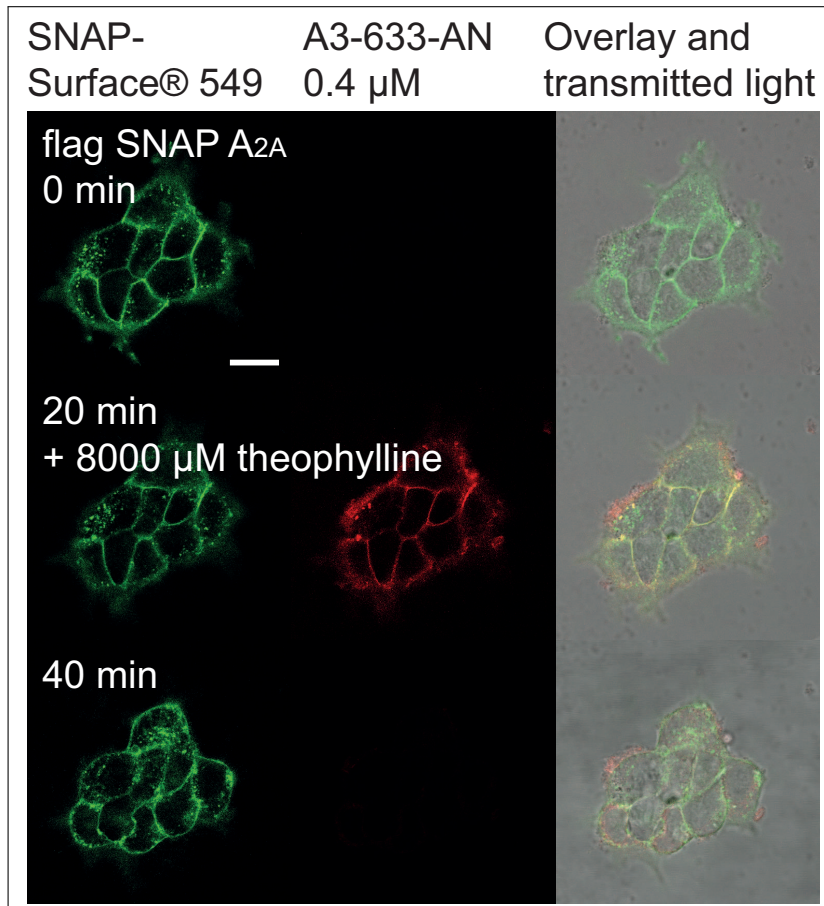
Figure 4.31: flag SNAP A$_{2A}$ labeled with SNAP-Surface$^®$ 549 and supplemented with A3-633-AN 0.4 μM at t= 0 min (first row), addition of 8000 μM theophylline at t= 20 min (second row) and competitive binding of both ligands until t= 40 min (third row). White bar refers to 20 μm

Flag SNAP A$_{2A}$, labeled with SNAP-Surface$^®$ 549, was investigated with A3-633-AN where a final concentration of 0.4 μM was added to cells at starting point of time series (figure 4.31). First binding of fluorescent antagonist was observed at t= 2 min and became clearly visible at t= 20 min as red fluorescence at the plasma membrane of cells. Now adenosine receptor antagonist theophylline with a final concentration of 8000 μM was added to cells and was able to completely displace fluorescent antagonist within further 20 min.
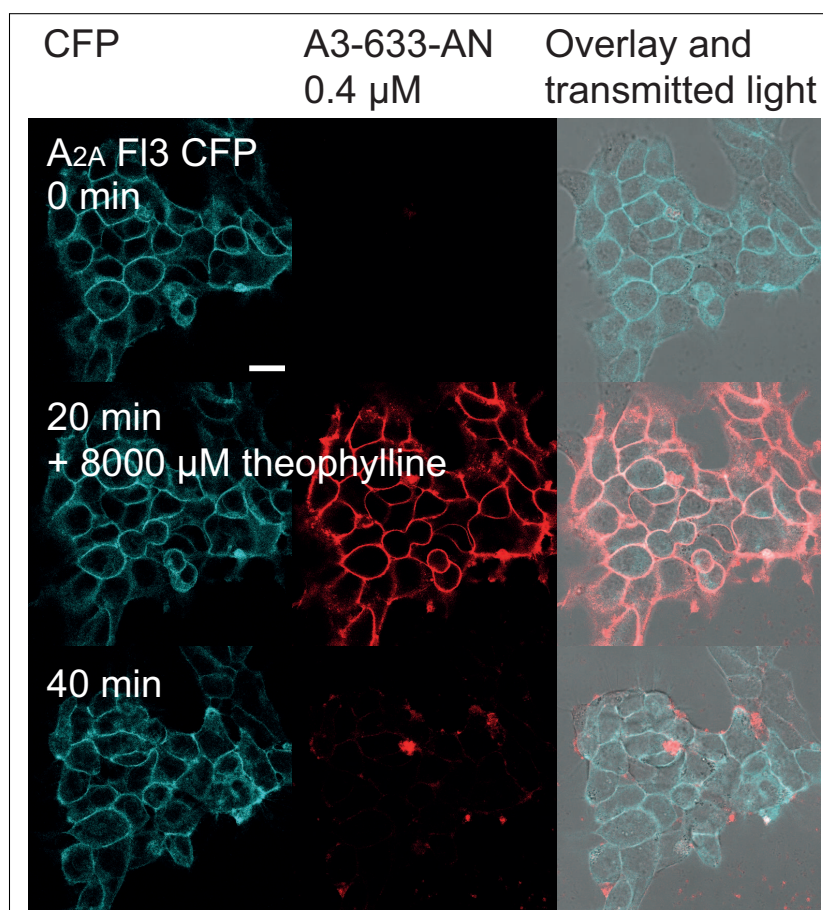
Figure 4.32: A_{2A} Fl3 CFP supplemented with A3-633-AN 0.4 μM at t= 0 min (first row), addition of 8000 μM theophylline at t= 20 min (second row) and competitive binding of both ligands until t= 40 min (third row). White bar refers to 20 μm

A_{2A} Fl3 CFP was probed with A3-633-AN where a final concentration of 0.4 μM was added to cells at starting point of time series (figure 4.32). First binding of fluorescent antagonist was observed at t= 2 min and red fluorescence at the plasma membrane became clearly visible at t= 20 min. Now theophylline with a final concentration of 8000 μM was added to cells and was not fully able to displace fluorescent antagonist within additional 20 min.

4.3 SNAP A_1 Fl3 CFP and SNAP A_{2A} Fl3 CFP

For getting more insight into receptor ligand interactions and resulting receptor conformational changes at the same time, FlAsH CFP based receptor sensors on the one hand and SNAP and CLIP tagged receptor sensors on the other hand were now

combined in one receptor sensor. Two different receptor sensors were investigated with all these fluorophores, called SNAP A_1 Fl3 CFP and SNAP A_{2A} Fl3 CFP. Principle of these fluorescent receptor sensors and theoretical binding of a fluorescent ligand are shown in figure 4.33.
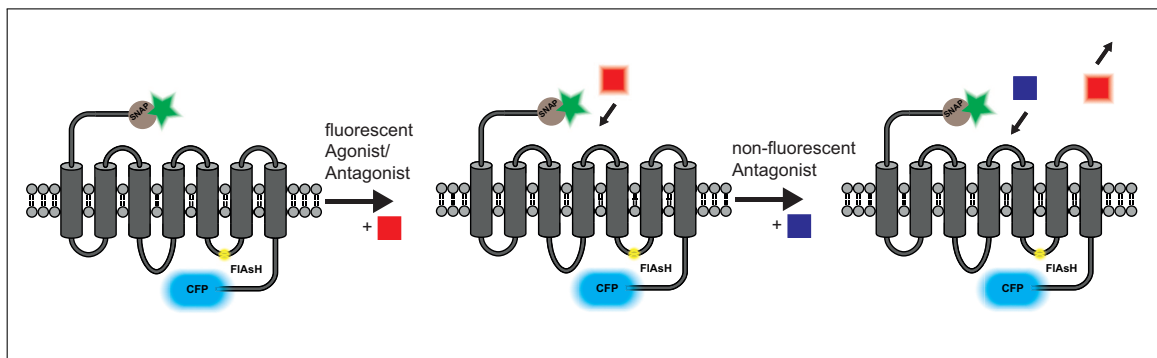

Figure 4.33: Principle of a fluorescent ligand binding at a N-terminal SNAP tagged receptor sensor that is labeled with a green fluorescent dye and has additional fluorophores included which are FlAsH in the third intracellular loop and CFP at the C-terminus of receptor. Fluorescent ligand, labeled with a red fluorescent dye binds at the receptor where the green and red fluorescent dye would make FRET possible in theory. The conformational change of receptor could be seen in a change in FRET ratio of the FRET pair CFP and FlAsH. After binding fluorescent ligand is displaced with a non-fluorescent antagonist which could be visible in a change in FRET ratio between the green and red fluorophore because of loss of the red fluorescence and also in a change in FRET ratio of CFP and FlAsH.

4.3.1 Development of SNAP A_1 Fl3 CFP and SNAP A_{2A} Fl3 CFP

Former introduced A_1R and $A_{2A}R$ sensors were the starting point for development of SNAP A_1 Fl3 CFP and SNAP A_{2A} Fl3 CFP.

Plasmids containing A_1 FlAsH3 CFP and flag SNAP A_1 were the basis for SNAP A_1 Fl3 CFP receptor sensor. Combination of these plasmids led to a new receptor sensor including a flag tagged SNAP sequence at the N-terminus of A_1R, the FlAsH binding motif in the third intracellular loop of A_1R and CFP encoding sequence at the C-terminus of A_1R, expressed in pcDNA 3. This construct was called SNAP A_1 FlAsH3 CFP.

For SNAP A_{2A} Fl3 CFP receptor sensor plasmids containing flag SNAP A_{2A} and A_{2A} FlAsH3 CFP in were combined resulting in an $A_{2A}R$ sensor with flag-tag and SNAP-

sequence before the N-terminus of $A_{2A}R$, the $A_{2A}R$ with FlAsH binding sequence in the third intracellular loop of $A_{2A}R$ and CFP encoding sequence at the C-terminus of $A_{2A}R$. This construct was called SNAP A_{2A} Fl3 CFP.

HEK 293 cells stably expressing the receptor sensor of interest were established for both receptors which will be beneficial for the required double labeling procedure with FlAsH and the SNAP dye in future investigations.

4.3.2 Confocal analysis of SNAP A_1 Fl3 CFP and SNAP A_{2A} Fl3 CFP sensors and behavior in FRET experiments
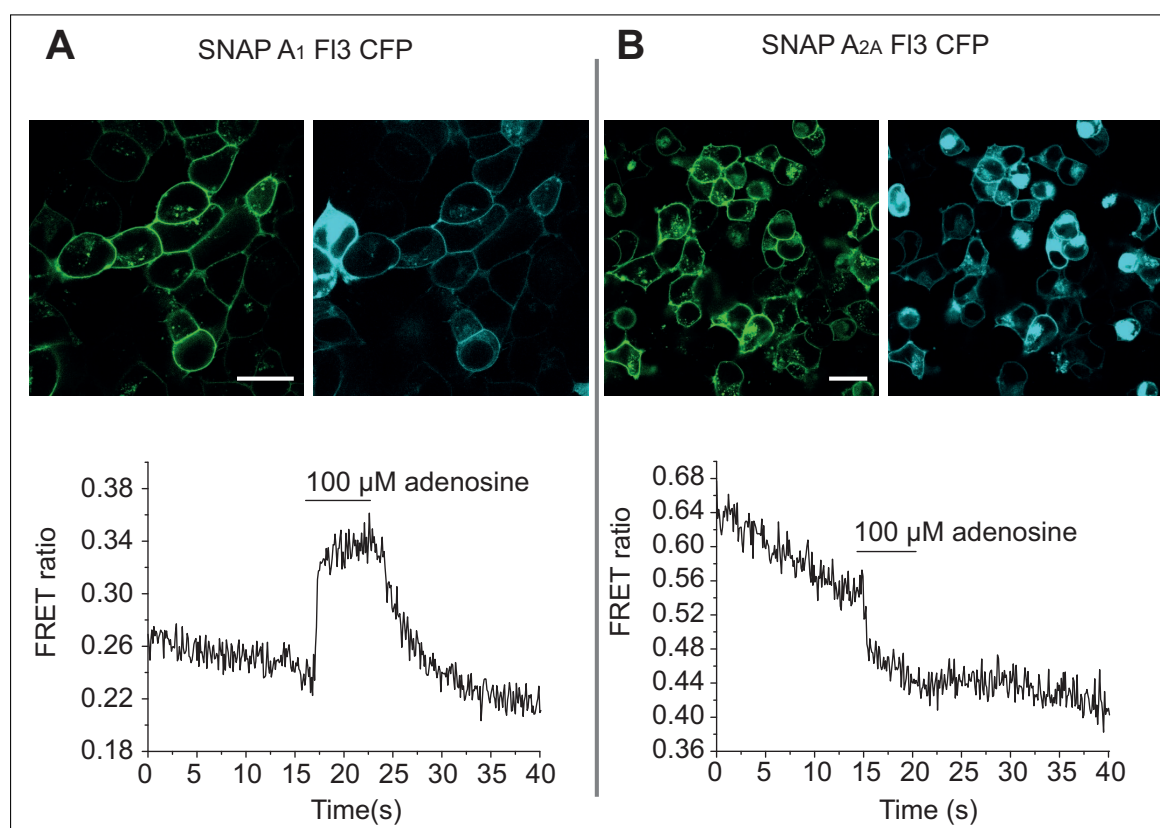
Figure 4.34: Confocal analysis and FRET experiments of **(A)** SNAP A_1 Fl3 CFP and **(B)** SNAP A_{2A} Fl3 CFP. Confocal images show emission of receptor sensor labeled with SNAP-Surface® 549 (green) and CFP emission of the same cells (cyan). White bars refer to 20 μm. Representative FRET trace shows a change in FRET ratio upon stimulation of receptors with 100 μM adenosine. FRET ratio increased for SNAP A_1 Fl3 CFP and decreased for SNAP A_{2A} Fl3 CFP.

HEK 293 cells expressing either SNAP A_1 Fl3 CFP or SNAP A_{2A} Fl3 CFP were

labeled with SNAP-Surface® 549 and were investigated with a confocal microscope. CFP and SNAP-Surface® 549 were excited and emission of both fluorophores was improved. Confocal analysis confirmed that receptor sensor was folded correctly concerning the fluorescent proteins and receptor sensors were located in the plasma membrane of cells (figure 4.34).

In a second approach HEK 293 cells expressing either SNAP A_1 Fl3 CFP or SNAP A_{2A} Fl3 CFP were labeled with FlAsH and FRET experiments were carried out with adenosine 100 μM. Both receptor sensors were successful in performing FRET, FRET ratio increased upon agonist stimulation of receptor for SNAP A_1 Fl3 CFP (figure 4.34 (A)) and decreased for SNAP A_{2A} Fl3 CFP (figure 4.34 (B)) which was consistent with the direction of change in FRET ratio for A_1 Fl3 CFP and A_{2A} Fl3 CFP.

These first experiments are very promising for future investigations with these receptor sensors which could lead to more insight into receptor behavior upon ligand binding.

5 Discussion

Adenosine receptors are widely distributed throughout the human body which makes them an attractive target for drug design. But the structural knowledge of this receptor family is still limited. To increase the knowledge about their dynamical behavior upon ligand binding, two members of this family, namely the A_1R and $A_{2A}R$ were investigated within the scope of this project. All experiments throughout this work were carried out in HEK 293 cells either expressing fluorescent A_1R or $A_{2A}R$ sensors. HEK 293 cells are a suitable host system as the only adenosine receptor endogenously expressed is the $A_{2B}R$ [161]. So there should be no interference between naturally occurring and transfected receptors during the experimental procedures.

The aim of this work was to elucidate differences in receptor dynamical movement for various ligands at the A_1R and $A_{2A}R$ and to emphasize the role of single amino acids in the A_1R with the help of FRET experiments.

5.1 Comparison of A_1 Fl3 CFP and A_{2A} Fl3 CFP revealed differences between the two adenosine receptor subtypes

The first time-resolved FRET based research in living cells described by Vilardaga and coworkers [138] was the starting point for a very promising field of research. The previously published A_{2A} Fl3 CFP receptor sensor [118] with the discontinuous tetracysteine FlAsH binding motif CCPGCC in the third intracellular loop and CFP tagged to the truncated C-terminus was shown to be suitable for FRET experiments [118]. The C-terminal truncation of the $A_{2A}R$ sensor did not affect receptor function concerning its downstream signaling [118]. This sensor was the base for the A_1 Fl3 CFP receptor sensor investigated within the scope of this work where the FlAsH binding motif was inserted into the third intracellular loop and

CFP was tagged to the C-terminus of receptor. FlAsH, with which receptors were labeled just before measurement [162] was already successfully applied for previous studies [118][186][139]. Its 40 times smaller size compared to YFP may contribute to the fact that FlAsH has no disturbing effects on downstream signaling which was previously shown for the $A_{2A}R$ [118].

The here investigated A_1 Fl3 CFP receptor sensor was pharmacologically functional regarding radioligand saturation binding experiments (figure 4.2 A) and inhibition of adenylate cyclase (figure 4.3). Furthermore, the A_1R sensor was stably expressed in the plasma membrane of HEK 293 cells (figure 4.2 A). Pharmacological functionality of A_{2A} Fl3 CFP was previously confirmed (figure 4.2 B) [118] and receptor sensor A_1 Fl3 CFP turned out to be suitable for FRET experiments (figure 4.2 A) which was the starting point for comparative FRET experiments with the two receptor subtypes. The first difference observed was the opposite direction of the FRET ratio upon ligand stimulation of the receptor sensors. The FRET ratio increased for A_1R sensor and decreased for $A_{2A}R$ sensor upon agonist stimulation of receptors. The exact reason for this phenomenon is not yet clear but could be correlated to the fact that FlAsH is a very small biarsenic molecule that is tightly bound to receptor structure through its tetracysteine binding motif [117]. Therefore it is able to exhibit tiniest alterations in receptor and fluorophore orientation which could be visible in an alteration of direction of the FRET ratio. FRET measurements were performed with the physiological agonist adenosine and the agonists NECA which has an equal specificity for all adenosine receptor subtypes, the $A_{2A}R$ selective agonist CGS 21680 and the A_1R selective agonist CPA. Examination of FRET experiments revealed that this approach is suitable for the comparative investigation of the A_1R and the $A_{2A}R$ subtype of the adenosine receptor family as well as for the previously published intramolecular receptor sensors of the muscarinic acetylcholine receptor family [140]. Within the work presented here differences in receptor dynamical movements of the A_1R and $A_{2A}R$ upon stimulation with various ligands could be investigated. Furthermore, measurement of the direct interaction of the physiological agonist adenosine became possible with FRET experiments. This is striking because so far direct pharmacological characterization of adenosine with radioligand binding studies was difficult since it is ubiquitously distributed in membrane preparations [30].

Comparison of the amplitudes of the FRET ratio that was observed upon ligand stimulation of the receptor sensors (figure 4.5) exhibited differences between ligands

and receptor subtypes. Direct comparison of the signal amplitude evoked by the subtype selective ligand CPA revealed that the signal height and conformational change of receptor was higher for A_1R when compared to the signal height at the $A_{2A}R$. For the $A_{2A}R$ selective ligand CGS 21680 direct comparison of signal amplitudes revealed higher intramolecular FRET signals and thus stronger conformational changes for the $A_{2A}R$ than for the A_1R. Moreover, comparison of the FRET traces exhibited that the various ligands explored had different association- and dissociation-times (τ_{on} and τ_{off}) at the two adenosine receptor subtypes investigated. This kind of approach was previously published for subtypes of the muscarinic acetylcholine receptor family [140]. Regarding the A_1R and $A_{2A}R$, differences were especially noticeable for the receptor-subtype selective ligands CPA and CGS 21680. The A_1R selective agonist CPA showed a remarkable longer dissociation time at the A_1R compared to the $A_{2A}R$ whereas CGS 21680, which has a higher specificity for the $A_{2A}R$, caused only tiny FRET ratio changes at the A_1R that were not evaluable regarding association- and dissociation-times. Concerning the $A_{2A}R$, CGS 21680 had the longest association time compared to the other ligands investigated. However, in sum of all experiments at the $A_{2A}R$, CGS 21680 had no remarkable different dissociation time compared to the other ligands.

The results presented here enable the direct comparison of the A_1R and $A_{2A}R$ and provide information about differences in ligand binding behavior regarding dynamical receptor movement upon ligand binding and ligand binding kinetics for the two members of the adenosine receptor family. These observations can lead to a better understanding of these receptors in the future and may lead to the development of new subtype selective drugs.

5.2 A_1 Fl3 CFP and its mutants revealed new insights into receptor dynamical behavior

The intramolecular A_1R FRET sensor presented here and its mutants designed on base of the previously published A_{2A} FlAsH 3 CFP (A_{2A} Fl3 CFP) sensor [118] and on base of the crystal structure of the $A_{2A}R$ bound to an antagonist [25] revealed new insights into receptor ligand binding behavior. With help of the $A_{2A}R$ crystal structure, amino acids that form the ligand binding pocket were selected and transferred to the A_1R sequence with help of sequence alignment so that a direct comparison of effects of certain mutants was possible. Following single amino acid mutations

in the A_1R were developed: I69V, L88A, T91A, W247A, H251A, N254A, H264A and T277A or T277S with the FRET pair CFP and FlAsH. CFP was C-terminally tagged to the receptor and the CCPGCC binding motif of the small biarsenic fluorophore FlAsH was inserted into the third intracellular loop of each A_1R mutant investigated. Figure 5.1 shows the hypothetical binding pocket of the A_1R, derived from crystallization studies of the $A_{2A}R$.
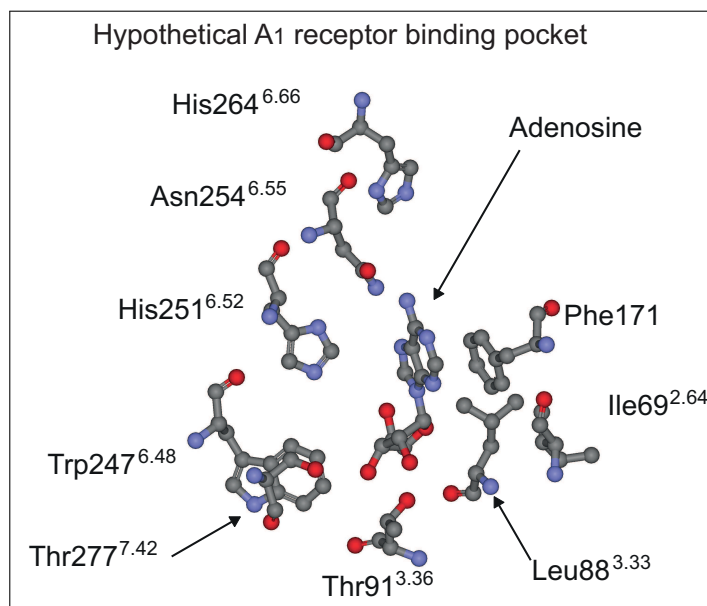

Figure 5.1: Hypothetical binding pocket of the A_1R, referred from the A_{2A} binding pocket

5.2.1 Involvement of single amino acids in the A_1R in the cellular distribution

Expression of A_1 Fl3 CFP revealed that fluorophores attached to receptor did not hinder expression in the plasma membrane of cells. This was also true for the mutants of A_1 Fl3 CFP where amino acids mutated did not hinder expression in the plasma membrane of cells except for mutations in the positions 3.33 where leucine was mutated into an alanine (L88A), 6.52 where histidine was mutated into an alanine (H251A) and 6.55 where asparagine was mutated into an alanine (N254A). It was previously shown that mutation of single amino acids in GPCRs can hinder their proper plasma membrane expression due to incorrect folding of receptor domains [187]. However, according to previous findings which showed that small ligands, if available in cell culture medium, could help to stabilize receptor in the

plasma membrane of receptors [176], incubation with the adenosine receptor antagonist theophylline led to stable expression of mutated receptor sensors in the plasma membrane of cells. Thus, contact of receptor and ligands investigated was enabled which made FRET experiments feasible on all A_1R sensors developed in this project. Figure 4.13 shows a FRET measurement without and with theophylline pretreatment at the L88A mutant of the A_1R.

5.2.2 Investigation of ligand binding behavior at the A_1R via FRET measurements

Intramolecular FRET sensors were previously shown to be suitable for the generation of concentration response curves where the signal height evoked by a distinct ligand concentration was plotted against the ligand concentration [140]. In the case of A_1 Fl3 CFP and its mutants a concentration dependent change in FRET ratio led to concentration response curves like previously published for members of the muscarinic acetylcholine receptor family [140]. The EC_{50} values investigated for the ligands examined at the A_1R sensor were much higher than the high affinity K_d values investigated in previously published studies [27][67]. However, EC_{50} values that were found for the A_1 Fl3 CFP receptor sensor were in better accordance with the low affinity K_d values investigated in binding studies for the A_1R [67]. The EC_{50} value found for NECA at the A_1 Fl3 CFP receptor sensor (2.6 μM) was in good agreement with the low affinity binding value of NECA at the A_1R (1.2 μM) [67], whereas affinity for CPA at A_1 Fl3 CFP receptor sensor (2.6 μM) was 10 fold shifted if compared to the earlier findings where ligand affinity at A_1R was 0.3 μM [67]. The reason for the EC_{50} values investigated here that are more in accordance with the low affinity K_d values previously investigated is likely that FRET experiments in this study were performed in living cells. That means receptors were investigated under non equilibrium conditions with no receptor reserve present whilst classical pharmacological receptor characterization like radioligand binding studies was mostly done under equilibrium conditions [27]. Values that were investigated for the A_1R sensor are in good agreement with values that were investigated in FRET experiments with members of the muscarinic acetylcholine receptor family [140]. Activation of the A_1 Fl3 CFP receptor sensor occurred within the range of milliseconds which is consistent with findings from previously published FRET experiments with GPCR

receptor sensors [138][118][141][139][140][182]. For all ligands investigated examination of EC_{50} values was feasible at the unmutated A_1R sensor (see table 4.3).

Influence on ligand binding affinity for the A_1R mutants investigated is summarized in table 5.1 at the end of this section, exact EC_{50} and K_i values for the ligands investigated are summarized in the table 4.3 in the chapter results.

Mutation in position 2.64 where isoleucine was mutated into a valine led to a marginal decrease of agonists and antagonist binding affinities in FRET experiments when compared to the unmutated receptor sensor. The highest decrease in ligand affinity was observed for CPA (11 fold) which confirms a previous study that found that amino acids in TM 1-4 are important for receptor subtype-selective binding of ligands [76]. However, previous findings, suggesting that I69 interacts with the ribose moiety of agonists [188], seem less likely regarding the $A_{2A}R$ based A_1R model and the overall marginally affinity shift in FRET experiments.

Leucine in position 3.33 was also previously found to be involved in A_1R binding of ligands [76]. After theophylline pretreatment there was a change in FRET ratio detectable for all agonists and the antagonist investigated regarding the A_1 Fl3 CFP L88A when leucine 88 was mutated into an alanine. Investigation resulted in decreased ligand binding affinity for agonists as well as the antagonist. The involvement in agonist and antagonist binding is consistent with previous binding studies [73]. Within the scope of this work L88 was found to be marginally involved in binding of the N^6-modified agonist CPA where only a slight loss in ligand binding affinity was observed. Whereas earlier investigations found L88 to influence N^6-modified agonist affinities more than the not N^6-modified agonist affinities [73].

Former findings suggested that threonine in position 3.36 is involved in agonist and antagonist binding and a remarkable loss in ligand binding affinity was observed when threonine was mutated into an alanine [76][73]. During FRET experiments the involvement in ligand binding of T91 could be confirmed since there was no change in FRET ratio detectable for A_1 Fl3 CFP T91A although determination of FRET efficiency confirmed correct folding of proteins. These findings were underlined by an A_1R model, based on the active-conformation $A_{2A}R$ crystal structure. When A_1R was modeled with NECA it was seen that T91 built H-bonds to 5'CO-NH-ethyl group of NECA and thus was involved in agonist binding [80].

For histidine in position 264 (6.66) that was mutated to an alanine the outcomes of FRET experiments were consistent with the findings from Peeters and coworkers in 2012 where this mutant showed the same activity as unmutated A_1R [189]. Thus,

H264 seems to be more involved in ligand binding in the $A_{2A}R$, as previously shown in the antagonist bound crystal structure [25], than in the ligand binding process in the A_1R.

Earlier studies found the amino acid threonine in position 277 (7.42) to be involved in ribose moiety binding of ligands since there was a remarkable decrease in agonist binding affinity if this amino acid was mutated to an alanine [75][190]. A previous modeling study where the A_1R model was based on the $A_{2A}R$ crystal structure in the active conformation confirmed the involvement of T277 in agonist ribose moiety binding [80]. The results within this work were consistent with the previous findings. Throughout FRET experiments with A_1 Fl3 CFP T277A any change in FRET ratio was detectable although correct folding of protein was confirmed via FRET efficiency determination. However, if threonine in position 277 was mutated into the structurally related serine, there were no obviously shifted ligand affinities for adenosine, NECA, CPA and theophylline observable which was also investigated in previously published radioligand binding studies[77].

Former mutational investigation of asparagine (6.55) mutated into an alanine in the $A_{2A}R$ reported a complete loss in ligand binding [52]. The results of the FRET experiments with A_1 Fl3 CFP N254A were consistent for adenosine and NECA where a clear loss in ligand binding affinity could be observed. Interestingly, ligand binding affinity of CPA was nearly not shifted compared to the unmutated receptor sensor. Thus asparagine (6.55) seems to have larger impact on ribose binding than on binding or recognition of the N^6 position in adenosine as it was stated in a previously published modeling study [80].

In earlier work histidine (6.52) was found to be a highly conserved amino acid among adenosine receptor subtypes, with mild to no influence on A_1R ligand binding affinity if mutated to a leucine [74]. Within this project histidine 251 of the A_1R was mutated into an alanine. Previous data exist for the $A_{2A}R$ where histidine (6.52) was mutated into an alanine which led to a crucial loss of agonist and antagonist affinity [52]. FRET measurements with adenosine and CPA at A_1 Fl3 CFP H251A did not show markedly shifted ligand affinities compared to unmutated receptor sensor and were in good agreement with the previous findings at the A_1R [74]. Remarkably, NECA caused huge changes in FRET ratio and had long dissociation rates compared to CPA and adenosine. Because of the long dissociation rate during FRET experiments after supplementing NECA, EC_{50} values could not be determined due to the limited volume of the "Attofluor" cell chamber used. Further investigation

of A_1 H251A co-expressed with the G_i FRET sensor revealed that there was only a small change in FRET ratio for NECA compared to CPA and adenosine. Therefore histidine in position 251 seems to be more involved in ribose moiety binding and recognition of NECA for the intracellular signal transfer compared to the other ligands examined. The involvement in the binding of NECA was previously investigated with help of an A_{2A}R based A_1R modeling study where histidine 251 was shown to built H-bonds to the 5'CO-NH-ethyl group of NECA [80].

For all A_1 Fl3 CFP receptor sensors investigated, the change in FRET ratio occurred as an increase in FRET ratio, except for mutation in position 6.48, A_1 Fl3 CFP W247A, where a decrease in FRET ratio could be observed. Absolute value of change in FRET ratio was smaller for A_1 Fl3 CFP W247A compared to A_1 Fl3 CFP but ligand affinity was only little shifted compared to the unmutated receptor sensor. Amino acid in position 6.48 was found to be highly conserved among GPCRs and is a part of the CWXP motif where it was found to act as a rotamer toggle switch amongst other amino acids [191][180] and to be involved in receptor activation upon ligand binding [192]. The movement of tryptophan 6.48 and its influence upon agonist stimulation was previously shown for the A_{2A}R in a molecular dynamic simulation study [193]. Furthermore, it was earlier investigated that mutation of tryptophan 6.48 into a phenylalanine in the A_3R hinders internalization of receptor upon stimulation with distinct agonist and leads to an impairment of G protein coupling [194] which underlines the importance of this amino acid regarding receptor activation. The opposite direction of the FRET ratio of A_1 Fl3 CFP W247A compared to the unmutated receptor sensor could be a hint for a different movement of receptor transmembrane domains upon activation resulting from an altered spatial orientation of fluorophores to each other, like previously described [140]. In contrast to the findings in the A_3R of Stoddart and co-workers [194] experiments of A_1 W247A co-expressed with the G_i FRET sensor showed G protein activation and signal amplitude for the G_i FRET sensor was not markedly different from the G_i signal evoked by the unmutated A_1R co-expressed with the G_i FRET sensor. Taken together, there was one group of amino acids, in positions 3.33 (leucine), 6.52 (histidine) and 6.55 (asparagine) that caused problems in membrane localization concerning the A_1R.

	$\leq$ 10 fold shift in ligand affinity compared to A_1 Fl3 CFP	$\geq$ 10 fold shift in ligand affinity compared to A_1 Fl3 CFP	$\geq$ 1000 fold shift in ligand affinity compared to A_1 Fl3 CFP
Adenosine	I69V, W247A, H251A, H264A, T277S	L88A	T91A, N254A, T277A
CPA	L88A, W247A, H251A, N254A, H264A, T277S	I69V, T91A, T277A	
NECA	I69V, W247A, H264A, T277S	L88A, T91A, N254A, T277A	
Theophylline	I69V, W247A, H251A, H264A, T277S	L88A	

Table 5.1: Impact of amino acids regarding A_1R ligand binding

However, there was no disturbance of plasma membrane localization for the amino acid mutations that were previously investigated in the $A_{2A}R$ [170]. Amino acid histidine 6.66 seemed to have more impact on ligand binding in the $A_{2A}R$, which was investigated in the crystal structure [25] and in FRET experiments [170], than in the A_1R. Furthermore, there were amino acids that were found to be involved in overall ligand binding in the A_1R, which were threonine 3.36 and threonine 7.42. Both amino acids showed less influence in ligand binding in FRET experiments with the $A_{2A}R$ [170]. Moreover, there were amino acids in the A_1R that were found to be more involved in binding the adenine moiety of adenosine and its derivatives, which was isoleucine 2.64 and amino acids that are more involved in binding the ribose moiety like leucine 3.33, asparagine 6.55 and histidine 6.52.

With the previously described FRET based experiments it was possible to gain new insights into dynamical receptor activation movements of A_1R and $A_{2A}R$ that were investigated in a high-resolution real time setting in living cells. In case of the intramolecular A_1R FRET sensor and its mutants it became feasible to elucidate the role of single amino acids in the ligand binding process where some of the findings from previous studies could be confirmed and new conclusions could be drawn.

5.3 Combining fluorescence-based receptor labeling techniques - future directions

During the past years fluorescence tagged receptor sensors turned out to be very useful tools for the investigation of receptor dynamical movements upon ligand stimulation [119]. A further step was the investigation of receptor ligand interactions employing fluorescent ligands and receptor distribution in living cells with help of confocal microscopy [131]. Beside the previously described intracellular FRET sensors with C-terminally tagged CFP and FlAsH in the third intracellular loop of receptors, there were several approaches that tagged receptors at the N-terminal end with fluorescent GFP-derivatives where it could be shown that there was an altered FRET ratio upon binding of a fluorescent ligand [131].

Within this project the SNAP and CLIP based label techniques were employed which were previously investigated [120][124]. Resulting flag CLIP A_1R, flag CLIP $A_{2A}R$, flag SNAP A_1R and flag SNAP $A_{2A}R$ were located in the plasma membrane of cells. Binding of the fluorescent adenosine receptor agonist A-633-AG and antagonist A3-633-AN was successfully examined at flag SNAP A_1R and flag SNAP $A_{2A}R$ with help of time series at the confocal microscope. The binding process of the fluorescent ligands at receptors could also successfully be shown for A_1 Fl3 CFP and A_{2A} Fl3 CFP. For further examination of fluorescent ligands, their binding properties can be characterized with a non-fluorescent ligand that competes for the binding site with the fluorescent ligand [149]. Within this project the competitive binding was successful when theophylline and the fluorescent ligands were investigated at the previously mentioned receptor sensors. The competitive binding of fluorescent ligands was previously shown for A_1R and A_3R [156]. The results of the time series at the A_1R and $A_{2A}R$ sensors, investigated within this project, with fluorescent adenosine receptor ligands shown here are very promising and exhibit the opportunity for further investigations. Further experiments with a perfusion system would be interesting to obtain the dynamical resolution of ligand receptor interaction over time and to minimize concentration of the fluorescent ligand. Furthermore, the combination of the SNAP and CLIP technique gives the opportunity to monitor different structures in one cell at the same time like previously described [195]. Within the scope of this work it was possible to label CLIP tagged $A_{2A}R$ and SNAP tagged A_1R simultaneously.

The next step was to combine the fluorescent labeling techniques for receptors which

resulted in the fluorescent receptor sensors SNAP A_1 Fl3 CFP and SNAP A_{2A} Fl3 CFP which represent promising tools for elucidating receptor dynamical movements and receptor ligand binding interactions at the same time. A complete pharmacologically characterization of these receptor sensors will be absolutely necessary. However, first confocal analysis regarding receptor distribution and first FRET experiments with the agonist adenosine look very promising (see figure 4.34).

These receptor sensors reveal a lot of opportunities for a better understanding of the A_1R and A_{2A}R function. In combination with fluorophore tagged orthosteric ligands it would be possible to unravel the influence of allosteric ligands. Allosteric ligands do not compete for the binding site with an orthosteric ligand. They mediate their effect via the allosteric ligand binding site and thus influence receptor function either positive or negative via modulation of the orthosteric binding behavior [196]. Another important point is that even in highly structural conserved receptor families it seems that there are noticeable differences regarding the shape of allosteric binding sites of different receptor family members [196]. The effect of allosteric modulators was previously investigated with CFP FlAsH based FRET sensors of the muscarinic acetylcholine receptor family [139]. In the SNAP FlAsH CFP tagged receptor sensors investigated here the influence of the allosteric modulator could be examined simultaneously regarding orthosteric ligand binding and receptor dynamical movement. FRET between FlAsH and CFP could indicate receptor movement whilst influence of the allosteric modulator on the orthosteric ligand binding could be investigated via FRET between the fluorescent ligand and the SNAP tag at the receptor.

With respect to receptor heterodimers an allosteric effect was recently shown in case of the A_{2A}R and D_2R [158] and it became possible to examine allosteric modulation at A_3R homodimers [197]. Furthermore, May and coworkers were able to show that the dissociation rate of A_1R and A_3R was distinct when an allosteric modulating substance was present from the dissociation rate when no allosteric enhancer was present, with help of fluorescent ligands and receptors [198].

The SNAP tagged FlAsH CFP based receptor sensors invented here reveal a combination of the former named labeling techniques and can add additional information regarding receptor movement simultaneously with information about the ligand binding process. This could be really helpful for a better understanding of these receptors and thus the development of new adenosine receptor subtype specific drugs.

6 Summary

6.1 Summary

Adenosine receptors that belong to the rhodopsin-like G protein-coupled receptors (GPCRs) are involved in a lot of regulatory processes and are widely distributed throughout the body which makes them an attractive target for drugs. However, pharmacological knowledge of these receptors is still limited. A big advance regarding the structural knowledge of adenosine receptors was the development of the first crystal structure of the adenosine A_{2A} receptor in 2008 [25]. The crystal structure revealed the amino acids that form the ligand binding pocket of the receptor and depicted the endpoint of receptor movement in the ligand binding process.

Within the scope of this work two members of the adenosine receptor family were investigated, namely the adenosine A_1 and the A_{2A} receptor (A_1R, $A_{2A}R$). A_1R was generated on base of the previously developed $A_{2A}R$ [118]. Receptors were tagged with fluorophores, with the cyan fluorescent protein (CFP) at the C-terminal end of receptor and the Fluorescein Arsenical Hairpin binder (FlAsH) binding sequence within the third intracellular loop of receptors. Resulting fluorescent receptor sensors A_1 Fl3 CFP and A_{2A} Fl3 CFP were investigated with help of Fluorescence Resonance Energy Transfer (FRET) measurements within living cells. FRET experiments enable the examination of alteration in the distance of two fluorophores and thus the observation of receptor dynamical movements.

For comparison of A_1R and $A_{2A}R$ regarding receptor dynamical movement upon ligand binding, fluorescent receptor sensors A_1 Fl3 CFP and A_{2A} Fl3 CFP were superfused with various ligands and the outcomes of FRET experiments were compared regarding signal height of FRET ratio evoked by the distinct ligand that is correlated to the conformational change of receptor upon ligand binding. Beside the different direction of FRET ratio upon ligand binding at A_1R and $A_{2A}R$ sensor, there were differences observable when signal height and association and dissociation kinetics of the various ligands investigated were compared to each other. Differences

between the adenosine receptor subtypes were especially remarkable for the A_1R subtype selective agonist CPA and the $A_{2A}R$ subtype selective agonist CGS 21680. Another part of the project was to investigate the influence of single amino acids in the ligand binding process within the fluorescent A_1R sensor. Amino acid positions were derived from the crystal structure of the $A_{2A}R$ forming the ligand binding pocket [25] and these amino acids were mutated in the A_1R structure. Investigation of the A_1R sensor and its mutants regarding confocal analysis showed involvement of some amino acids in receptor localization. When these amino acids were mutated receptors were not expressed in the plasma membrane of cells. Some amino acids investigated were found to be involved in the ligand binding process in general whereas other amino acids were found to have an influence on the binding of distinct structural groups of the ligands investigated.

In a further step, A_1R and $A_{2A}R$ were N-terminally tagged with SNAP or CLIP which allowed to label receptor sensors with multiple fluorophores. With this technique receptor distribution in cells could be investigated with help of confocal analysis. Furthermore, ligand binding with fluorescent adenosine receptor ligands and their competition with help of a non-fluorescent antagonist was examined at the SNAP tagged A_1R and $A_{2A}R$.

Finally the previously developed receptor sensors were combined to the triple labeled receptor sensors SNAP A_1 Fl3 CFP and SNAP A_{2A} Fl3 CFP which were functional regarding FRET experiments and plasma membrane expression was confirmed via confocal analysis.

In the future, with the help of this technique, interaction between fluorescent ligand and SNAP tagged receptor can be monitored simultaneously with the receptor movement that is indicated by the distance alteration between FlAsH and CFP. This can lead to a better understanding of receptor function and its dynamical movement upon ligand binding which may contribute to the development of new and more specific drugs for the A_1R and $A_{2A}R$ in the future.

6.2 Zusammenfassung

Adenosin Rezeptoren, die zur Gruppe der Rhodopsin-ähnlichen G Protein-gekoppelten Rezeptoren (GPCRs) gehören, sind in eine Vielzahl regulatorischer Prozesse eingebunden und weit im Körper verbreitet. Das macht sie zu einer interessanten Zielstruktur für Arzneistoffe. Das Wissen über die Struktur der Adenosin Rezeptoren

ist jedoch noch begrenzt. Ein großer Fortschritt zu mehr strukturellem Wissen war die Entwicklung der ersten Kristallstruktur des Adenosin A_{2A} Rezeptors im Jahr 2008 [25]. Mit der Kristallstruktur wurden die Aminosäuren bekannt, die die Ligandenbindetasche dieses Rezeptors formen. Zudem gab die Kristallstruktur Einblick in den Endpunkt der dynamischen Rezeptorbewegung nach Ligandenbindung.

Im Rahmen der hier vorgestellten Arbeit wurden zwei Mitglieder der Adenosin Rezeptor Familie, der Adenosin A_1 Rezeptor und der Adenosin A_{2A} Rezeptor (A_1R, A_{2A}R), genauer untersucht. Der A_1R wurde auf Basis des vor kurzem veröffentlichten A_{2A}R [118] entwickelt. Die Rezeptoren wurden mit Fluorophoren versehen, zum einen mit dem cyan fluoreszierenden Protein (CFP) am C-Terminus des Rezeptors und zum anderen mit der Bindesequenz des kleinen Fluorophors "Fluorescein Arsenical Hairpin binder" (FlAsH) in der dritten intrazellulären Schleife des Rezeptors. Die daraus resultierenden Rezeptorsensoren A_1 Fl3 CFP und A_{2A} Fl3 CFP wurden mit Hilfe des Fluoreszenz Resonanz Energie Transfers (FRET) in lebenden Zellen erforscht. FRET Messungen ermöglichen es, eine Änderung der Distanz zwischen den beiden Fluorophoren und damit Rezeptorbewegungen zu untersuchen.

Um A_1R und A_{2A}R bezüglich dynamischer Rezeptorbewegungen nach Ligandenbindung vergleichen zu können, wurden die fluoreszierenden Rezeptorsensoren A_1 Fl3 CFP und A_{2A} Fl3 CFP mit verschiedenen Liganden umspült. Die Ergebnisse der FRET Messungen bezüglich ihrer Höhe des FRET Ratio wurden verglichen, welche mit der Konformationsänderung des Rezeptors nach Ligandenbindung zusammenhängt. Neben der unterschiedlichen Richtung des FRET Ratio nach Ligandenbindung am A_1R und A_{2A}R Sensor waren Unterschiede bezüglich der Signalhöhe und der Bindungs- und Dissoziationskinetiken feststellbar, wenn die verschiedenen Liganden miteinander verglichen wurden. Unterschiede zwischen den Adenosin Rezeptor Subtypen waren speziell für den A_1R subtypselektiven Agonist CPA und für den A_{2A}R subtypselektiven Agonist CGS 21680 feststellbar.

Einen weiteren Punkt in diesem Projekt stellte die Erforschung des Einflusses, den einzelne Aminosäuren im fluoreszierenden A_1R Sensor auf den Prozess der Ligandenbindung haben, dar. Die Position der Aminosäuren wurde der Kristallstruktur des A_{2A}R entnommen [25] und entsprechende Aminosäuren im A_1R mutiert. Die konfokalmikroskopische Analyse des A_1R Sensors und seiner Mutanten ergab, dass einige Aminosäuren direkt an der zellulären Expression des Rezeptors beteiligt waren. Wurden diese Aminosäuren mutiert, wurde der Rezeptor nicht in der Plasmamembran der Zellen exprimiert. Einige Aminosäuren die untersucht wurden,

hatten einen generellen Einfluss auf die Bindung der Liganden, andere Aminosäuren hatten mehr Einfluss auf die Bindung bestimmter struktureller Gruppen der untersuchten Liganden.

In einem weiteren Schritt wurden A_1R und $A_{2A}R$ am N-terminalen Rezeptorende mit SNAP oder CLIP versehen, was eine Markierung der Rezeptoren mit einer Vielzahl an Fluorophoren erlaubt. Mit Hilfe dieser Technik konnte die Verteilung der Rezeptoren in der Zelle mit konfokaler Mikroskopie untersucht werden. Des Weiteren wurde die Bindung von fluoreszierenden Adenosin Rezeptor Liganden und deren Verdrängung mit einem nicht-fluoreszierenden Adenosin Rezeptor Antagonist erforscht.

Am Ende des Projekts wurden die zuvor beschriebenen fluoreszierenden Rezeptorsensoren zu dreifach fluorophormarkierten Rezeptorsensoren kombiniert, was zu den Sensoren SNAP A_1 Fl3 CFP und SNAP A_{2A} Fl3 CFP führte. Beide Rezeptorsensoren waren funktionell bezüglich FRET Experimenten und der Expression in der Plasmamembran der Zellen.

In Zukunft können mit dieser Methode gleichzeitig die Bindung von fluoreszierenden Liganden am SNAP-markierten Rezeptor, so wie die Rezeptorbewegung beobachtet werden, die durch eine Distanzänderung zwischen CFP und FlAsH angezeigt wird. Das kann zu einem besseren Verständnis der Rezeptorfunktion und der dynamischen Rezeptorbewegung nach Ligandenbindung führen, die in Zukunft zur Entwicklung spezifischerer Wirkstoffe am A_1R und $A_{2A}R$ beitragen könnte.
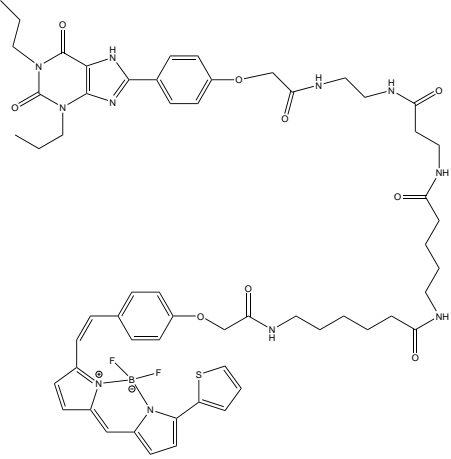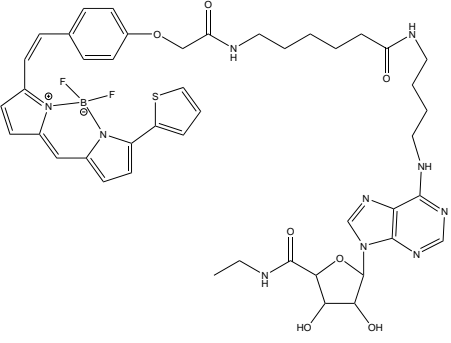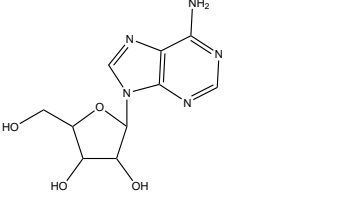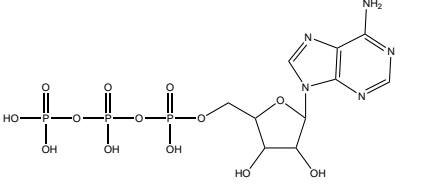
7 Abbreviations
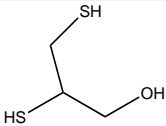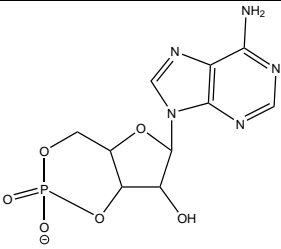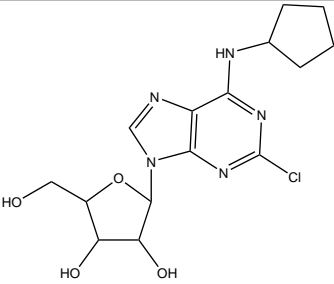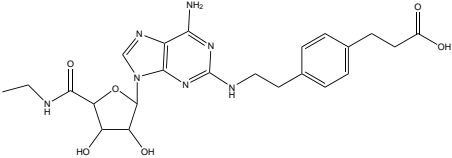
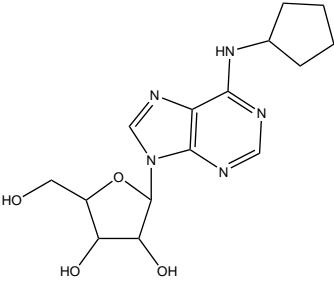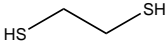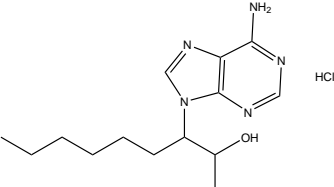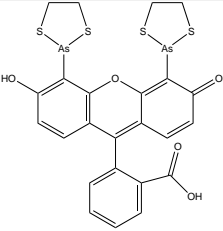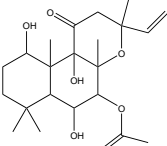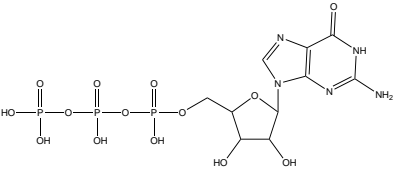| Abbreviation	Meaning
A-633-AG	Fluorescent adenosine receptor agonist, NECA-derivative
A3-633-AN	Fluorescent adenosine receptor antagonist, XAC-derivative
A_1R	Adenosine A_1 receptor
A_1 Fl3 CFP	A_1 FlAsH3 CFP (fluorescent A_1 receptor sensor that carries FlAsH binding motif in the third intracellular loop and CFP at the C-terminus of receptor)
$A_{2A}R$	Adenosine A_{2A} receptor
A_{2A} Fl3 CFP	$A_{2A}R$ FlAsH3 CFP (fluorescent $A_{2A}R$ receptor sensor that carries FlAsH binding motif in the third intracellular loop and CFP at the truncated C-terminus of receptor)
ABEA	N^6-(4-amonibutyl)-5'-ethylamino-5'oxo-5'-deoxyadenosine
Ado	Adenosine
ADA	Adenosine deaminase or Adenosine aminohydrolase
AGT	O^6-alkylguanine-DNA alkyltransferase
Amp	Ampicillin
AR	Adenosine receptor
ATP	Adenosine triphosphate
BAL	British Anti-Lewisite (2,3 Dimercapto-1-propanol)
BSA	Bovine serum albumine
cAMP	Cyclic adenosine monophosphate
$CaCl_2$	Calcium chloride
CCPA	2-Chloro-N^6-cyclopentyladenosine
CFP	Cyan fluorescent protein
CGS 21680	2-p-(2-Carboxyethyl)phenetylamino-5'-N-ethylcarboxamidoadenosine
CPA	N^6-Cyclopentyladenosine
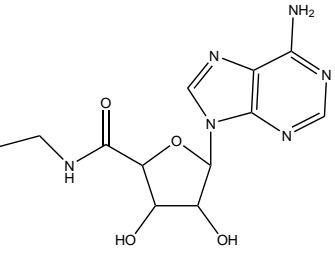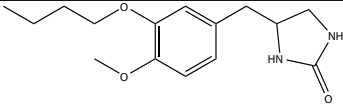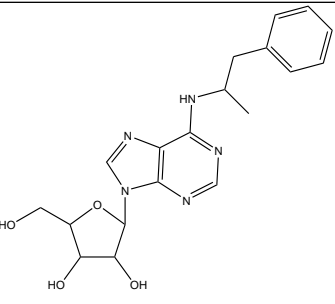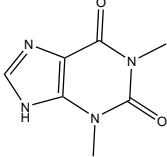
DMEM	Dulbecco's modified eagle medium
DMSO	Dimethylsulfoxide
dNTP	Deoxynucleotide
DPBS	Dulbecco's phosphate buffered saline
DPSS	Diode pumped solid state laser
ECFP	Enhanced cyan fluorescent protein
EDT	1,2 Ethanedithiol
EDTA	Ethylenediaminetetraacetic acid
EHNA	Erythro-9-(2-Hydroxy-3-nonyl) adenine
EL	Extracellular loop (of a receptor)
EtBr	Ethidiumbromide
EtOH	Ethanol
FCS	Fetal calve serum
FlAsH	Fluorescein Arsenical Hairpin Binder
G 418	Geneticin sulfate
GDP	Guanosine-5'diphosphate
GTP	Guanosine-5'triphosphate
GFP	Green fluorescent protein
HEK 293	Human embryonic kidney cells, line 293
HEPES	4-(2-hydroxyethyl)-1-piperazineethanesulfonic acid
H_2O_2	Hydrogenperoxide
Iso	Isopropanol
KCl	Potassium chloride
KH_2PO_4	Potassium di-hydrogen phosphate
LB-Medium	Lysogeny broth Medium
$MgCl_2$	Magnesium chloride
Na_2CO_3	Di-sodium-carbonate
Na_2HPO_4	Di-sodium-hydrogenphosphate
NaOH	Sodium hydroxide
NECA	5'-N-Ethylcarboxamidoadenosine
p.a.	Pro analysi
PDE 4	Phosphodiesterase 4
PEG	Poly ethylene glycol

Pen/Strep	Penicillin/ Streptomycin
R-PIA	(-)N^6-(2-phenylisopropyl)adenosine
RT	Room temperature (20 - 25 °C)
SDS	Sodium dodecyl sulfate
TM	Transmembrane domain (of a receptor)
Theo	Theophylline
TRIS	Tris(hydroxymethyl)aminomethane or 2-Amino-2-hydroxymethyl-propane-1,3-diol
TSB	Transformation Storage Buffer
XAC	Xanthine amine congener
YFP	Yellow fluorescent protein
ZnAc	Zinc acetate

8 Ligands- Structures and Properties

Name	Properties	Chemical Structure
A3-633-AN	Fluorescent AR antagonist	
A-633-AG	Fluorescent AR agonist	
Adenosine	AR agonist	
ATP	Cellular energy source	

BAL	Chelating agent	
cAMP	Second messenger	
CCPA	A_1R agonist	
CGS 21680	$A_{2A}R$ agonist	
CPA	A_1R agonist	
EDT	Thiol	
EHNA	Adenosine deaminase inhibitor	

FlAsH	Fluorescein derivative for intracellular labeling	
Forskolin	Adenylate cyclase activator	
GTP	Cellular energy source	
NECA	AR agonist	
RO-20-1724	PDE 4 inhibitor	
R-PIA	AR agonist	
Theophylline	AR antagonist	

9 Bibliography

[1] Dohlman, H. G.; Caron, M. G. and Lefkowitz, R. J., *Biochemistry*, 1987, **26**(10), 2657–2664.

[2] Lander, E. S.; Linton, L. M.; Birren, B.; Nusbaum, C.; Zody, M. C.; Baldwin, J. and et al., , *Nature*, 2001, **409**(6822), 860–921.

[3] Venter, J. C.; Adams, M. D.; Myers, E. W.; Li, P. W.; Mural, R. J.; Sutton, G. G. and et al., , *Science (New York, N.Y.)*, 2001, **291**(5507), 1304–1351.

[4] Lefkowitz, R. J., *Trends in pharmacological sciences*, 2004, **25**(8), 413–422.

[5] Almén, M. S.; Nordström, Karl J V, ; Fredriksson, R. and Schiöth, H. B., *BMC biology*, 2009, **7**, 50.

[6] Fredriksson, R. and Schiöth, H. B., *Molecular pharmacology*, 2005, **67**(5), 1414–1425.

[7] Ji, T. H.; Grossmann, M. and Ji, I., *Journal of Biological Chemistry*, 1998, **273**(28), 17299–17302.

[8] Wess, J., *Pharmacology & therapeutics*, 1998, **80**(3), 231–264.

[9] Gilman, A. G., *The Journal of clinical investigation*, 1984, **73**(1), 1–4.

[10] Hepler, J. R. and Gilman, A. G., *Trends in biochemical sciences*, 1992, **17**(10), 383–387.

[11] Hamm, H. E., *Journal of Biological Chemistry*, 1998, **273**(2), 669–672.

[12] Lohse, M. J.; Benovic, J. L.; Codina, J.; Caron, M. G. and Lefkowitz, R. J., *Science (New York, N.Y.)*, 1990, **248**(4962), 1547–1550.

[13] Attramadal, H.; Arriza, J. L.; Aoki, C.; Dawson, T. M.; Codina, J.; Kwatra, M. M.; Snyder, S. H.; Caron, M. G. and Lefkowitz, R. J., *The Journal of biological chemistry*, 1992, **267**(25), 17882–17890.

[14] Lefkowitz, R. J. and Shenoy, S. K., *Science (New York, N.Y.)*, 2005, **308**(5721), 512–517.

[15] Takeda, S.; Kadowaki, S.; Haga, T.; Takaesu, H. and Mitaku, S., *FEBS Letters*, 2002, **520**(1-3), 97–101.

[16] Fredriksson, R.; Lagerström, M. C.; Lundin, L.-G. and Schiöth, H. B., *Molecular pharmacology*, 2003, **63**(6), 1256–1272.

[17] Vassilatis, D. K.; Hohmann, J. G.; Zeng, H.; Li, F.; Ranchalis, J. E.; Mortrud, M. T.; Brown, A.; Rodriguez, S. S.; Weller, J. R.; Wright, A. C.; Bergmann, J. E. and Gaitanaris, G. A., *Proceedings of the National Academy of Sciences of the United States of America*, 2003, **100**(8), 4903–4908.

[18] Kolakowski, L. F., *Receptors & channels*, 1994, **2**(1), 1–7.

[19] Baldwin, J. M., *The EMBO journal*, 1993, **12**(4), 1693–1703.

[20] Schwartz, T. W., *Current opinion in biotechnology*, 1994, **5**(4), 434–444.

[21] Ballesteros, J. A. and Weinstein, H. In *Receptor Molecular Biology*, Vol. 25 of *Methods in Neurosciences;* Elsevier, 1995; pages 366–428.

[22] Heifetz, A.; Schertler, Gebhard F X, ; Seifert, R.; Tate, C. G.; Sexton, P. M.; Gurevich, V. V.; Fourmy, D.; Cherezov, V.; Marshall, F. H.; Storer, R. I.; Moraes, I.; Tikhonova, I. G.; Tautermann, C. S.; Hunt, P.; Ceska, T.; Hodgson, S.; Bodkin, M. J.; Singh, S.; Law, R. J. and Biggin, P. C., *Naunyn-Schmiedeberg's archives of pharmacology*, 2015, **388**(8), 883–903.

[23] Palczewski, K., *Science*, 2000, **289**(5480), 739–745.

[24] Magnani, F.; Shibata, Y.; Serrano-Vega, M. J. and Tate, C. G., *Proceedings of the National Academy of Sciences of the United States of America*, 2008, **105**(31), 10744–10749.

[25] Jaakola, V.-P.; Griffith, M. T.; Hanson, M. A.; Cherezov, V.; Chien, Ellen Y T, ; Lane, J. R.; Ijzerman, A. P. and Stevens, R. C., *Science (New York, N.Y.)*, 2008, **322**(5905), 1211–1217.

[26] Shonberg, J.; Kling, R. C.; Gmeiner, P. and Löber, S., *Bioorganic & medicinal chemistry*, 2015, **23**(14), 3880–3906.

114

[27] Fredholm, B. B.; IJzerman, A. P.; Jacobson, K. A.; Klotz, K. N. and Linden, J., *Pharmacological reviews*, 2001, **53**(4), 527–552.

[28] Piirainen, H.; Ashok, Y.; Nanekar, R. T. and Jaakola, V.-P., *Biochimica et biophysica acta*, 2011, **1808**(5), 1233–1244.

[29] Holanda, A. D., ; Asth, L.; Santos, A. R.; Guerrini, R.; de P Soares-Rachetti, V., ; Calo', G.; André, E. and Gavioli, E. C., *Life sciences*, 2015, **120**, 8–12.

[30] Fredholm, B. B.; Irenius, E.; Kull, B. and Schulte, G., *Biochemical pharmacology*, 2001, **61**(4), 443–448.

[31] Chen, J.-F.; Eltzschig, H. K. and Fredholm, B. B., *Nature Reviews Drug Discovery*, 2013, **12**(4), 265–286.

[32] Olah, M. E., *The Journal of biological chemistry*, 1997, **272**(1), 337–344.

[33] Kull, B.; Svenningsson, P. and Fredholm, B. B., *Molecular pharmacology*, 2000, **58**(4), 771–777.

[34] Corvol, J. C.; Studler, J. M.; Schonn, J. S.; Girault, J. A. and Hervé, D., *Journal of neurochemistry*, 2001, **76**(5), 1585–1588.

[35] Ledent, C.; Vaugeois, J. M.; Schiffmann, S. N.; Pedrazzini, T.; El Yacoubi, M.; Vanderhaeghen, J. J.; Costentin, J.; Heath, J. K.; Vassart, G. and Parmentier, M., *Nature*, 1997, **388**(6643), 674–678.

[36] Chen, J. F.; Huang, Z.; Ma, J.; Zhu, J.; Moratalla, R.; Standaert, D.; Moskowitz, M. A.; Fink, J. S. and Schwarzschild, M. A., *The Journal of neuroscience : the official journal of the Society for Neuroscience*, 1999, **19**(21), 9192–9200.

[37] Jordan, J. E.; Zhao, Z. Q.; Sato, H.; Taft, S. and Vinten-Johansen, J., *The Journal of pharmacology and experimental therapeutics*, 1997, **280**(1), 301–309.

[38] Kanda, T.; Jackson, M. J.; Smith, L. A.; Pearce, R. K.; Nakamura, J.; Kase, H.; Kuwana, Y. and Jenner, P., *Experimental neurology*, 2000, **162**(2), 321–327.

[39] Doré, A. S.; Robertson, N.; Errey, J. C.; Ng, I.; Hollenstein, K.; Tehan, B.; Hurrell, E.; Bennett, K.; Congreve, M.; Magnani, F.; Tate, C. G.; Weir, M. and Marshall, F. H., *Structure (London, England : 1993)*, 2011, **19**(9), 1283–1293.

[40] Congreve, M.; Andrews, S. P.; Doré, A. S.; Hollenstein, K.; Hurrell, E.; Langmead, C. J.; Mason, J. S.; Ng, I. W.; Tehan, B.; Zhukov, A.; Weir, M. and Marshall, F. H., *Journal of medicinal chemistry*, 2012, **55**(5), 1898–1903.

[41] Hino, T.; Arakawa, T.; Iwanari, H.; Yurugi-Kobayashi, T.; Ikeda-Suno, C.; Nakada-Nakura, Y.; Kusano-Arai, O.; Weyand, S.; Shimamura, T.; Nomura, N.; Cameron, A. D.; Kobayashi, T.; Hamakubo, T.; Iwata, S. and Murata, T., *Nature*, 2012, **482**(7384), 237–240.

[42] Liu, W.; Chun, E.; Thompson, A. A.; Chubukov, P.; Xu, F.; Katritch, V.; Han, G. W.; Roth, C. B.; Heitman, L. H.; Ijzerman, A. P.; Cherezov, V. and Stevens, R. C., *Science (New York, N.Y.)*, 2012, **337**(6091), 232–236.

[43] Xu, F.; Wu, H.; Katritch, V.; Han, G. W.; Jacobson, K. A.; Gao, Z.-G.; Cherezov, V. and Stevens, R. C., *Science (New York, N.Y.)*, 2011, **332**(6027), 322–327.

[44] Lebon, G. and Tate, C. G., *Médecine sciences : M/S*, 2011, **27**(11), 926–928.

[45] Lebon, G.; Warne, T.; Edwards, P. C.; Bennett, K.; Langmead, C. J.; Leslie, Andrew G W, and Tate, C. G., *Nature*, 2011, **474**(7352), 521–525.

[46] Lebon, G.; Edwards, P. C.; Leslie, Andrew G W, and Tate, C. G., *Molecular pharmacology*, 2015, **87**(6), 907–915.

[47] Keränen, H.; Gutiérrez-de Terán, H. and Åqvist, J., *PloS one*, 2014, **9**(10), e108492.

[48] Keränen, H.; Åqvist, J. and Gutiérrez-de Terán, H., *Chemical communications (Cambridge, England)*, 2015, **51**(17), 3522–3525.

[49] Jiang, Q.; van Rhee, A M, ; Kim, J.; Yehle, S.; Wess, J. and Jacobson, K. A., *Molecular pharmacology*, 1996, **50**(3), 512–521.

[50] Bertheleme, N.; Strege, A.; Bunting, S. E.; Dowell, S. J. and Byrne, B., *PloS one*, 2014, **9**(3), e89613.

[51] Lee, Y.; Choi, S. and Hyeon, C., *PLoS computational biology*, 2015, **11**(2), e1004044.

[52] Kim, J.; Wess, J.; van Rhee, A M, ; Schöneberg, T. and Jacobson, K. A., *The Journal of biological chemistry*, 1995, **270**(23), 13987–13997.

[53] Jaakola, V.-P.; Lane, J. R.; Lin, J. Y.; Katritch, V.; Ijzerman, A. P. and Stevens, R. C., *The Journal of biological chemistry*, 2010, **285**(17), 13032–13044.

[54] Zhukov, A.; Andrews, S. P.; Errey, J. C.; Robertson, N.; Tehan, B.; Mason, J. S.; Marshall, F. H.; Weir, M. and Congreve, M., *Journal of medicinal chemistry*, 2011, **54**(13), 4312–4323.

[55] Kim, S.-K.; Gao, Z.-G.; van Rompaey, P.; Gross, A. S.; Chen, A.; van Calenbergh, S. and Jacobson, K. A., *Journal of medicinal chemistry*, 2003, **46**(23), 4847–4859.

[56] Jacobson, K. A.; Van Galen, P J, and Williams, M., *Journal of medicinal chemistry*, 1992, **35**(3), 407–422.

[57] Jarvis, M. F.; Schulz, R.; Hutchison, A. J.; Do, U. H.; Sills, M. A. and Williams, M., *The Journal of pharmacology and experimental therapeutics*, 1989, **251**(3), 888–893.

[58] Londos, C.; Cooper, D. M. and Wolff, J., *Proceedings of the National Academy of Sciences of the United States of America*, 1980, **77**(5), 2551–2554.

[59] Koeppen, M.; Eckle, T. and Eltzschig, H. K., *PloS one*, 2009, **4**(8), e6784.

[60] Arrigoni, E.; Rainnie, D. G.; McCarley, R. W. and Greene, R. W., *The Journal of neuroscience : the official journal of the Society for Neuroscience*, 2001, **21**(3), 1076–1085.

[61] Rainnie, D. G.; Grunze, H. C.; McCarley, R. W. and Greene, R. W., *Science (New York, N.Y.)*, 1994, **263**(5147), 689–692.

[62] Johansson, B.; Halldner, L.; Dunwiddie, T. V.; Masino, S. A.; Poelchen, W.; Giménez-Llort, L.; Escorihuela, R. M.; Fernández-Teruel, A.; Wiesenfeld-Hallin, Z.; Xu, X. J.; Hårdemark, A.; Betsholtz, C.; Herlenius, E. and Fred-

holm, B. B., *Proceedings of the National Academy of Sciences of the United States of America*, 2001, **98**(16), 9407–9412.

[63] Ramos-Zepeda, G.; Schröder, W.; Rosenow, S. and Herrero, J. F., *European journal of pharmacology*, 2004, **499**(3), 247–256.

[64] Mathôt, R. A.; van Schaick, E A, ; Langemeijer, M. W.; Soudijn, W.; Breimer, D. D.; IJzerman, A. P. and Danhof, M., *The Journal of pharmacology and experimental therapeutics*, 1994, **268**(2), 616–624.

[65] Sun, D.; Samuelson, L. C.; Yang, T.; Huang, Y.; Paliege, A.; Saunders, T.; Briggs, J. and Schnermann, J., *Proceedings of the National Academy of Sciences of the United States of America*, 2001, **98**(17), 9983–9988.

[66] Brown, R.; Ollerstam, A.; Johansson, B.; Skøtt, O.; Gebre-Medhin, S.; Fredholm, B. and Persson, A. E., *American journal of physiology. Regulatory, integrative and comparative physiology*, 2001, **281**(5), R1362–7.

[67] Klotz, K. N.; Hessling, J.; Hegler, J.; Owman, C.; Kull, B.; Fredholm, B. B. and Lohse, M. J., *Naunyn-Schmiedeberg's archives of pharmacology*, 1998, **357**(1), 1–9.

[68] Beukers, M. W.; Chang, L. C. W., ; von Frijtag Drabbe Künzel, J. K., ; Mulder-Krieger, T.; Spanjersberg, R. F.; Brussee, J. and IJzerman, A. P., *Journal of medicinal chemistry*, 2004, **47**(15), 3707–3709.

[69] Kolb, P.; Phan, K.; Gao, Z.-G.; Marko, A. C.; Sali, A. and Jacobson, K. A., *PloS one*, 2012, **7**(11), e49910.

[70] IJzerman, A. P.; Van Galen, P J, and Jacobson, K. A., *Drug design and discovery*, 1992, **9**(1), 49–67.

[71] Libert, F.; Schiffmann, S. N.; Lefort, A.; Parmentier, M.; Gérard, C.; Dumont, J. E.; Vanderhaeghen, J. J. and Vassart, G., *The EMBO journal*, 1991, **10**(7), 1677–1682.

[72] Henderson, R.; Baldwin, J. M.; Ceska, T. A.; Zemlin, F.; Beckmann, E. and Downing, K. H., *Biochemical Society transactions*, 1990, **18**(5), 844.

[73] Rivkees, S. A.; Barbhaiya, H. and IJzerman, A. P., *The Journal of biological chemistry*, 1999, **274**(6), 3617–3621.

118

[74] Olah, M. E.; Ren, H.; Ostrowski, J.; Jacobson, K. A. and Stiles, G. L., *The Journal of biological chemistry*, 1992, **267**(15), 10764–10770.

[75] Townsend-Nicholson, A. and Schofield, P. R., *The Journal of biological chemistry*, 1994, **269**(4), 2373–2376.

[76] Rivkees, S. A.; Lasbury, M. E. and Barbhaiya, H., *The Journal of biological chemistry*, 1995, **270**(35), 20485–20490.

[77] Tucker, A. L.; Robeva, A. S.; Taylor, H. E.; Holeton, D.; Bockner, M.; Lynch, K. R. and Linden, J., *The Journal of biological chemistry*, 1994, **269**(45), 27900–27906.

[78] Barbhaiya, H.; McClain, R.; Ijzerman, A. and Rivkees, S. A., *Molecular pharmacology*, 1996, **50**(6), 1635–1642.

[79] Scholl, D. J. and Wells, J. N., *Biochemical pharmacology*, 2000, **60**(11), 1647–1654.

[80] Tosh, D. K.; Phan, K.; Deflorian, F.; Wei, Q.; Gao, Z.-G. and Jacobson, K. A., *ACS medicinal chemistry letters*, 2011, **2**(8), 626–631.

[81] Kobilka, B. K. and Deupi, X., *Trends in pharmacological sciences*, 2007, **28**(8), 397–406.

[82] Lean, A. d.; Stadel, J. M. and Lefkowitz, R. J., *The Journal of biological chemistry*, 1980, **255**(15), 7108–7117.

[83] Samama, P.; Cotecchia, S.; Costa, T. and Lefkowitz, R. J., *The Journal of biological chemistry*, 1993, **268**(7), 4625–4636.

[84] Weiss, J. M.; Morgan, P. H.; Lutz, M. W. and Kenakin, T. P., *Journal of theoretical biology*, 1996, **178**(2), 151–167.

[85] Koshland, D. E., *Proceedings of the National Academy of Sciences of the United States of America*, 1958, **44**(2), 98–104.

[86] Hall, D. A., *Molecular pharmacology*, 2000, **58**(6), 1412–1423.

[87] Frauenfelder, H.; Sligar, S. G. and Wolynes, P. G., *Science (New York, N.Y.)*, 1991, **254**(5038), 1598–1603.

[88] Nygaard, R.; Frimurer, T. M.; Holst, B.; Rosenkilde, M. M. and Schwartz, T. W., *Trends in pharmacological sciences*, 2009, **30**(5), 249–259.

[89] Rosenbaum, D. M.; Rasmussen, S. G. and Kobilka, B. K., *Nature*, 2009, **459**(7245), 356–363.

[90] Lebon, G.; Bennett, K.; Jazayeri, A. and Tate, C. G., *Journal of molecular biology*, 2011, **409**(3), 298–310.

[91] Stephenson, R. P., *British journal of pharmacology and chemotherapy*, 1956, **11**(4), 379–393.

[92] Kenakin, T. P., *Pharmacological reviews*, 1984, **36**(3), 165–222.

[93] Copeland, R. A.; Pompliano, D. L. and Meek, T. D., *Nature reviews. Drug discovery*, 2006, **5**(9), 730–739.

[94] Tummino, P. J. and Copeland, R. A., *Biochemistry*, 2008, **47**(20), 5481–5492.

[95] Lu, H. and Tonge, P. J., *Current opinion in chemical biology*, 2010, **14**(4), 467–474.

[96] Lu, H.; England, K.; Am Ende, C.; Truglio, J. J.; Luckner, S.; Reddy, B. G.; Marlenee, N. L.; Knudson, S. E.; Knudson, D. L.; Bowen, R. A.; Kisker, C.; Slayden, R. A. and Tonge, P. J., *ACS chemical biology*, 2009, **4**(3), 221–231.

[97] Louvel, J.; Guo, D.; Agliardi, M.; Mocking, Tamara A M, ; Kars, R.; Pham, T. P.; Xia, L.; Vries, H. d.; Brussee, J.; Heitman, L. H. and Ijzerman, A. P., *Journal of medicinal chemistry*, 2014, **57**(8), 3213–3222.

[98] Guo, D.; Hillger, J. M.; Ijzerman, A. P. and Heitman, L. H., *Medicinal research reviews*, 2014, **34**(4), 856–892.

[99] Zwier, J. M.; Roux, T.; Cottet, M.; Durroux, T.; Douzon, S.; Bdioui, S.; Gregor, N.; Bourrier, E.; Oueslati, N.; Nicolas, L.; Tinel, N.; Boisseau, C.; Yverneau, P.; Charrier-Savournin, F.; Fink, M. and Trinquet, E., *Journal of biomolecular screening*, 2010, **15**(10), 1248–1259.

[100] Guo, D.; Xia, L.; van Veldhoven, J. P. D., ; Hazeu, M.; Mocking, T.; Brussee, J.; Ijzerman, A. P. and Heitman, L. H., *ChemMedChem*, 2014, **9**(4), 752–761.

[101] Guo, D.; Mulder-Krieger, T.; Ijzerman, A. P. and Heitman, L. H., *British journal of pharmacology*, 2012, **166**(6), 1846–1859.

[102] Stokes, G. G., *Philosophical Transactions of the Royal Society of London*, 1852, (142), 463–562.

[103] Herschel, J. F. W., , *Philosophical Transactions of the Royal Society of London*, 1845, (135), 143–145.

[104] Shimomura, O.; Johnson, F. H. and SAIGA, Y., *Journal of cellular and comparative physiology*, 1962, (59), 223–239.

[105] Chalfie, M.; Tu, Y.; Euskirchen, G.; Ward, W. W. and Prasher, D. C., *Science (New York, N.Y.)*, 1994, **263**(5148), 802–805.

[106] Heim, R.; Prasher, D. C. and Tsien, R. Y., *Proceedings of the National Academy of Sciences of the United States of America*, 1994, **91**(26), 12501–12504.

[107] Heim, R. and Tsien, R. Y., *Current biology : CB*, 1996, **6**(2), 178–182.

[108] Tsien, R. Y., *Annual review of biochemistry*, 1998, **67**, 509–544.

[109] Frommer, W. B.; Davidson, M. W. and Campbell, R. E., *Chemical Society reviews*, 2009, **38**(10), 2833–2841.

[110] Goedhart, J.; Stetten, D. v.; Noirclerc-Savoye, M.; Lelimousin, M.; Joosen, L.; Hink, M. A.; van Weeren, L.; Gadella, T. W. J., and Royant, A., *Nature communications*, 2012, **3**, 751.

[111] Nagai, T.; Ibata, K.; Park, E. S.; Kubota, M.; Mikoshiba, K. and Miyawaki, A., *Nature biotechnology*, 2002, **20**(1), 87–90.

[112] Zhang, J.; Campbell, R. E.; Ting, A. Y. and Tsien, R. Y., *Nature reviews. Molecular cell biology*, 2002, **3**(12), 906–918.

[113] Griffin, B. A., *Science*, 1998, **281**(5374), 269–272.

[114] Griffin, B. A.; Adams, S. R.; Jones, J. and Tsien, R. Y., *Methods in enzymology*, 2000, (327), 565–578.

[115] Adams, S. R.; Campbell, R. E.; Gross, L. A.; Martin, B. R.; Walkup, G. K.; Yao, Y.; Llopis, J. and Tsien, R. Y., *Journal of the American Chemical Society*, 2002, **124**(21), 6063–6076.

[116] Pomorski, A. and Kręzel, A., *Chembiochem : a European journal of chemical biology*, 2011, **12**(8), 1152–1167.

[117] Madani, F.; Lind, J.; Damberg, P.; Adams, S. R.; Tsien, R. Y. and Gräslund, A. O., *Journal of the American Chemical Society*, 2009, **131**(13), 4613–4615.

[118] Hoffmann, C.; Gaietta, G.; Bünemann, M.; Adams, S. R.; Oberdorff-Maass, S.; Behr, B.; Vilardaga, J.-P.; Tsien, R. Y.; Ellisman, M. H. and Lohse, M. J., *Nature methods*, 2005, **2**(3), 171–176.

[119] Lohse, M. J.; Nuber, S. and Hoffmann, C., *Pharmacological reviews*, 2012, **64**(2), 299–336.

[120] Keppler, A.; Gendreizig, S.; Gronemeyer, T.; Pick, H.; Vogel, H. and Johnsson, K., *Nature biotechnology*, 2003, **21**(1), 86–89.

[121] Gronemeyer, T.; Chidley, C.; Juillerat, A.; Heinis, C. and Johnsson, K., *Protein engineering, design & selection : PEDS*, 2006, **19**(7), 309–316.

[122] Keppler, A.; Pick, H.; Arrivoli, C.; Vogel, H. and Johnsson, K., *Proceedings of the National Academy of Sciences of the United States of America*, 2004, **101**(27), 9955–9959.

[123] Keppler, A.; Kindermann, M.; Gendreizig, S.; Pick, H.; Vogel, H. and Johnsson, K., *Methods (San Diego, Calif.)*, 2004, **32**(4), 437–444.

[124] Gautier, A.; Juillerat, A.; Heinis, C.; Corrêa, I. R.; Kindermann, M.; Beaufils, F. and Johnsson, K., *Chemistry & biology*, 2008, **15**(2), 128–136.

[125] Lakowicz, J. R., *Principles of fluorescence spectroscopy*, Springer, New York, 3rd ed ed., 2006.

[126] Jablonski, A., *Nature*, 1933, **131**(3319), 839–840.

[127] Rücker, G.; Neugebauer, M. and Willems, G. G., *Instrumentelle pharmazeutische Analytik: Lehrbuch zu spektroskopischen, chromatographischen, elektrochemischen und thermischen Analysenmethoden ; mit 81 Tabellen*, Wiss. Verl.-Ges., Stuttgart, 4., durchges. und aktualisierte aufl ed., 2008.

[128] Förster, T., *Annalen der Physik*, 1948, **437**(1-2), 55–75.

[129] Piston, D. W. and Kremers, G.-J., *Trends in biochemical sciences*, 2007, **32**(9), 407–414.

[130] Pollok, B. A. and Heim, R., *Trends in cell biology*, 1999, **9**(2), 57–60.

[131] Ciruela, F.; Jacobson, K. A. and Fernández-Dueñas, V., *ACS chemical biology*, 2014, **9**(9), 1918–1928.

[132] Ward, R. J. and Milligan, G., *Biochimica et biophysica acta*, 2014, **1838**(1 Pt A), 3–14.

[133] Deupi, X. and Standfuss, J., *Current opinion in structural biology*, 2011, **21**(4), 541–551.

[134] Tsien, R. Y.; Bacskai, B. J. and Adams, S. R., *Trends in cell biology*, 1993, **3**(7), 242–245.

[135] Trzaskowski, B.; Latek, D.; Yuan, S.; Ghoshdastider, U.; Debinski, A. and Filipek, S., *Current Medicinal Chemistry*, 2012, **19**(8), 1090–1109.

[136] Lohse, M. J.; Nikolaev, V. O.; Hein, P.; Hoffmann, C.; Vilardaga, J.-P. and Bünemann, M., *Trends in pharmacological sciences*, 2008, **29**(3), 159–165.

[137] Lohse, M. J.; Bünemann, M.; Hoffmann, C.; Vilardaga, J.-P. and Nikolaev, V. O., *Current opinion in pharmacology*, 2007, **7**(5), 547–553.

[138] Vilardaga, J.-P.; Bünemann, M.; Krasel, C.; Castro, M. and Lohse, M. J., *Nature biotechnology*, 2003, **21**(7), 807–812.

[139] Maier-Peuschel, M.; Frölich, N.; Dees, C.; Hommers, L. G.; Hoffmann, C.; Nikolaev, V. O. and Lohse, M. J., *The Journal of biological chemistry*, 2010, **285**(12), 8793–8800.

[140] Ziegler, N.; Bätz, J.; Zabel, U.; Lohse, M. J. and Hoffmann, C., *Bioorganic & medicinal chemistry*, 2011, **19**(3), 1048–1054.

[141] Zürn, A.; Zabel, U.; Vilardaga, J.-P.; Schindelin, H.; Lohse, M. J. and Hoffmann, C., *Molecular pharmacology*, 2009, **75**(3), 534–541.

[142] Nikolaev, V. O.; Hoffmann, C.; Bünemann, M.; Lohse, M. J. and Vilardaga, J.-P., *The Journal of biological chemistry*, 2006, **281**(34), 24506–24511.

[143] Gilman, A. G., *Annual review of biochemistry*, 1987, **56**, 615–649.

[144] Neer, E. J., *Cell*, 1995, **80**(2), 249–257.

[145] Janetopoulos, C.; Jin, T. and Devreotes, P., *Science (New York, N.Y.)*, 2001, **291**(5512), 2408–2411.

[146] Bünemann, M.; Frank, M. and Lohse, M. J., *Proceedings of the National Academy of Sciences of the United States of America*, 2003, **100**(26), 16077–16082.

[147] Goedhart, J.; van Weeren, L.; Adjobo-Hermans, M. J. W., ; Elzenaar, I.; Hink, M. A. and Gadella, T. W. J., , *PloS one*, 2011, **6**(11), e27321.

[148] Anderson, M. J. and Cohen, M. W., *The Journal of Physiology*, 1974, **237**(2), 385–400.

[149] McGrath, J. C.; Arribas, S. and Daly, C. J., *Trends in pharmacological sciences*, 1996, **17**(11), 393–399.

[150] Baker, J. G.; Middleton, R.; Adams, L.; May, L. T.; Briddon, S. J.; Kellam, B. and Hill, S. J., *British journal of pharmacology*, 2010, **159**(4), 772–786.

[151] Vernall, A. J.; Stoddart, L. A.; Briddon, S. J.; Hill, S. J. and Kellam, B., *Journal of medicinal chemistry*, 2012, **55**(4), 1771–1782.

[152] Vernall, A. J.; Hill, S. J. and Kellam, B., *British journal of pharmacology*, 2014, **171**(5), 1073–1084.

[153] Kozma, E.; Jayasekara, P. S.; Squarcialupi, L.; Paoletta, S.; Moro, S.; Federico, S.; Spalluto, G. and Jacobson, K. A., *Bioorganic & medicinal chemistry letters*, 2013, **23**(1), 26–36.

[154] Jacobson, K. A.; Ukena, D.; Padgett, W.; Kirk, K. L. and Daly, J. W., *Biochemical pharmacology*, 1987, **36**(10), 1697–1707.

[155] Middleton, R. J.; Briddon, S. J.; Cordeaux, Y.; Yates, A. S.; Dale, C. L.; George, M. W.; Baker, J. G.; Hill, S. J. and Kellam, B., *Journal of medicinal chemistry*, 2007, **50**(4), 782–793.

[156] Stoddart, L. A.; Vernall, A. J.; Denman, J. L.; Briddon, S. J.; Kellam, B. and Hill, S. J., *Chemistry & biology*, 2012, **19**(9), 1105–1115.

[157] Brand, F.; Klutz, A. M.; Jacobson, K. A.; Fredholm, B. B. and Schulte, G., *European journal of pharmacology*, 2008, **590**(1-3), 36–42.

[158] Fernández-Dueñas, V.; Gómez-Soler, M.; Jacobson, K. A.; Kumar, S. T.; Fuxe, K.; Borroto-Escuela, D. O. and Ciruela, F., *Journal of neurochemistry*, 2012, **123**(3), 373–384.

[159] Graham, F. L.; Smiley, J.; Russell, W. C. and Nairn, R., *The Journal of general virology*, 1977, **36**(1), 59–74.

[160] Ho, S. N.; Hunt, H. D.; Horton, R. M.; Pullen, J. K. and Pease, L. R., *Gene*, 1989, **77**(1), 51–59.

[161] Cooper, J.; Hill, S. J. and Alexander, S. P., *British journal of pharmacology*, 1997, **122**(3), 546–550.

[162] Hoffmann, C.; Gaietta, G.; Zürn, A.; Adams, S. R.; Terrillon, S.; Ellisman, M. H.; Tsien, R. Y. and Lohse, M. J., *Nature protocols*, 2010, **5**(10), 1666–1677.

[163] Jost, C. A.; Reither, G.; Hoffmann, C. and Schultz, C., *Chembiochem : a European journal of chemical biology*, 2008, **9**(9), 1379–1384.

[164] Bradford, M. M., *Analytical biochemistry*, 1976, (72), 248–254.

[165] Cheng, Y. and Prusoff, W. H., *Biochemical pharmacology*, 1973, **22**(23), 3099–3108.

[166] Gibson, S. K. and Gilman, A. G., *Proceedings of the National Academy of Sciences of the United States of America*, 2006, **103**(1), 212–217.

[167] Goedhart, J.; van Weeren, L.; Hink, M. A.; Vischer, N. O. E., ; Jalink, K. and Gadella, T. W. J., , *Nature methods*, 2010, **7**(2), 137–139.

[168] Martin, P.; Albagli, O.; Poggi, M. C.; Boulukos, K. E. and Pognonec, P., *BMC biotechnology*, 2006, **6**, 4.

[169] Klotz, K. N.; Lohse, M. J.; Schwabe, U.; Cristalli, G.; Vittori, S. and Grifantini, M., *Naunyn-Schmiedeberg's archives of pharmacology*, 1989, **340**(6), 679–683.

[170] Dang, T. N. Fret-based analysis of ligand binding and activation of the human adenosine a2a receptor, Master's thesis, Rheinische Friedrich-Wilhelms-Universität Bonn, Bonn, 2011.

[171] Lane, J. R.; Klein Herenbrink, C.; van Westen, G. J. P., ; Spoorendonk, J. A.; Hoffmann, C. and Ijzerman, A. P., *Molecular pharmacology*, 2012, **81**(3), 475–487.

[172] Thompson, J. D.; Higgins, D. G. and Gibson, T. J., *Nucleic Acids Research*, 1994, **22**(22), 4673–4680.

[173] Hartl, F. U.; Bracher, A. and Hayer-Hartl, M., *Nature*, 2011, **475**(7356), 324–332.

[174] Morello, J. P.; Salahpour, A.; Laperrière, A.; Bernier, V.; Arthus, M. F.; Lonergan, M.; Petäjä-Repo, U.; Angers, S.; Morin, D.; Bichet, D. G. and Bouvier, M., *The Journal of clinical investigation*, 2000, **105**(7), 887–895.

[175] Petäjä-Repo, U. E.; Hogue, M.; Bhalla, S.; Laperrière, A.; Morello, J.-P. and Bouvier, M., *The EMBO journal*, 2002, **21**(7), 1628–1637.

[176] Zhang, X.; Stevens, R. C. and Xu, F., *Trends in biochemical sciences*, 2015, **40**(2), 79–87.

[177] Fredholm, B. B., *European journal of respiratory diseases. Supplement*, 1980, **109**, 29–36.

[178] Biaggioni, I.; Paul, S.; Puckett, A. and Arzubiaga, C., *The Journal of pharmacology and experimental therapeutics*, 1991, **258**(2), 588–593.

[179] Seifert, R. and Wenzel-Seifert, K., *Naunyn-Schmiedeberg's archives of pharmacology*, 2002, **366**(5), 381–416.

[180] Smit, M. J.; Vischer, H. F.; Bakker, R. A.; Jongejan, A.; Timmerman, H.; Pardo, L. and Leurs, R., *Annual review of pharmacology and toxicology*, 2007, **47**, 53–87.

[181] Vilardaga, J.-P.; Steinmeyer, R.; Harms, G. S. and Lohse, M. J., *Nature chemical biology*, 2005, **1**(1), 25–28.

[182] Hoffmann, C.; Nuber, S.; Zabel, U.; Ziegler, N.; Winkler, C.; Hein, P.; Berlot, C. H.; Bünemann, M. and Lohse, M. J., *Molecular pharmacology*, 2012, **82**(2), 236–245.

[183] Mirzadegan, T.; Benkö, G.; Filipek, S. and Palczewski, K., *Biochemistry*, 2003, **42**(10), 2759–2767.

[184] McAllister, S. D.; Hurst, D. P.; Barnett-Norris, J.; Lynch, D.; Reggio, P. H. and Abood, M. E., *The Journal of biological chemistry*, 2004, **279**(46), 48024–48037.

[185] Buschmann, V.; Weston, K. D. and Sauer, M., *Bioconjugate chemistry*, 2003, **14**(1), 195–204.

[186] Zürn, A.; Klenk, C.; Zabel, U.; Reiner, S.; Lohse, M. J. and Hoffmann, C., *Bioconjugate chemistry*, 2010, **21**(5), 853–859.

[187] Málaga-Diéguez, L.; Yang, Q.; Bauer, J.; Pankevych, H.; Freissmuth, M. and Nanoff, C., *Molecular pharmacology*, 2010, **77**(6), 940–952.

[188] Xie, K.-Q.; Cao, Y. and Zhu, X.-Z., *Biochemical pharmacology*, 2006, **71**(6), 865–871.

[189] Peeters, M. C.; Wisse, L. E.; Dinaj, A.; Vroling, B.; Vriend, G. and IJzerman, A. P., *Biochemical pharmacology*, 2012, **84**(1), 76–87.

[190] Heitman, L. H.; Mulder-Krieger, T.; Spanjersberg, R. F.; von Frijtag Drabbe Künzel, J. K., ; Dalpiaz, A. and Ijzerman, A. P., *British journal of pharmacology*, 2006, **147**(5), 533–541.

[191] Shi, L.; Liapakis, G.; Xu, R.; Guarnieri, F.; Ballesteros, J. A. and Javitch, J. A., *The Journal of biological chemistry*, 2002, **277**(43), 40989–40996.

[192] Katritch, V.; Cherezov, V. and Stevens, R. C., *Annual review of pharmacology and toxicology*, 2013, (53), 531–556.

[193] Yuan, S.; Hu, Z.; Filipek, S. and Vogel, H., *Angewandte Chemie (International ed. in English)*, 2015, **54**(2), 556–559.

[194] Stoddart, L. A.; Kellam, B.; Briddon, S. J. and Hill, S. J., *British journal of pharmacology*, 2014, **171**(16), 3827–3844.

[195] Schultz, C.; Schleifenbaum, A.; Goedhart, J. and Gadella, T. W. J., , *Chembiochem : a European journal of chemical biology*, 2005, **6**(8), 1323–1330.

[196] Proska, J. and Tucek, S., *Molecular pharmacology*, 1995, **48**(4), 696–702.

[197] May, L. T.; Bridge, L. J.; Stoddart, L. A.; Briddon, S. J. and Hill, S. J., *FASEB journal : official publication of the Federation of American Societies for Experimental Biology*, 2011, **25**(10), 3465–3476.

[198] May, L. T.; Self, T. J.; Briddon, S. J. and Hill, S. J., *Molecular pharmacology*, 2010, **78**(3), 511–523.

10 Publications and conferences attended

10.1 Publications

Stumpf, A. D., Hoffmann, C.; Strategien zur Proteinmarkierungen für die Fluoreszenzmikroskopie – Wer die Wahl hat, hat die Qual, *GIT Labor-Fachzeitschrift, 2015, 5 (59): 24-27*

Stumpf, A. D. and Hoffmann, C.; Optical probes based on G-protein-coupled receptors – added work or added value?, under revision in *the British Journal of Pharmacology*

Stumpf, A. D., Ziegler, N., Zabel, U., Schmitt, S., van Unen, J., Goedhart, J., Hill, S. J. and Hoffmann, C.; Investigation of A_1 - adenosine receptor sensors and receptor activation by fluorescence resonance energy transfer in living cells. Manuscript in preparation

Dang, T. N.*, Ziegler, N.*, **Stumpf, A. D.**, Zabel, U., Müller C., Lohse, M. J., Lane, R., IJzermann, A. and Hoffmann, C.; Investigation of A_{2A} - adenosine receptor activation by fluorescence resonance energy transfer in living cells. Manuscript in preparation

(* contributed equally)

10.2 Conferences attended

19 - 20 Oct 2011, BIO BANG, international Symposium, Graduate School of Life Sciences, University of Würzburg, Germany

07 – 09 Oct 2012, GPCR Symposium of the Rudolf Virchow Center, University of Würzburg, Germany
Stumpf, A. D., Ziegler, N., Zabel, U., Winkler, C., Nuber, S., Bätz, J, Lohse, M. J., Hoffmann, C; Comparison of A_1 - and A_{2A} - receptor via fluorescence microscopy

16 – 17 Oct 2012, EPOS, 7th international Symposium, Graduate School of Life Sciences, University of Würzburg, Germany
Stumpf, A. D., Ziegler, N., Zabel, U., Winkler, C., Nuber, S., Bätz, J, Lohse, M. J., Hoffmann, C.; Comparison of A_1 - and A_{2A} - receptor via fluorescence microscopy

05 – 08 Apr 2013, 79. Jahrestagung der Deutschen Gesellschaft für Pharmakologie und Toxikologie, Halle, Germany
Stumpf, A. D., Ziegler, N., Zabel, U., Lohse, M. J., Hoffmann, C.; Comparison of A_1 - and A_{2A} - receptor activation dynamics via fluorescence resonance energy transfer microscopy; *Naunyn-Schmiedeberg's Archieves of Pharmacology, 2013 (386), 83, Suppl. 1*

03 – 06 Oct 2013, EMBO/EMBL Symposium: Seeing is believing - Imaging the Processes of Life, Heidelberg, Germany
Stumpf, A. D., Ziegler, N., Dang, T N., Schmitt, S., Zabel, U., Lohse, M. J., Hoffmann, C; Comparison of A_1 - and A_{2A} - receptor dynamics using FRET - based receptor sensors

01 – 04 Apr 2014, 80. Jahrestagung der Deutschen Gesellschaft für Pharmakologie und Toxikologie, Hannover, Germany
Stumpf, A. D., Ziegler, N., Schmitt, S., Dang, T N., Zabel, U., Lohse, M. J., Hoffmann, C.; Mutational analysis of A_1 - and A_{2A} - receptor dynamics via FRET measurements

28. – 29 Apr 2014, 5th BPS Focused Meeting on Cell Signalling, University of Leicester, United Kingdom

Stumpf, A. D., Ziegler, N., Dang, T N., Schmitt, S., Zabel, U., Lohse, M. J., Hoffmann, C.; Mutational analysis of A_1 - and A_{2A} - receptor dynamics via FRET measurements

23 – 27 Jul 2014, Purines 2014 – Nucleotides, Nucleosides and Nucleobases, International Conference in Signaling Drugs and Targets, Bonn, Germany

Stumpf, A. D., Ziegler, N., Schmitt, S., Dang, T N., Zabel, U., Lohse, M. J., Hoffmann, C.; Mutational analysis of A_1 - and A_{2A} - receptor dynamics via FRET measurements

11 acknowledgment

I want to give thanks to all the people who made this work possible.

I want to thank the members of the doctorate committee.
First and foremost I want to thank my first supervisor Prof. Dr. C. Hoffmann for giving me the opportunity to do my PhD thesis at the Institute of Pharmacology and Toxicology in his working group and for his great supervision.
Special thanks goes to Prof. Dr. C. Sotriffer for being my second supervisor and for the valuable discussions about my work at our meetings.
I want to thank Prof. Dr. S. Hill for filling the position of the third supervisor in my thesis and for fruitful discussions and valuable help concerning this project.
I want to thank Prof. Dr. M. Gessler for his time to be the chairperson for my doctorate committee.

I came in a working group with really nice and helpful colleagues that made the start in this new chapter of my life as comfortable as it could be. Special thanks to Nicole Ziegler and Dr. Susanne Nuber for introducing me to lab and microscopic methods and for their patience whenever I had questions.
I wanna thank the whole working group of Prof. Dr. C. Hoffmann for their helpfulness and the good working atmosphere which made my time in the Institute of Pharmacology and Toxicology a good and interesting time.

Finally I want to thank my family and my friends for their support- without you this work would not have been possible.

12 Affidavit/Eidesstattliche Erklärung

12.1 Affidavit

I hereby confirm that my thesis entitled "Development of fluorescent FRET receptor sensors for investigation of conformational changes in adenosine A_1 and A_{2A} receptors" is the result of my own work. I did not receive any help or support from commercial consultants. All sources and/ or materials applied are listed and specified in the thesis.

Furthermore, I confirm that this thesis has not yet been submitted as a part of another examination process neither in identical nor in similar form.

12.2 Eidesstattliche Erklärung

Hiermit erkläre ich an Eides statt, die Dissertation "Entwicklung fluoreszenter FRET Rezeptor-Sensoren zur Untersuchung von Konformationsänderungen in Adenosin A_1 und A_{2A} Rezeptoren" eigenständig, d.h. insbesondere selbstständig und ohne Hilfe eines kommerziellen Promotionsberaters angefertigt und keine anderen als die von mir angegebenen Quellen und Hilfsmittel verwendet zu haben.

Ich erkläre außerdem, dass die Dissertation weder in gleicher noch in ähnlicher Form bereits in einem anderen Prüfungsverfahren vorgelegen hat.

Würzburg, ...

Ort,Datum   *Unterschrift*